

SCUOLA DI SCIENZE

Dipartimento di Chimica Industriale "Toso Montanari"

Corso di Laurea Magistrale in

Chimica Industriale

Classe LM-71 - Scienze e Tecnologie della Chimica Industriale

**Theoretical and experimental studies of gold
catalysts for glucose oxidation**

Tesi di laurea sperimentale

CANDIDATO

Alessia Ventimiglia

RELATORE

Chiar.mo Prof. Nikolaos Dimitratos

CORRELATORE

Chiar.mo Prof. Ivan Rivalta

Chiar.mo Prof. Marco Garavelli

Eleonora Monti

Sessione II

Anno Accademico 2019-2020

ABSTRACT

The glucaric acid (GLA) has been identified as a “top value-added chemical from biomass” that can be employed for many uses; for instance, it could be a precursor of adipic acid, a monomer of Nylon-6,6. GLA can be synthesized by the oxidation of glucose (GLU), passing through the intermediate gluconic acid (GLO). In recent years, a new process has been sought to obtain GLA in an economic and environmental sustainable way, in order to replace the current use of HNO_3 as a stoichiometric oxidant, or electrocatalysis and biochemical synthesis, which show several disadvantages. Thereby, this work is focused on the study of catalysts based on gold nanoparticles supported on activated carbon for the oxidation reaction of GLU to GLA using O_2 as an oxidant agent and NaOH as base. The sol-immobilization method leads us to obtain small and well dispersed nanoparticles, characterized by UV-Vis, XRD and TEM techniques. Repeating the reaction on different batches of catalyst, both the synthesis and the reaction were confirmed to be reproducible. The effect of the reaction time feeding GLO as reagent was studied: the results show that the conversion of GLO increases as the reaction time increases; however, the yields of GLA and Other increase up to 1 hour, and then they remain constant. In order to obtain information on the catalytic mechanism at the atomistic level, a computational study based on density functional theory and atomistic modeling of the gold nano-catalyst were performed. Highly symmetric (icosahedral and cubo-octahedral) and distorted Au_{55} nanoparticles have been optimized along with Au(111) and Au(100) surfaces. Distorted structures were found to be more stable than symmetrical ones due to relativistic effects. On these various models the adsorptions of various species involved in the catalysis have been studied, including OH^- species, GLU and GLO. The study carried out aims to provide a method for approaching to the study of nanoparticellary catalytic systems.

1. <u>Introduction</u>	1
1.1. Catalysis: concept and historical context.....	1
1.1.1. Homogeneous catalysis.....	3
1.1.2. Heterogeneous catalysis.....	4
1.2. Biorefinery.....	7
1.2.1 Biorefinery: definition.....	8
1.2.2. Biorefineries platform molecules: glucaric acid.....	11
1.2.3. Synthesis of glucaric acid.....	15
1.3. Nanoparticles.....	19
1.3.1. Nanoparticles: synthetic methods.....	20
1.3.2. Bimetallic nanoparticles.....	26
1.3.3. Bimetallic nanoparticles: synthetic methods.....	26
1.4. Gold nanoparticles.....	27
1.4.1 Gold nanoparticles: main reactions.....	27
1.4.2 Glucose oxidation: mechanism of reaction.....	29
1.5. Glucose oxidation: a computational point of view.....	31
1.5.1. Computational chemistry in heterogeneous catalysis.....	31
1.5.2. Mechanism of glucose oxidation.....	32
2. <u>Scope</u>	34
3. <u>Theoretical and experimental background</u>	35
3.1. Experimental section.....	35
3.1.1. Preparation of catalysts.....	36
3.1.2. Characterization of catalysts.....	37

3.1.2.1. UV-Vis spectroscopy.....	37
3.1.2.2. X-Ray Diffraction (XRD).....	39
3.1.2.3. Transmission electron microscopy (TEM).....	40
3.1.3. Catalytic testing-Oxidation reactions	41
3.1.3.1. Reactor.....	41
3.1.3.2. Preparation of the reaction solutions.....	42
3.1.4. Sample treatments.....	43
3.1.5. Analysis of products.....	43
3.1.5.1. HPLC (High-performance liquid chromatography)	43
3.1.5.2. Calculation of reaction product concentration	45
3.2. Computational studies of glucose oxidation.....	49
3.2.1. Fundamental of quantum mechanics	49
3.2.2. DFT theory	50
3.2.3. The functionals.....	53
3.2.4. Basis sets	54
3.2.5. Effective Core Potential	55
4. <u>Results and discussion</u>.....	56
4.1. Experimental part: results.....	56
4.1.1. Synthesis and characterisation of materials.....	56
4.1.1.1. UV-Vis analysis.....	57
4.1.1.2. XRD analysis.....	58
4.1.1.3. TEM analysis.....	59
4.1.2. Glucose oxidation.....	61
4.2. Computational results.....	65
4.2.1. Modeling Gold Nanoparticles: structures and reactivity.....	65
4.2.2. Bare Gold Nanoparticles.....	66
4.2.3. Bare Gold Nanoparticles: Au ₅₅	67
4.2.4. Bare Gold Nanoparticles: Au(100) and Au(111).....	70
4.2.5. Study of the mechanism of the reaction: Preliminary consideration.....	72

4.2.6. OH ⁻ adsorption on Au ₅₅ clusters.....	72
4.2.7. OH ⁻ adsorption on Au(100) and Au(111).....	76
4.2.8. Glucose and OH ⁻ adsorption on Au ₅₅ clusters.....	79
4.2.9. Gluconic acid and OH ⁻ adsorption on Au ₅₅ clusters.....	82
5. <u>Conclusions</u>.....	84
6. <u>Future work</u>.....	86
7. <u>Reference</u>.....	87

1. Introduction

1.1. Catalysis: concept and historical context

The term “catalysis” was proposed in 1835 by Jöns Jakob Berzelius (1779-1848): [1] it comes from the Greek words *kata*, that means “down”, and *lyein*, meaning “loosen”. But this phenomenon has its origins long before: it has been used for thousands of years for fermentation processes, although the theory behind it was not known. In 1781 Antoine Augustin observed that by mixing potato starch with distilled water and cream of tartar (potassium hydrogen tartrate), the starch acquired a sweet taste after a few months. Döbereiner (1780-1849) discovered by heating the starch in water in the presence of mineral alcohols, it worked converted into alcohol. In 1811 Sigismund Konstantin Kirchhoff (1764-1833) saw that, by heating an aqueous solution of amide in the presence of acids, rubber, distirina and sugar were obtained.

The study of catalysis had its foundations between the late eighteenth and early nineteenth centuries, with the accumulation of experimental data which show the presence of foreign substances in various chemical reactions. At the beginning of the nineteenth century the properties of some metals, such as platinum, were noted, hypothesizing the functioning mechanism of homogeneous catalysis based on an unstable intermediate. In 1830s physical adsorption was proposed as a catalysis mechanism.

At the end of the nineteenth century by J.H. Van 't Hoff and W.H. Nernst (from 1898) was given a definitions of catalysis based entirely on the variation of the speed of a reaction in the presence of a catalyst. Giving a similar definition, W. Ostwald won the Nobel prize in 1909 for his studies on chemical equilibrium and catalysis. He defined catalysis like "the acceleration of a slow chemical process due to the presence of one foreign and unnecessary substance in itself to the reaction "pointing out that "It is necessary without any change in the energy situation [thermodynamics]" and that “At the end of the same process, the foreign substance can be considered as removed”. [2]

Catalysis is a chemical phenomenon where the speed of a chemical reaction undergoes changes due to the intervention of a substance (or a mixture of substances) called catalyst, which is not consumed by the progress of the reaction itself. It has a kinetic nature: the catalyst in fact acts

on the intermediate stages of a reaction, without modifying the initial and final one, thus not modifying the probability that a reaction takes place.

The basic principle is the variation of the reaction mechanism, preferring paths with a lower activation energy, increasing the reaction speed, as reported in Figure 1.

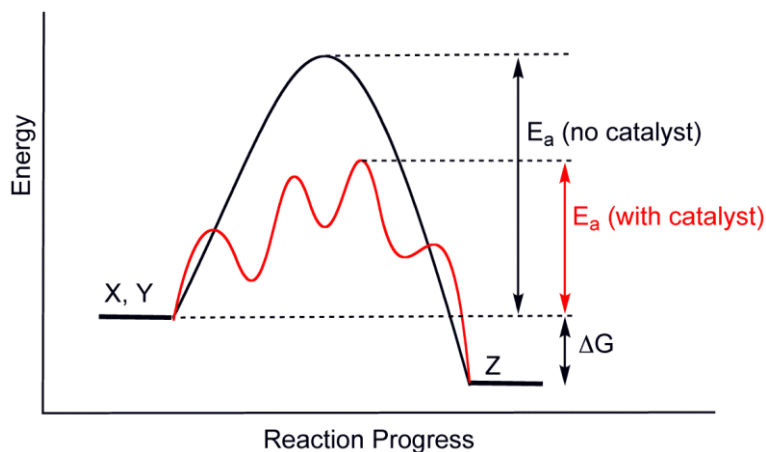


Figure 1: Variation of the reaction mechanism using a catalyst

Catalysts can be classified in several ways based on the chemical nature, the physical state or the type of reaction; however, the commonly classification used is based on number of phases present in the reaction system, such as:

- **homogeneous**, when the catalyst is in the same phase in which the reactants are present;
- **heterogeneous**, when the catalyst and the reactants are not in the same phase.

The characteristics of a catalyst may be defined by different parameters:

activity: it corresponds to the speed with which a chemical reaction proceeds towards equilibrium in the presence of the catalyst in question. It is related to the law of Arrhenius, which relates the speed constant to the temperature:

$$k = k_0 e^{-\Delta E/RT} \quad 1.1)$$

where k is the velocity constant; k_0 is the pre-exponential factor, which it was considered constant for not too high temperature variations; ΔE the activation energy; R the gas constant; T the temperature;

- **selectivity**, which is linked to the ability to slow down unwanted reactions;

- **stability:** the catalyst must be stable over time, since loss of stability (deactivation) leads to a decrease in activity and selectivity. The possible causes of deactivation are: mechanical (particle deterioration, abrasion); thermal (component volatility, phase changes, formation of new compounds, sintering); chemical (poisoning, coke deposition; physical (fouling).

Theoretically, a catalyst should carry out a catalytic cycle ad infinitum without undergoing modifications and without reducing its activity, but in reality this is not true it will become inactive.

Two other indicators are important: the Turn Over Number (TON) and the Turn Over Frequency (TOF); studying these can give us an idea of how the catalyst can change. In particular, the TON indicates the number of moles of substrate that a mole of catalyst can convert per second; instead the TOF is used to refer to the turnover per unit time. [3].

1.1.1. Homogeneous catalysis

As previously said, a catalyst is considered homogeneous when it is in the same phase as the reaction medium. For a homogeneous catalyst all active sites are equal to each other; furthermore, since it is homogeneously distributed in the reaction mixture, many active sites are available to interact with the substrate. For all these reasons it is usually possible to conduct reactions in mild conditions and without using a large amount of catalyst. Another advantage is that for homogeneous catalysts it is not necessary to consider the diffusion rate in the understanding of catalytic chemistry.

Among the industrial processes where homogeneous catalysis is used there are: oxidation, carbonylation, hydroformylation, oligomerization, polymerization, hydrocyanation and synthesis of fine chemicals, among other processes. [4]

The homogeneous catalysts used in industrial chemistry are generally organometallic compounds. In particular, transition metals play a central role in catalytic processes. This is due to their electronic configuration: having the d-orbitals partially filled, the formation of bonds with ligands is favoured, so as to be available for other reactions.

Among the possible binders of the organometallic complexes are CO, N₂, CN, RNC, PR₃, π -aryl, π -allyl, $-\text{SiR}_3$ and π -acyl. Tolman [5] proposed that the functioning of the catalytic cycle is based on a defined rule of 16 or 18 electrons (Figure 2). It gives importance to the oxidation state and to the coordination number of the metal centre of the catalytic complex.

The two main postulates of the rules are:

- Diamagnetic organometallic complexes of transition metals exist only if the valence shell of the central metal contains 16 or 18 electrons.
- Intermediates that form during the reaction must also contain 16 or 18 valence shell electrons.

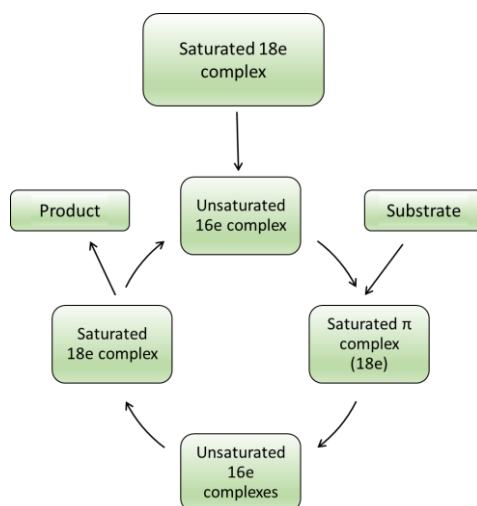


Figure 2: Cycle explaining the 16/18 electron rule

The main disadvantage of homogeneous catalysis is found in the difficulty to separate and recovering the catalyst from the reaction medium since the catalysts are in the same phase as the reactants and products. This makes the process unfavorable from an economic and environmental point of view, therefore difficult to achieve on a large scale. Moreover, there are mass transfer problems when one of the reagents is a gas; in a gas-liquid reaction there is the problem of the gas diffusion at the gas-liquid interface and in the liquid film.

1.1.2. Heterogeneous catalysis

Heterogeneous catalysts are for definition in a different phase from reaction medium and they are generally in solid phase. The use of heterogeneous catalysts in the chemical industry began in the early 1800s with Faraday, who discovered the use of platinum for oxidation reactions. [6] During the second world war, Pt-Al₂O₃ was used for the dehydrogenation of methyl

cyclohexane to toluene. After the war, heterogeneous catalysts such as Ni-aluminosilicate were used for oil hydrocracking and high boiling point: this allowed to obtain fuels, leading to the automotive industry revolution. Heterogeneous catalysts are used for a great number of chemical reactions, such as oxidation, nitration, coupling, condensation, and hydrogenation.

Chemical reactions take place through the adsorption of the reagents on the surface of the catalyst: The American chemist-physicist I. Langmuir [7] in 1916 proposed a model called the *adsorption isotherm* (later the *isotherm of Langmuir*), which explains adsorption by assuming an adsorbate behaves as an ideal gas at isothermal conditions. The model used for this formulation is still considered valid only for some borderline cases, since the assumption that the solid surface is uniform and the equivalent adsorption sites, that there are no interactions between adsorbed molecules and that only a single layer of molecules is adsorbed, represents an extreme simplification for the treatment of adsorption / desorption kinetics.

This model, however, provided the impetus to formulate new studies related to the adsorption mechanism on catalytic surfaces, up to the model Langmuir - Hinshelwood still used today.

The Langmuir - Hinshelwood theory is the one most used to explain the kinetics of heterogeneous catalyst processes. The equation that explains the kinetics of heterogeneous catalysts is as follows [10]:

$$r = \frac{dC}{dt} = \frac{k_r KC}{1+KC} \quad 1.2)$$

where r represents the rate of reaction that changes with time, C is the concentration and k the rate constant.

This theory is based on fundamental assumptions:

- Concentration gradients of the reagents in correspondence with the external film and inside the granules are negligible
- Concentration of each reagent at each point of the active surface equal to the concentration in the bulk of the homogeneous adsorbed phase.

The term r is represented by the initial velocity r_0 , which can be expressed as a function of the initial concentration C_0 or the equilibrium concentration C_{eq} : [8]

$$r_0 = \frac{k_r KC_0}{1+KC_0} \quad 1.3)$$

$$r_0 = \frac{k_r K C_{eq}}{1 + K C_{eq}} \quad 1.4)$$

Some years after the formulation of the Langmuir equation, Eley and Rideal, in 1939, proposed the reaction mechanism between chemisorbed and physisorbed molecules. Rideal proposed that a reaction not only occurs between chemisorbed molecules or a chemisorbed molecule and a molecule colliding with it from the gas phase, but can also occur between a chemisorbed molecule and a physisorbed one, holding the latter in a Van der Waals trough, without adsorbing.

For the reaction:



Rate equation is: $r = k C_S \theta_A C_A$

Considering the steady state approximation for AS and considering the reaction the limiting step, we obtain:

$$r = k C_B C_S \frac{k_1 C_A}{1 + k_1 C_A} \quad 1.6)$$

At low concentrations of A, $r = k C_B C_S k_1 C_A$ and the order is one with respect to A.

At high concentrations of A, $r = k C_B C_S$, and the order is zero with respect to A.

The reaction cycle using a heterogeneous catalyst takes place in 7 main steps (reported in Figure 3):

1. Diffusion of the reagents from the bulk of the homogeneous phase to the external surface of the CT (external diffusion);
2. Diffusion within the catalytic granule (intraparticle);
3. Adsorption of reagents on the catalyst;
4. Surface reaction of adsorbed reagents;
5. Desorption of the products from the surface of the catalyst;
6. Diffusion of products from inside the catalyst to the external surface (internal counter-diffusion);
7. External diffusion of products.

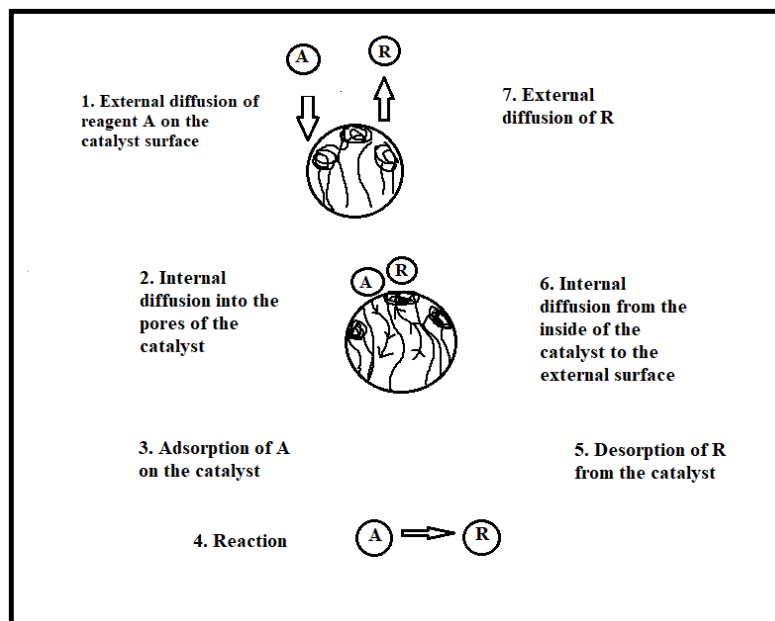


Figure 3: 7 steps of reaction in presence of a heterogeneous catalyst

Stages 1, 2, 6 and 7 are physical processes of matter transfer, while stages 3, 4 and 5 are chemical phenomena.

The heterogeneous catalyst consists of several parts:

- **The active phase:** where the reaction takes place;
- **The support:** where the active phase is deposited;
- **The promoters:** they can be physical, which improve the physical properties (surface area, mechanical strength) or chemicals, which modify the activity and selectivity of the active phase (such as semiconductivity n or p).

The active phase is generally expensive, so the advantage of having a support is that it allows to use less of it. The support, in fact, gives optimum porosity and surface area to the active phase. It also increases the mechanical resistance of the catalyst; creates multifunctional CTs, introducing new sites (basic or acid); increases the heat exchange capacity (e.g. SiC).

1.2. Biorefinery

The current world energy needs are largely supplied by fossil fuels (coal, oil and natural gas). However, these resources are slowly running out. [9] Furthermore, there is scientific evidence of greenhouse gas (GHG) emissions, such as carbon dioxide (CO₂), methane

(CH₄) and nitrous oxide (N₂O), updated by the combustion of fossil fuels, are harmful to the Earth [10,11]. For all these reasons, in recent years the use of renewable raw materials, i.e. biomass, becomes a crucial issue for the future of the chemical process industries.

Chemical products depend heavily on fossil fuels: it is estimated that around 4% [12] of oil is invested in this sector, for the production of plastic and chemical products. To cope with these problems, the world industry is looking for new sources of energy and production methods: [13] Plant-based raw materials (i.e. biomass) are known to have the potential to replace fossil fuels as raw materials for industrial production and an energy source in the transport sector; [14] moreover, biomass is abundant (about 180 billion tons per year) and more uniform distributed on the planet, so the incorporation of biomass into the industrial profile can help to keep energy independence and develop new opportunities for the chemical industry. This approach is fully compatible with the sustainability principle development, ensuring economic development based on local renewable resources, create jobs in both industry and agriculture fields and protect the environment.

1.2.1. Biorefinery: definition

The biorefinery is a structure that integrates various processes and equipment to convert biomass, such as wood, corn, etc., into its building blocks, such as carbohydrates, proteins, triglycerides, as well as biofuels and chemicals. Therefore, it is based on the same principles as oil refineries but using biobased and sustainable resources. An ethical and political discussion point is that some of the biofuels and chemicals are produced from raw materials in competition with the food and feed industries from first generation. To overcome these problems, a second generation of biofuels and chemicals has been introduced, from raw materials based on waste, residues or biomass from non-food crops. Lignocellulosic crops have the advantage of being able to be grown on land unsuitable for agricultural crops.

The raw materials for the biorefinery are supplied by different sectors, as reported in Figure 4:



Figure 4: Sectors that supply biomass as a raw material

The main biomass feedstocks are the lignocellulose, made up of three different components: cellulose, hemicellulose e lignin. They can be found in different percentages depending on the substance.

Cellulose ($C_6H_{10}O_6$)_n (Figure 5) is a polysaccharide consisting of a large number of glucose molecules joined together by a β -glycosidic bond. It has a branched chain, which differentiates it from starch. This latter, in fact, can be easily hydrolyzed by enzymes and acid attacks; cellulose, on the other hand, is much more difficult to hydrolyze.

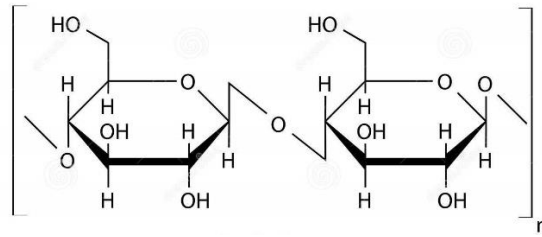


Figure 5: Cellulose structure

Hemicellulose ($C_5H_8O_5$)_n (Figure 6) is a polysaccharide which can be extracted from cellulose; it is relatively amorphous and scarcely soluble, but easier to hydrolyze than cellulose; it contains high hexose and pentose sugars.

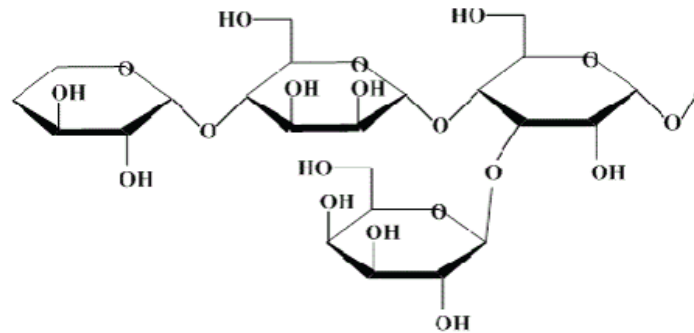


Figure 6: Hemicellulose structure

Lignin ($C_9H_{10}O_2$ (OCH_3)_n) is a heavy and complex organic polymer consisting mostly of phenolic compounds. It is found mainly in the cell wall of some plant cells and its main function is to give rigidity to the structure. It is composed essentially of many methoxylated derivatives of benzene, especially coniferyl, sinapyl and coumaryl alcohols, shown in Figure 7. [15] Cellulose and hemicellulose are polysaccharides hydrolysable in sugars and therefore usable in fermentation processes. Lignin, on the other hand, cannot be used in fermentation processes but is useful for other purposes, such as chemical extraction and energy generation.

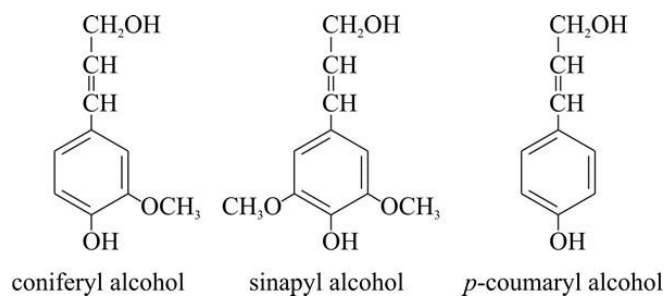


Figure 7: The three main components of lignin

1.2.2. Biorefineries platform molecules: glucaric acid

Bio-refineries must have a limited number of platform molecules, from which the chemicals are then derived. In particular, the fraction of carbohydrates collected from cellulose and hemicellulose from lignocellulosic biomass have a fundamental role for the formation of biochemical products: polysaccharides have in fact been hydrolyzed obtaining monosaccharides such as glucose, fructose and xylose, which can be converted in platform molecules with fermentative processes. The "Biomass Value-Added Chemicals" report published by the United States Department of Energy in 2004 [16] reported twelve molecules derived primarily from renewable sources, listed along with their potential in a bio-based chemical industry (Figure 8). The twelve building blocks can be subsequently converted to a number of high-value bio-based chemicals or materials. They are molecules with multiple functional groups that possess the potential to be transformed into new families of useful molecules.

Building blocks
1,4 succinic, fumaric and malic acids
Xylitol/arabinitol
Itaconic acid
Glycerol
3-hydroxybutyrolactone
Glutamic acid
Glucaric acid
Levulinic acid
Aspartic acid
3 hydroxy propionic acid
Sorbitol
2,5 furan dicarboxylic acid

Figure 8: The twelve building blocks with a great potential in a bio-based chemical industry (reported by the United States Department of Energy)

In this work we will focus on glucaric acid, that can be obtained from the oxidation of glucose.

Glucose

Glucose is an aldehyde monosaccharide; it is the most widespread organic compound in nature and is the product of chlorophyll photosynthesis. It is an aldohexose sugar as it is made up of six carbon atoms; it is a chiral molecule and is naturally present in the form of two enantiomers: the left-handed and the right-handed; the latter (D-glucose) is the most common: it is also present in the human body and is fundamental because it represents one of the major sources of energy. Glucose is produced industrially from starch through the use of acids or, with increasing popularity in recent years, through an enzymatic hydrolysis process.

World annual sugar production is around 20 million tons. [17] It is therefore a widely distributed raw material that is accessible from an economic point of view. Glucose is used as a platform molecule for the synthesis of chemicals and fuels (Figure 9). Starting from glucose it is possible to obtain alcohols such as ethanol and butanol through fermentative and enzymatic processes, but also to obtain organic acids such as citric acid and gluconic

acid. The latter is obtained by oxidation of the aldehyde group of glucose to obtain a carboxyl group. By oxidizing gluconic acid, glucaric acid can be obtained.

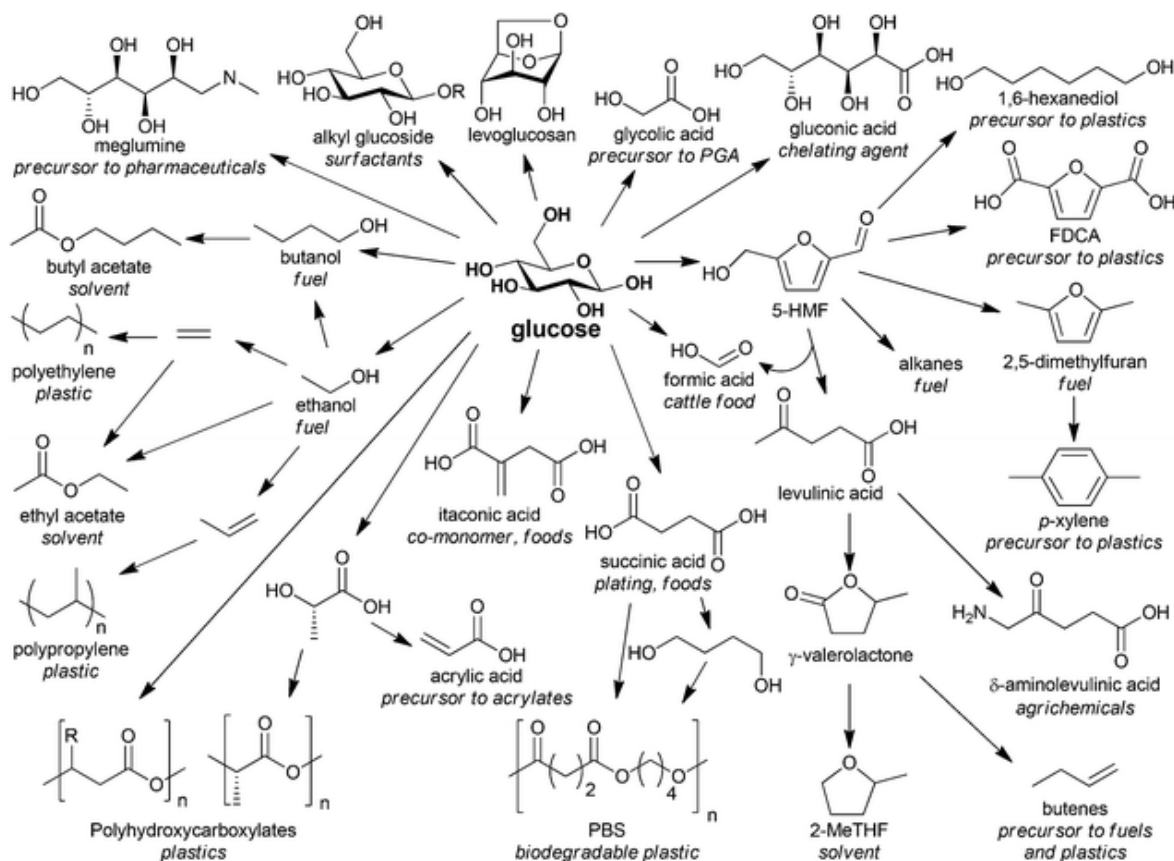


Figure 9: Derivative of glucose and their applications

Glucaric Acid

Glucaric acid, also known as saccharic acid, is a dicarboxylic polyhydroxy acid with structure $C_6H_{10}O_8$ obtained from the oxidation of both terminal groups of glucose to carboxylic groups, following the mechanism reported in the Figure 10. It is used as a chelating agent and raw material for pharmaceutical or food products. The gluconated ion in fact, with a net negative charge (anion), chelates Ca^{2+} , Fe^{2+} , Al^{3+} , and other heavy metals.

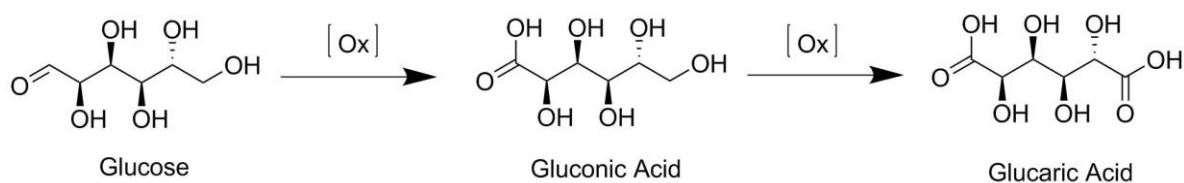


Figure 10: Mechanism of oxidation of glucose to glucaric acid

It can be obtained both in nature and in the laboratory: it is produced by some species of mammals and plants and together with D-glucaro-1,4-lactone it represents the final product of the metabolism of glucuronic acid. [18]

It has several possible uses: for example, it can be used in the medical field: it has been proposed as an anticancer agent [19], for the early diagnosis of heart attacks [20] and as a food supplement for the regulation of the cholesterol level. [21] Furthermore, it can be used as a metal corrosion inhibitor [22] and as a cationic sequestering agent for the production of phosphate-free detergents. [23]

Glucaric acid is a very interesting molecule for the chemical industry: salts and esters can be used for the production of new hyper-branched polyesters and its derivative, α -ketoglucarate, for the synthesis of innovative elastomers, [24] as shown in Figure 11.

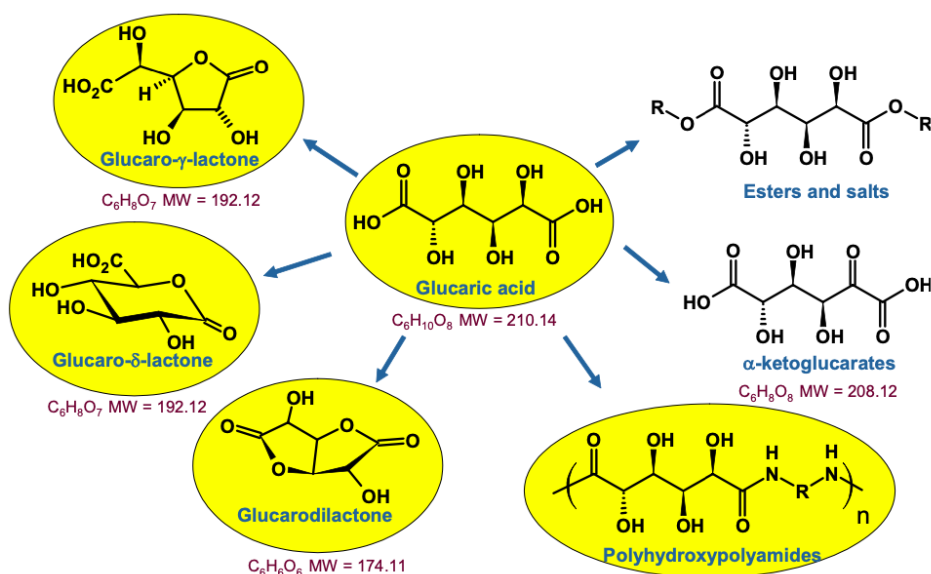


Figure 11: Chemical structure of glucaric acid and its derivatives

Particularly important is the process of catalytic reduction of glucaric acid to adipic acid, nylon-6.6 monomer (Figure 12). The global annual productions of adipic acid and its derivative ϵ -caprolactam are 2.2 and 4 million metric tons, respectively. [25] In 2012, more than 90% of the global adipic acid production relied on the nitric acid oxidation of cyclohexanol or a mixture of cyclohexanol – cyclohexanone (KA-oil), all derived from fossil-based benzene. For these reasons, a bio-based production of adipic acid starting from glucaric acid is interesting for the environment [26]. However, much of the interest of research on the synthesis of glucaric acid is mainly due to its potential use in polymer chemistry.

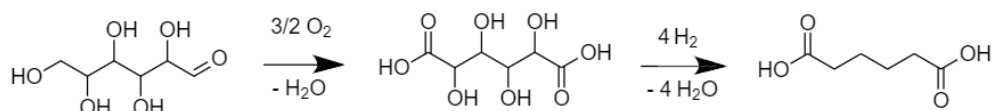


Figure 12: Synthesis of adipic acid starting from glucaric acid, obtained from biobased resources

1.2.3. Synthesis of glucaric acid

The most common method of obtaining glucaric acid is the oxidation of glucose via nitric acid, using the method introduced by Sohst-Tollens. This method has the advantage of being relatively simple, since nitric acid works both as an oxidant and as a solvent; consequently, it is still the most convenient, although it has many disadvantages and problems: indeed, it is not convenient from an economic and environmental point of view. HNO_3 , in fact, decomposes at NO_x , classified as air pollutants: its presence in the atmosphere is one of the causes of acid rain production, which causes damage to buildings and monuments. [27] It is therefore clear that it is necessary to find a new synthesis method that is less harmful from an environmental point of view.

In last years, various alternatives based on both chemical and biochemical processes have been proposed, even if none of them has proved economically advantageous to be developed on an industrial scale. [28] In the next paragraph it has been reported the main used.

Sohst-Tollens synthesis

As it has been already introduced, in 1888 the German chemists Sohst and Tollens proposed as a synthetic method of glucaric acid the oxidation of glucose by nitric acid, followed by the addition of potassium hydroxide in order to isolate the product as monopotassic glucarate. [29]

This process has numerous advantages: first of all, nitric acid, a relatively cheap reagent, is used both as an oxidant and as a solvent; furthermore, the reaction can be carried out at atmospheric pressure. In the 1950s a pilot plant was proposed for this process.

However, there are numerous problems for this process: nitric acid, as mentioned above, is a reagent considered to be polluting: during the reaction it is partially decomposed to NO_x and N₂O, which must be killed according to the regulations, leading to further costs. Furthermore, the reaction is poorly selective, leading to a low yield of glucaric acid; consequently, there is a low productivity and therefore an increase in costs due to the separation of the desired product from the by-products obtained during the reaction; furthermore, nitric acid is a strong acid, consequently the plant must be made using specific and expensive materials, leading high cost.

Glucaric acid production in recombinant E. Coli

In 2009 a mechanism of synthesis of glucaric acid starting from glucose was proposed by T.S. Moon et al., exploiting an enzymatic process with recombinant Escherichia Coli [30] through a complex genetic manipulation procedure. To perform the synthesis, three enzymes from three different organisms are transferred to Escherichia Coli (Figure 13).

This process has the advantage of being carried out at low temperatures, around 30 °C; it also does not require the use of oxidants or catalysts. The disadvantage is that the yield of glucaric acid is only 17%, therefore it is not a process achievable on an industrial scale as it would not lead to great economic advantages.

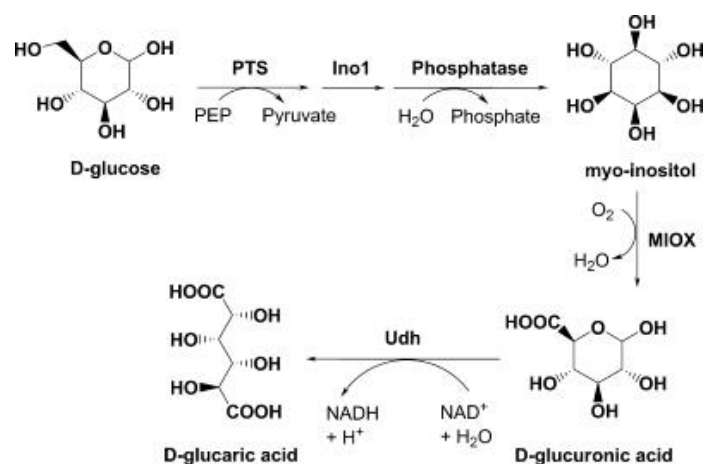


Figure 13: Pathway for the production of glucaric acid in recombinant *E. coli* [30]

Catalytic oxidation with vanadium pentoxide

Various mechanisms of glucaric acid synthesis have been proposed over the years using heterogeneous catalysts. In particular, V. Pamuk et al. have seen that in the presence of vanadium pentoxide supported on silica, a yield of 64% glucaric acid can be obtained in a cylindrical reactor air–molasses co-current downflow. [31] Specifically, it starts from a molasses containing 52% sucrose, oxidized with air in the presence of nitric acid, sulfuric acid and sodium nitrite. The latter helps the inversion reaction of sucrose and the oxidation of the glucose formed. The air has the function of oxidizing the glucose and nitrogen oxides that were formed during the reaction, in order to partially regenerate the nitric acid. The synthesis is carried out in a fixed bed reactor thermostated at 60° C.

This synthesis has numerous advantages: air is used as an oxidant, which is low cost; moreover, we start from molasses, a waste product of the sugar industry. However, there are problems with the use of high concentration strong acids and the formation of NO_x. Therefore, there is no convenient process from an economic and environmental point of view for a large-scale application.

Oxidation catalyzed by nitroxides

Merbouh et al. proposed to synthesize glucaric acid by oxidizing glucose by 4-acetamide-TEMPO [32] (Figure 14). In this process glucose is oxidized in the presence of catalytic quantities of the nitroxide, using potassium hypochlorite as a co-oxidant species. It is necessary to increase the basicity of the solution with NaOH up to a pH of 11,5. The reaction

is carried out between 0 to 5 °C. Finally, by adding ethanol the product precipitates in the form of monopotassium glucarate and therefore isolated. This synthesis has numerous advantages, among which the high selectivity and the high yield of glucaric acid (about 90%). However, the problem is not feasible on an industrial scale due to the high cost of the oxidizing agent.

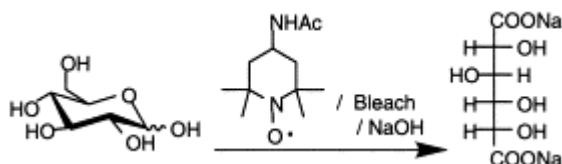


Figure 14: Glucose oxidation by 4-acetamide-TEMPO

Electrocatalytic oxidation of glucose

Another method of synthesis of glucaric acid is the oxidation of glucose in a catalytic reactor. The system consists of a nanoparticle MnO_2 anode deposited on a titanium electrode and a cathode consisting of a metal mesh around an electrode. The reaction occurs by applying a difference in potential between the two electrodes, causing the passage of electrons in the circuit. This leads to surprising results, with a yield of gluconic acid of 15% and 84% of glucaric acid. [33] This method has the advantage of not requiring the use of an oxidizing agent. In addition, the reaction is carried out under mild conditions, at a temperature of about 30° C, pH around 7 and with a current intensity of 6 mA cm⁻². However, although there are numerous advantages, the use of an electrocatalytic reactor on an industrial scale is too expensive to use. [34]

Catalytic oxidation with metallic nanoparticles

Over the years, various methods of synthesis of glucaric acid have been proposed using metal nanoparticles. Some noble metals, such as gold, platinum and palladium, on the nanometer scale are in fact particularly active for oxidation reactions. Furthermore, the possibility of supporting them, as seen above, allows their use as heterogeneous catalysts, therefore easily reusable and not subject to high separation costs. Gold nanoparticles are preferred because they do not undergo large leaching and poisoning phenomena, unlike those of Pd and Pt. [35]

1.3. Nanoparticles

Nanoparticles are particles with sizes ranging from 1 to 100 nm [36]. Although they appear to be a modern invention, they have been known for hundreds of years: for example, in the 11th century the artisans of Mesopotamia used them to generate a sparkling effect on the surface of the pottery.

Nanoparticles are a bridge between bulk materials and atomic or molecular structures. In fact, they have different properties compared to their large counterparts: they have a very high surface area to volume ratio; consequently, having the under coordinated surface atoms, they are more reactive. The high surface area therefore leads the nanoparticles to have interesting and unexpected properties.

Thanks to their special characteristics, in recent years, nanoparticles have become of great scientific interest, being used in numerous sectors, as reported in Figure 15.

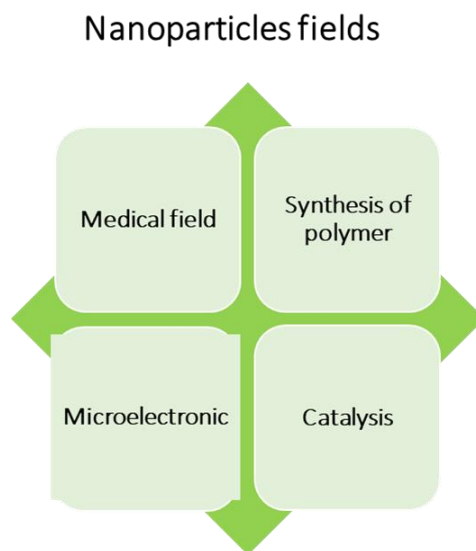


Figure 15: Fields of application of nanoparticles

In the medical field, for example, gold nanoparticles can be exploited to detect the presence of cancer cells. In addition to being biocompatible, they can be used as a scaffold for the transport of antibodies, which agglomerate in the vicinity of the cancer cells, highlighting them. This technique is advantageous because it is accurate and not very invasive. [37]

The clay nanoparticles are then used for the synthesis of polymers, as they increase their resistance by increasing the glass transition temperature. This allows to obtain nanocomposite polymers with significantly improved mechanical performance. Sometimes the nanoparticles are also tied to textile fibers to make the clothing more functional. [38]

In the field of microelectronics, metal nanoparticles are used for the production of printed circuits. They allow to lower the melting temperature of the conductive paste used to print the circuit, so that it is lower than the softening temperature of the card, made of polymeric material. The most conductive and weather-resistant metal is gold, but given its high cost, copper is often used. [39]

Nanoparticles have found wide use in the area of catalysis. Indeed, having a very high surface area they are more reactive, because of atoms on the surface with lower binding energy. This has allowed the use of bulk metals considered inactive for a long time. A significant example is gold: group VIII metals, copper (Cu), silver (Ag) and gold (Au), have the d-band fully occupied; For this reason, in bulk form, these metals are catalytically inactive as they do not have vacant sites in the d band; as we know, surface atoms, being undercoordinated, are reactive; in nanoparticles the surface to volume ratio is very high: as a consequence, as evidenced by the research of prof. M. Haruta [40] and prof. G. J. Hutchings [41], metals such as gold are catalytically active if their size falls below 10 nm, even at relatively low temperatures.

1.3.1. Nanoparticles: synthetic methods

Impregnation method

The impregnation method (IMP) is widely used for the preparation of different metal catalysts because it is simple and easy to control. In their Ki-Joong Kim work and Ho-Geun Ahn [42] report the synthesis of a bimetallic Pt-Au catalyst supported on ZnO / Al₂O₃ through a classic IMP and an incipient wetness impregnation (IW-IMP). The catalysts were characterized by ultraviolet-visible spectroscopy (UV-vis), X-ray diffraction (XRD), CO chemisorption, temperature-programmed reduction (TPR), X-ray photoelectron spectroscopy (XPS) and scanning transmission electron microscopy (STEM) in conjunction with energy dispersive spectroscopy (EDS).

The impregnation method (IMP)

Chlorinated precursors are used for Al₂O₃ support due to the strong interactions between precursor and support. 4% ZnO was loaded supported on alumina. H₂PtCl₆·5H₂O (Aldrich) and HAuCl₄·3 H₂O solutions were used as precursors of Pt and Au. Two grams of powder of the support of ZnO / Al₂O₃ were introduced and 20 ml of an aqueous solution of 2,47 10⁻² M HAuCl₄ and 1,95 10⁻² M H₂PtCl₆ at room temperature; the water was evaporated at 80° C, finally obtaining a paste. The catalyst obtained was dried and finally calcined.

The incipient wetness impregnation method (IW-IMP)

To prepare the catalyst with the incipient wetness impregnation method (IW-IMP) the necessary quantity of precursor was dissolved in deionized water; the volume of water used was chosen by imposing it equal to the volume of the pores of Al₂O₃. Keeping the ZnO / Al₂O₃ support under stirring, the freshly updated solution was added slowly and at room temperature for 20 minutes. The powder was dried for 24 hours and calcined for 3 hours at various temperatures.

For both methods it is necessary to pre-treat the catalysts with a reducing gas such as H₂ to remove the chlorine atoms coming from the solutions of the precursors, which is what would cause the sintering of the nanoparticles and therefore those of their size and of the latter.

This method has the advantages, besides being simple, to be capable to use different types of substrates and which do not require pH control. However, it does not allow to control the size of nanoparticles.

Anion adsorption

V. Pitchon and coworkers reported in their article [43] the direct anionic exchange (DAE). This method consists in a simple contact between a gold solution prepared with HAuCl₄ as precursor and alumina as support over a narrow range of pH. They start from the aqueous solutions of HAuCl₄ with concentrations of 10⁻², 1.44 × 10⁻³ or 2.23 × 10⁻⁴ M; support is Al₂O₃ (IEP=8-9). The solution is added to the support, then it is heated to 70° C and aged for an hour. The obtained product is filtered, washed with hot water, dried at 120° C and calcined at 300° C for 4 h. In Figure 16 we reported the method of synthesis. With this method, a loading of gold of 2% by weight is reached; the nanoparticles are large, about 10-20 nm. Their size depends on the presence of chlorine, which causes the sintering of the nanoparticles: to avoid this, it is possible to carry out a limited treatment with an ammonia solution, which however leads to a loss of

gold, reaching a final quantity of 1.5%. The dimensions of the nanoparticles are measured with HRTEM.

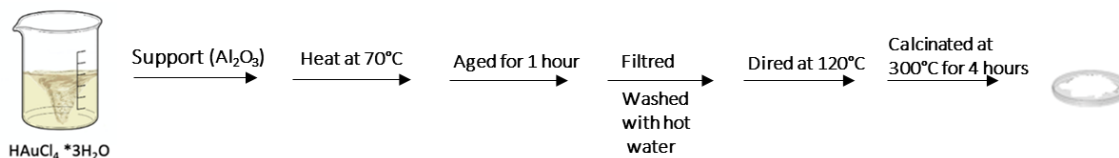


Figure 16: Scheme of anion adsorption method

This method is based on the direct anion exchange (AED) of the gold species with the hydroxyl groups of the medium. For this process, the isoelectric point (IEP) of the substrate is fundamental: if the pH of the solution is lower than the IEP: when the oxide surface is positively charged (OH^{2+} groups are present), consequently the anions present in the solution can adsorb; on the other hand, if the pH of the solution is higher than the IEP of the substrate, the substrate is negatively charged due to the presence of O^- surface groups, consequently the cations present in the solution are adsorbed.

As the preparation of the catalyst proceeded, Pitchon and colleagues noticed a continuous increase in the pH of the solution over time for all three prepared solutions [44]: for example, for a higher concentration of HAuCl_4 , 1.44×10^{-3} M, is observed an increase in pH from 2.9 to 3.7. At this pH, the gold species present in the solution are $[\text{AuCl}_3\text{OH}]^-$ and $[\text{AuCl}_2(\text{OH})_2]^-$: it is the latter being the main species that makes possible a reaction between the support and the complexes. The pH of the solution increases because the H^+ in the solution protonate the OH^- groups of Al_2O_3 forming OH_2 on the surface of the support (Figure 17).

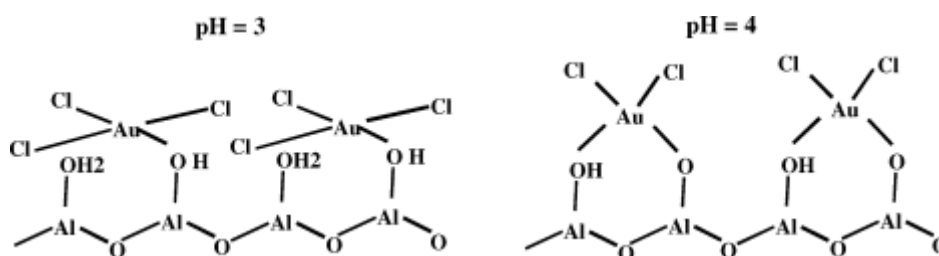


Figure 17: Mechanism of interaction of the gold complex with the alumina surface according to the pH

Sol-immobilization

Supported nanoparticles can be obtained in water by sol-immobilization method. In this technique, introduced by Prati and Martra in 1999 [45], metal nanoparticles are formed as sol, which are then stabilized by means of a support; the nanoparticles are obtained by reducing a solution of the metal precursor desired, for example HAuCl_4 to obtain gold nanoparticles, by means of a strong reducing agent like sodium borohydride, or reducing agent with lower strength, like hydrous hydrazine.

Nanoparticles are thermodynamically unstable in solution, therefore it is necessary to avoid that they aggregate [46]; consequently, before adding the support, it is necessary to add a stabilizing agent: this can be a steric, electrostatic or steric-electrostatic stabilizer (Figure 18). For electrostatic stabilization, the anions and cations that are in solution interact with the nanoparticles forming a double electric layer, which avoids their aggregation; electrostatic stabilization has the disadvantage of being sensitive to ionic strength and pH; in fact the addition of an electrolyte like NaCl can cause the agglomeration of the nanoparticles [47]; for these reasons steric stabilization is preferred, since it is not influenced by these factors; it consists in the adsorption of large molecules onto the surface of the nanoparticles: for steric reasons they consequently do not allow the nanoparticles to approach and therefore to agglomerate; some polymers, such as PVA (polyvinyl alcohol), combine steric and electrostatic effects. Part of the PVP adsorbs on the NP surface, while the other part dissolves freely in the suspension, creating a second protective shell. [48]

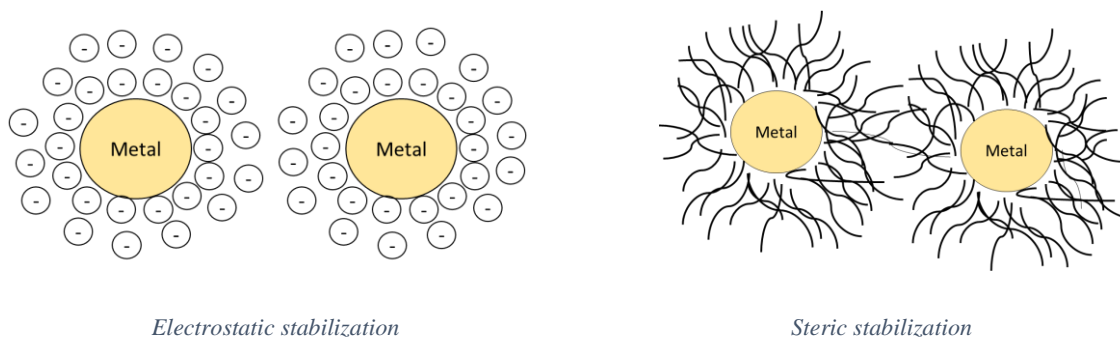


Figure 18: Scheme of electrostatic and steric stabilization

The stabilization of the nanoparticles is also fundamental for the immobilization phase through the support, as it increases their long-term stability. Moreover, this method allows to obtain nanoparticles with different shapes simply by varying the ionic environment (from the

octahedron to the cube, to the rhombic dodecahedron) [49]. Other parameters that influencing the morphology of the nanoparticles are metal, stabilizing agent and reducing agent concentration. [50,51] Indeed, it also turned out that a PVA / Au 3:1 weight ratio must not be exceeded, in order to avoid total immobilization of the NPs. [52] The immobilization of the nanoparticles allows to obtain a uniform and narrow size distribution of the latter on the surface of the support; the nanoparticles obtained with this method are not sensitive to pH, and furthermore it is possible to control their size, shape, oxidation state and final morphology.

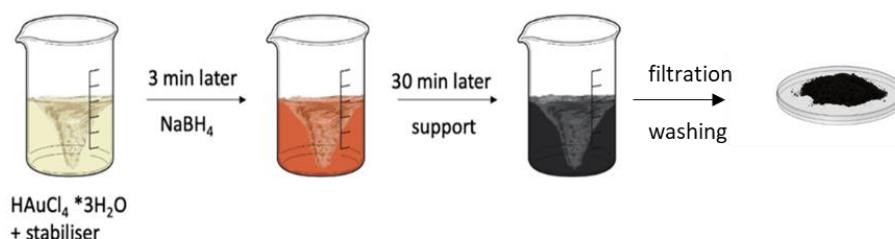


Figure 19: Sol immobilization preparation method

To support the nanoparticles in order to obtain the heterogeneous catalyst, the solution containing the nanoparticles must be brought to a pH lower than the isoelectric point of the support: this allows to facilitated the interactions between support and nanoparticles.

Deposition-precipitation

Deposition-Precipitation (DP) method consists in the deposition, by precipitation, of a hydroxide or hydrated oxide of the metal precursor on the surface of the support. The precursor of the metal, in fact, which is soluble, is rendered insoluble by increasing the pH: it has to be higher than the support IEP by the addition of a base. The procedure (Figure 20) generally consists in stirring a solution containing the support and the precursor of the soluble metal; the precipitating agent is added gradually for increasing the pH. Once the metal has precipitated on the support, the solid obtained is recovered, washed, dried and activated.

Zanella and collaborators [53] report the synthesis procedure of the catalysts with two different deposition-precipitation methods: with NaOH and with urea. They report for 1 g of support, in this case TiO₂, 100 mL of aqueous solution H₂AuCl₄ or [Au(en)₂]Cl₃ (4.2 10⁻³ M) (Au 8% wt). In the case of the reaction with NaOH, the temperature was set at 80° C and the pH adjusted to

8 with the addition of soda; the support and solution were left in contact for about an hour. For the reaction with urea, it was added to the solution of the gold precursor until it reached a concentration of 0,42 M. The reaction is carried out in the absence of light, so as not to decompose the precursor Gold.

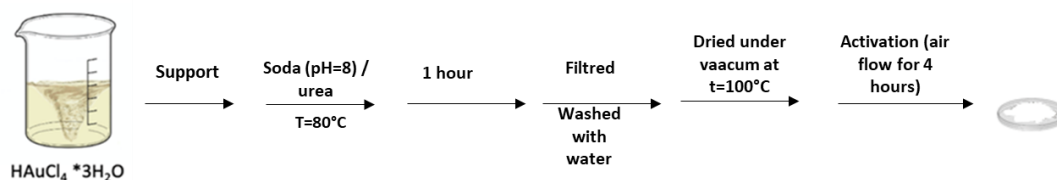


Figure 20: Deposition-precipitation synthetic method

Once the deposition is finished, the solid obtained is a state separated from the solution by centrifugation and washed several times with distilled water and dried under vacuum at room temperature or at 100° C. Finally, to activate the catalyst, it was calculated by a flow of industrial air at 300° C for 4 hours (50 mL /min).

In his work, Zanella and co-workers [54] propose a reaction mechanism. By XAS characterization, they demonstrated that a gold hydroxide structure is formed during NaOH DP. The dominating species in solution at the preparation pH (pH = 8) and the temperature of 80° C, are $[\text{AuCl}_2(\text{OH})_2]^-$ and $[\text{AuCl}(\text{OH})_3]^-$. [55] They observed that there is no chlorine in the close vicinity of gold in the catalyst prepared by DP NaOH. Moreover, the number of neighbours is found to be four and not three (indicates a square planar geometry of AuIII species). For these reasons they proposed that deposition could occur via a grafting reaction of the metal complexes with hydroxyl groups of the support surface.

For the DP urea preparation, the deposition of gold into the TiO_2 surface occurs from the precipitation of a gold compound, which is gold (III). Indeed, metallic gold does not form during DP urea preparation. For the reaction mechanism, it has been proposed that the gold species in the HAuCl_4 solution react with the ammonium ions or isocyanate ions, obtained by the decomposition of urea; while for the reaction between the isocyanate ions and gold there are no testimonials in the literature, the reactivity between gold and ammonia complexes is widely documented, in particular for the formation of planar square complexes of AuIII, such as $[\text{Au}(\text{NH}_3)_4]^{3+}$ [54]: it is obtained by slowly adding concentrated ammonia to the solution of

the gold precursor, keeping the pH below 5; [56] this process is similar to that which occurs during urea hydrolysis.

The products were characterized by inductively coupled plasma emission spectroscopy; calcinated Au / TiO₂ were analysed by TEM, X-ray (XANES and EXAFS) and RAMAN spectroscopy.

With this method it is possible to obtain 3-5 nanometer sized nanoparticles [57][58]. Furthermore, it is suitable for the deposition of gold on oxide supports with IEP higher than 5, such as magnesia, titania, alumina, zirconia, and ceria. It is not suitable for silica (IEP \approx 2), silica-alumina (IEP \approx 1), and tungsten (IEP \approx 1), activated carbon or zeolites.

The catalysts prepared from DP urea are more active than those obtained by the impregnation method, regardless of the quantity of gold. This is probably due to the fact that the impregnated catalysts have a larger particle size distribution than that of the catalysts obtained by urea DP.

1.3.2. Bimetallic nanoparticles

A bimetallic nanoparticle is a combination of two different metals that exhibit several new and improved properties. [59-61]

They have gained great interest from the scientific and industrial world thanks to their unique physicochemical properties; in fact, by blending two metals in one particle you can have more possibility to vary the properties of the obtained particle. They are used in various fields, including biomedical, imaging [62-72] and as catalysts: in fact, they often show higher catalytic activity compared to the corresponding monometallic nanoparticles.

1.3.3. Bimetallic nanoparticles: synthetic methods

As with monometallic nanoparticles, bimetallic ones can be summarized in two main ways: bottom-up method and top-down method.

For the bottom-up method it is necessary to start from solutions of the metal cations of interest in the form of soluble salts; subsequently these cations are reduced with suitable agents, which will then influence the properties of the particles. As seen above, the addition of stabilizers is required to prevent the nanoparticles from clumping. For bimetallic nanoparticles it is necessary to start from its solutions of the metal cations which will then constitute the nanoparticles. [73-76] The synthesis method can be of two types, depending on how the precursors are added: co-reduction method or subsequent reduction method. We speak of co-reduction method if both

pre-cursors are present at the same time, therefore they bind to each other according to a statistical mixture. Otherwise we speak of successive reduction method if one precursor is added after the other: the precursor of the metal that must form the core is added along with the stabilizing agent first. This is followed by the reducing agent. Once the complete reduction of the first metal is ensured, the second metal precursor is added: this can lead to the formation of core-shell structures. [77-80]

Considering that, for core-shell nanoparticles, the core will consist of the most noble metal, while the shell will be the least noble (Figure 21). For example, gold forms the core and silver forms the shell. If the opposite were done, first reducing Ag^+ to Ag to form the core, and subsequently adding Au^{3+} , the latter would oxidize the metallic silver that will dissolve; to avoid this problem you can proceed with the addition of an excess of strong oxidizing agents together with the more noble metal, but this does not always work and there are numerous complications to be taken into consideration. [81-84]

Among the top-down methods, the most used is laser ablation: a solid target, which in this case is a bimetallic alloy, is hit by a laser beam, allowing to obtain well dispersed bimetallic nanoparticles.

The most controllable top-down method is laser ablation. [85-89]

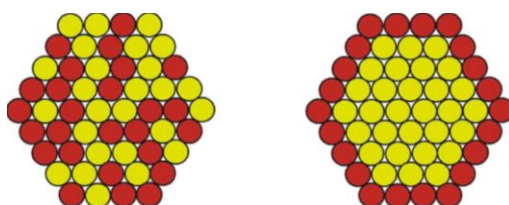
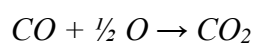


Figure 21: Alloy (left) and core shell (right) nanoparticles

1.4. Gold nanoparticles

1.4.1. Gold nanoparticles: main reactions

CO oxidation



Gold-based catalysts have a high activity for oxidation reactions. In particular, small nanoparticles, below 5 nm, are more active than larger ones. Among these reactions there is the oxidation of carbon monoxide [90], which allows to purify the combustion fumes by eliminating CO and breaking down the CO in the fuel cells. [91]

By varying the support, the activity of the catalyst varies: Au/Fe₂O₃ catalyst has the advantage of being active even at low temperatures (i.e. -76 ° C).

The mechanism of the reaction is not clear yet, but it has been hypothesized that oxidation occurs with a charge transfer from the electronic lacks present on the surface of the support towards the gold nanoparticles and that activates the metal in the oxidation reaction. [92]

Glycerol Oxidation

Gold-based catalysts are active, as evidenced by J. Hutchings and coworkers [93], for the selective oxidation of glycerol to glyceric acid in the presence of NaOH under stoichiometric conditions. Indeed, basic conditions are essential to obtain selective oxidation to glyceric acid and a high conversion of glycerol. They saw that with high concentration of NaOH, remarkably high selectivities to glyceric acid can be observed. The reaction is carried out at 60 ° C at a pressure of 3 bar. The support is based on carbon or graphite.

L. Prati and coworkers studied the oxidation reaction of glycerol using unsupported gold nanoparticles, stabilized in an aqueous environment by chelating agents, as a catalyst. The reaction was carried out at 50 ° C in the presence of a base. The catalysts showed a selectivity of 76% for the desired reaction [94] and a conversion of 90%. By varying the stabilizing agent, a variation in catalytic activity was observed: in particular, the catalysts in the presence of tetrakis(hydroxypropyl)phosphonium chloride (THPC) show a catalytic activity measured in terms of TOF 3 to 15 times greater than nanoparticles stabilized with sodium citrate or PVA. Using THPC and PVA as stabilizers, they were able to obtain nanoparticles of about 2 nm.

Glucose oxidation to glucaric acid

Prati and co-workers [95] studied the possibility of oxidizing glucose to glucaric acid with a catalyst based on gold nanoparticles, in order to replace Pt and Pd which give leaching phenomena, as mentioned above. They conducted the reaction under basic reaction conditions (pH = 7-9.5) and at moderate temperatures (50 ° C). For the first step of the reaction, from glucose to gluconic acid, they found a selectivity greater than 99%, without leaching phenomena.

They noted that basic conditions are required for this reaction: by raising the pH to 9.5, in fact, an increase in the initial velocity of the formation reaction of gluconic acid was observed.

1.4.2. Glucose oxidation: mechanism of reaction

There is no numerous information on the mechanism and stoichiometry of the oxidation reaction of gold with gold nanoparticles. Rossi and co-workers [96] in 2005 focused on their study and noted that, in this reaction, hydrogen peroxide is formed by a two-electron reduction of O_2 catalysed by gold. This occurs not only in the case of molecular hydrogen as a reducing agent, but also using more complex organic molecules as glucose, as reported in Figure 22.

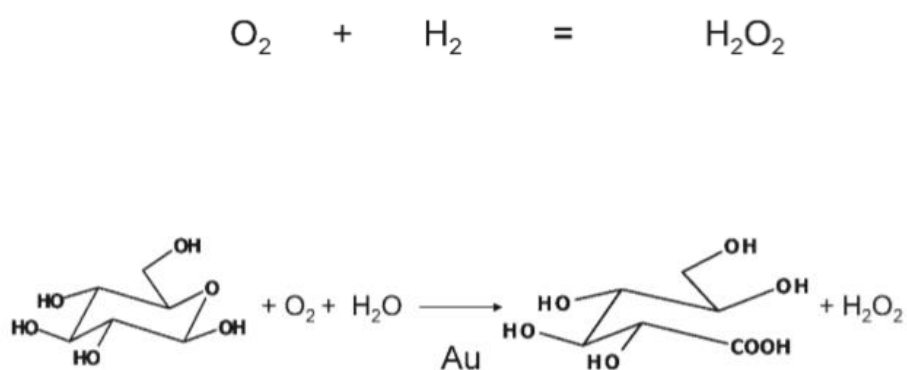


Figure 22: Mechanism of glucose oxidation studied by Rossi and co-workers [96]

In addition, the importance of a basic environment for this reaction was investigated. In particular, hydrated glucose anion, obtained by the reaction of glucose with OH^- , binds to the gold nanoparticle (Figure 23), forming electron-rich gold species. Molecular oxygen is activated by nucleophilic attack from the electron-rich Glucose-Au nanoparticle complex: a two-electron transfer occurs from the adsorbed glucose anion to the activated molecular oxygen. The discussion is valid if we consider it as dioxogold intermediate either $Au^+ - O_2^-$ or $Au^{2+} - O_2^{2-}$.

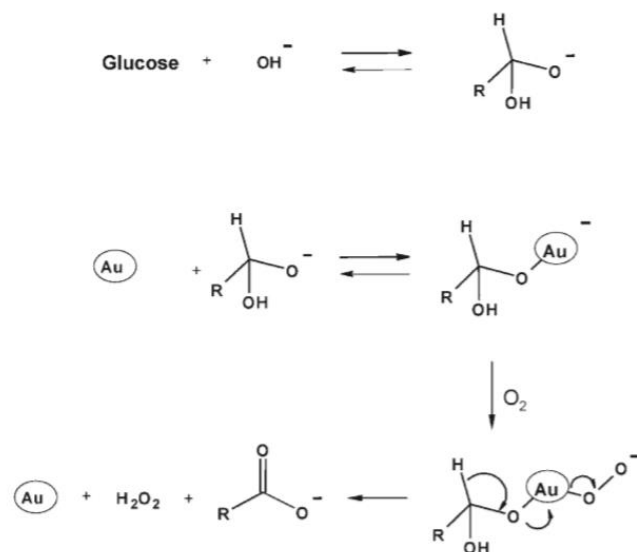


Figure 23: Proposed mechanism of oxidation of glucose by Rossi and co-workers [96]

Saliger and co-workers studied the oxidation reaction of glucose with gold nanoparticles under alkaline conditions, using both molecular oxygen and hydrogen peroxide as the oxidizing agent. [97] They saw that the two reactions with the two oxidizing agents have similar activation energies and comprise the same rate-determining step in the 30-60 °C temperature range. This has led to the imputation that the effective oxidizing agent is in both cases O_2 , which is obtained in the case of hydrogen peroxide from its decomposition.

1.5. Glucose oxidation: a computational point of view

1.5.1. Computational chemistry in heterogeneous catalysis

Computational chemistry developed only around the beginning of the twentieth century. The reason was lack of machines sufficiently powerful to perform simulations: the number of floating-point operations per second and the memory capacity are the most important parameters that determine the possibility of performing simulations in reasonable times. At the beginning of the 1960s, the advent of computational sciences in numerous sectors led to a real scientific revolution, producing significant technological innovations, changing the conception of science known up to that time. For these reasons only in the last years of the twentieth century computational chemistry has reached a great development. Computational has then joined experimental research allowing to understand the results obtained in the laboratory, comparing the measurements with the calculations; in some cases, it also allows predictions of results and to obtain additional information not accessible even with the most advanced experimental techniques.

In the field of heterogeneous catalysis, the synergy between computational and experimental chemistry has opened up a new approach for the study of catalytic systems: indeed, this cooperation has allowed us to understand reactive mechanisms of catalytic systems and the existence of preferred active sites for a large part of heterogeneous systems currently in use. [98,99]

Computational chemistry methods can be summarized in two main categories: methods based on quantum mechanics (QM) and those based on classical mechanics. The former allows to obtain information at the atomic and molecular level on the electronic structure of chemical systems, which is out of reach for methods based on classical mechanics. Consequently, a QM approach must be preferred for the study of heterogeneous catalysis processes, since it allows to determine the chemical reactivity of catalytic processes.

QM studies are based on the solution of the Schrödinger's equation [100]; however, this is impossible to solve exactly for multielectronic systems, and it requires involvement of several approximations that allow the treatment of the large number of particles present in a chemical system. Among the various QM methods developed so far, the "density functional theory" (DFT) [101] represents the main tool for the study of reactivity in catalytic system. This method,

based on the so-called “mono-determinant” approach, offers the great advantage of possessing good accuracy both for the calculation of structural and energy properties at a reasonable computational cost.

1.5.2. Mechanism of glucose oxidation

Ishimoto and co-workers computationally studied by DFT the oxidation mechanism of glucose to gluconic acid on Au catalyst in direct alkaline fuel cell. [102] They started from a cube-octahedral structure (i.e. a Au_{55} cluster) to model small gold nanoparticles and, since the oxidation reaction takes place under alkaline conditions, they decided to analyze the adsorption of a hydroxyl group (OH^-) on the gold cluster, comparing it with that of H_2O . From the results obtained in their study, it can be concluded that the adsorption of OH^- is favoured on the Au_{55} structure with cube-octahedral symmetry. Subsequently, they moved toward the study of the oxidation of the aldehyde group of glucose to carboxylic group, proposing two possible adsorption of glucose on the cube-octahedral Au_{55} structure: i) the direct adsorption of glucose on the Au surface or ii) the adsorption of glucose on top of an adsorbed OH^- group. It was found that the direct adsorption of glucose on Au surface is 13 kJ/mol favoured compared to that on the OH^- adsorbed on the cluster.

Considering a direct adsorption of glucose on the Au surface, two possible reaction mechanisms have been studied (see Figure 24): i) an H-transfer from the aldehyde group to the gold surface, and subsequently the attack of an adjacent surface OH^- group to the glucose aldehydic group; ii) an attack of the OH^- from the Au surface to the aldehyde group of glucose, followed by the H-transfer from the carboxylic group to the gold surface. Comparing the energetics of the two mechanisms it appears that the second is the favourite one. The rate determining step (RDS) turns out to be the transfer of OH^- from the gold surface to the aldehyde group of glucose, forming a tetrahedral intermediate.

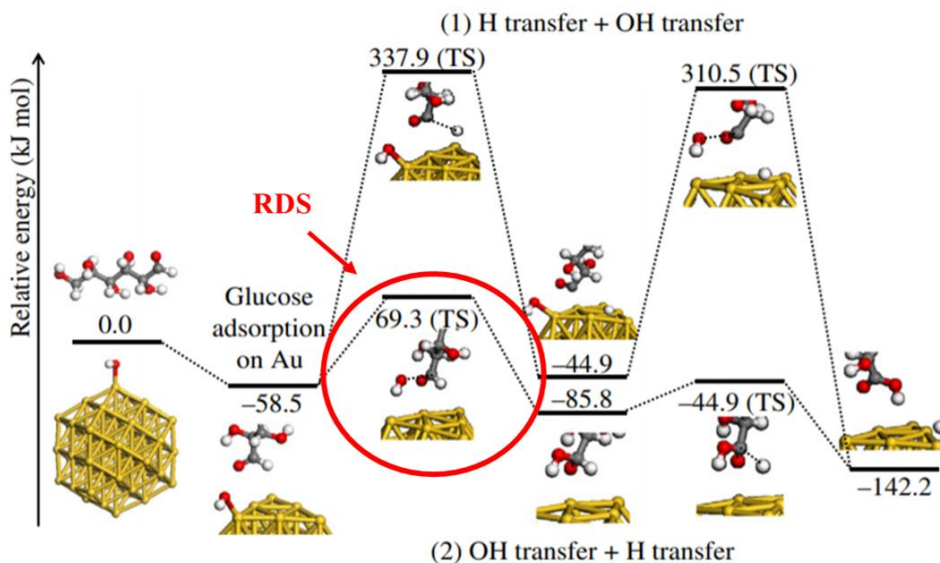


Figure 24: Reaction energy diagram of oxidation reaction assuming direct adsorption of glucose on Au surface [102]

In conclusion, Ishimoto *et al.* proposed a catalytic cycle summarized in Figure 25. First of all, glucose adsorbs on OH^- adsorbed on Au surface; OH^- in alkaline solution interacts with CHO group of glucose, forming water by proton transfer from CHO group to OH^- in aqueous phase. Gluconic acid is then formed by OH transfer from Au surface.

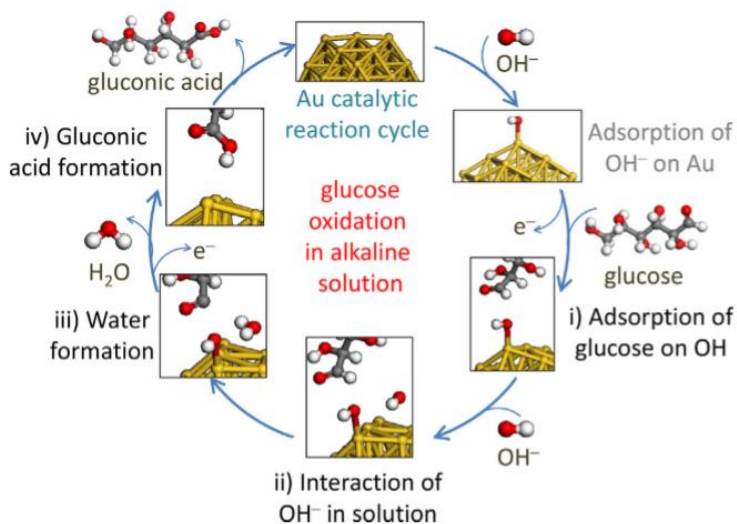


Figure 25: Proposed mechanism of glucose oxidation in alkaline solution [103]

2. Scope

It has been found that gold nanoparticle-based catalysts are stable and are reactive for oxidation reactions. For these reasons, in this work heterogeneous catalysts of gold nanoparticles supported on activated carbon were synthesized using the sol immobilization technique. Subsequently, the catalysts were characterized by various techniques, such as UV-VIS spectroscopy, X-ray diffraction and TEM, in order to evaluate the formation of gold nanoparticles and to know their average size.

The synthesized catalysts were then tested for the oxidation reaction of glucose to glucaric acid in liquid phase under basic conditions, using oxygen as an oxidizing agent. Three different batches of catalysts were tested in order to evaluate the reproducibility of the operator, both for the synthesis phase of the materials and for the reaction. The effect of the reaction time parameter was investigated by carrying out the reactions for 15 minutes, 1 hour and two hours.

It was decided to combine the experimental study with a computational one based on DFT. In particular, a modeling using Au₅₅ gold clusters (representing small nanoparticle) and Au(100) and Au(111) surface clusters, which are the main exposed surfaces present in (medium-size) gold nanoparticles, was performed. Subsequently, on the DFT optimized structures, the study of the adsorption of reactants and products of glucose oxidation was carried out, in particular: OH⁻, glucose and gluconic acid. The aim was to propose a method to approach from a computational point of view the study of nanoparticulate catalytic systems, studying the structure of the clusters and the adsorption of the various surface species.

3. Theoretical and experimental background

3.1. Experimental section

In this chapter it was reported:

- Materials and procedures for synthesis and characterization of catalysts
- Reaction scheme
- A description of the analytical techniques and the procedures used for data analysis.

In Table 1 all the reagents used for the synthesis of the catalysts, the glucose oxidation reaction and the HPLC calibration are reported.

Compound	Formula	Molecular weight (g/mol)	Purity
Activated carbon NORIT SX1G	Carbon	/	Information not provided
Arabinose	C ₅ H ₁₀ O ₅	150,13	>98%
Formic acid	CH ₂ O ₂	46,02	>95%
Fructose	C ₆ H ₁₂ O ₆	180,16	≥99%
Glyceric acid	C ₃ H ₆ O ₄	106,08	>97%
Glycolic acid	C ₂ H ₄ O ₃	76,05	99%
Glucose	C ₆ H ₁₂ O ₆	180,16	>99%
Gluconic acid	C ₆ H ₁₂ O ₇	196,16	97%
Glucaric acid	C ₆ H ₁₀ O ₈	210,14	98%
Lactic acid	C ₃ H ₆ O ₃	90,08	85%
Mannose	C ₆ H ₁₂ O ₆	180,16	99%
Mesoxalic acid	C ₃ H ₂ O ₅	118	98%
Oxalic acid	C ₂ H ₂ O ₄	90,03	>99%
Polyvinyl alcohol	(C ₂ H ₄ O) _n	13.000-23.000	87-89% hydrolyzed
Tartaric acid	C ₄ H ₆ O ₆	150,09	>99%
Tartronic acid	C ₃ H ₄ O ₅	120,06	>97%
Tetrachloroauric acid trihydrate	HAuCl ₄ *3H ₂ O	393,83	>99%
Sodium borohydride	NaBH ₄	37,83	≥98%
Sodium hydroxide	NaOH	39,99	>98%
2-keto-D-gluconic acid (2KDG)	C ₆ H ₁₀ O ₇	194	99%
5-keto-D-gluconic acid (5KDG)	C ₆ H ₁₀ O ₇	194	98%

Table 1: Reagents used for catalyst preparation, oxidation reaction of glucose, calibration curves for HPLC

3.1.1. Preparation of catalysts

Supported gold nanoparticle catalysts were prepared using the sol immobilization technique. All the catalysts were prepared in order to obtain a metal loading of 1 wt%.

A fresh aqueous solution of PVA was prepared. In details, the stabilizing agent, PVA (0,1010 g) was added and dissolved in 10 mL of distilled water using a flask. After that, the flask was placed on a plate at 60 ° C and was stirred for a period of 5 minutes. In the meantime, the gold metal precursor solution was prepared: 0,0209 g of $\text{HAuCl}_4 \cdot 3\text{H}_2\text{O}$ were dissolved in 385 mL of distilled water and the solution was stirred at room temperature. After that, 0,643 mL of the PVA aqueous solution previously prepared was added, keeping the solution stirred (PVA: Au = 0,65:1 weight ratio). After three minutes, the reducing agent NaBH_4 was added (0,0096 g in 2.5 mL of distilled water; NaBH_4 : Au = 5:1 molar ratio) and the solution immediately turned from yellow to dark red, indicating the formation of gold colloidal nanoparticles. After 30 minutes, the support was added, Activated Carbon (0,99 g) and the solution was acidified with sulphuric acid up to $\text{pH} = 2$ for enhancing the immobilisation of the gold colloidal nanoparticles onto the support. The slurry solution was left under stirring at room temperature for one hour. At this point the solution was filtered with a Buchner filter. The catalyst was washed with abundant distilled water (about 1 L) in order to remove the impurities, until the washing water had reached neutral pH. The catalyst was left to dry overnight at room temperature and subsequently dried in an oven for 4 hours at 80 ° C (Figure 26).

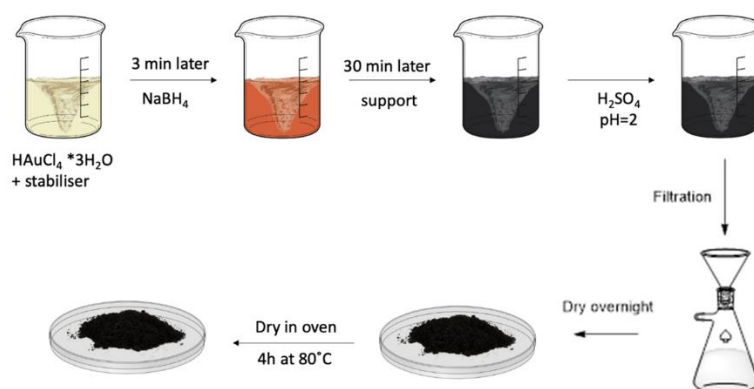


Figure 26: Preparation of catalyst with sol-immobilization technique

3.1.2. Characterization of catalysts

3.1.2.1. UV-VIS spectroscopy

UV-VIS spectroscopy is an analytical technique based on molecular absorption: when a molecule is hit by radiation with a wavelength between 200-400 nm (UV) or 400-800 nm (visible), it absorbs energy, leading to electronic transitions from a ground state to an excited one. In details, electron moves from a molecular orbital level to one of higher energy level, and this phenomenon is called electronic transitions. Therefore, for the transition to take place, the radiation must have a frequency comparable to or greater than the energy gap between the ground and the excited state. Beyond that, it is necessary to respect other criteria, the *selection rules*: the first says that "in an electronic transition there must be a strong redistribution of the charge and therefore a concrete variation of the dipolar moment ". The second, called *the rule of orbital symmetry*, states that " the total spin in a transition must be conserved".

With this technique it is therefore possible to perform analysis on different types of molecules that respect the selection rules, in particular: metals of block d, organic compounds containing a high number of conjugated double bonds and biological macromolecules (generally in the liquid phase).

Gold nanoparticles solution could be studied using this technique; indeed, the solutions of the metals of the d block are often colored due to electronic transitions of the d orbitals: these, degenerate, undergo an energetic separation when they are hit by a photon ($h\nu$).

UV-VIS spectroscopy permit also to perform quantitative analysis thanks to the Lambert-Beer law. In fact, when a monochromatic light beam with a specific intensity (I_0) hits a sample of thickness l in a medium, part of the radiation is absorbed by the sample and a part is reflected with residual intensity I_1 . The ratio between the reflected light and the incident light can be indicated as Transmittance T:

$$T = \frac{I_1}{I_0}$$

We can therefore define another quantity, the absorbance A, which is related to the transmittance by the following equation:

$$A = -\log \frac{T}{100}$$

For a solution, the Lambert-Beer law is:

$$A = l\epsilon_{\lambda}M$$

where ϵ_{λ} is the molar extinction coefficient, M the concentration of the solution and l the geometric path. The value of ϵ_{λ} is considered constant for a given substance at a given wavelength and for a given range of concentrations.

The spectrophotometer consists of:

- Energy source, which in this case is a Tungsten filament for the visible range (350 – 700 nm) and a Deuterium lamp for the UV range (190 – 400 nm);
- Monochromator, which has the aim to select the radiation in the range around the wavelength of interest;
- Cuvette, which contains the sample solution;
- Signal detector.

The spectrophotometer can be single beam or double beam (Figure 27): in the single beam, the radiation affects only the sample of interest; in the double beam one there is a sector rotating mirror (or chopper) which reflects the beam of the source, directing it alternately towards the reference and towards the sample. The reference beam intensity is taken as 0 absorbance and the ratio of the two beam intensities is displayed. The instrument used is a Perkin Elmer UV-VIS-NIR Lambda 19 with a double beam.

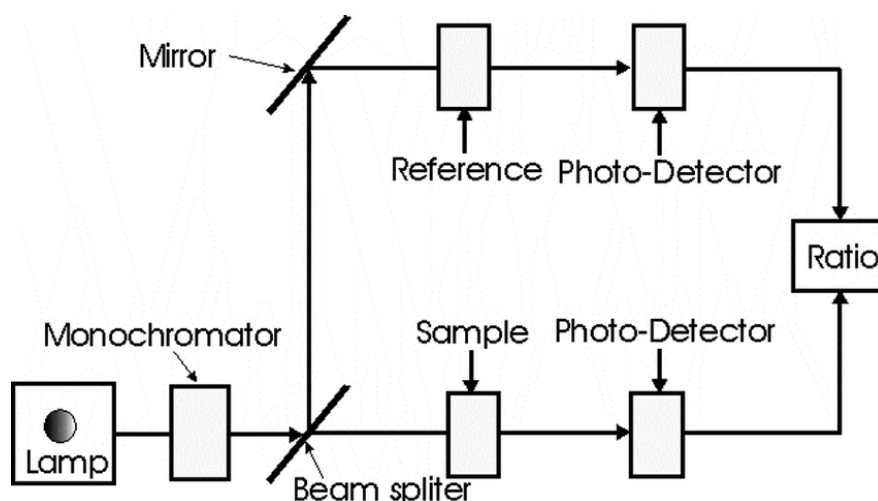


Figure 27: Double beam spectrophotometer operation diagram [104]

3.1.2.2. X-ray Diffraction (XRD)

X-ray diffraction is an analytical technique that allows the study of crystalline solids. It is based on the phenomenon of diffusion (or scattering): when an X-ray beam hits a sample, its electrons vibrate, so the radiation is diffused, propagating in different directions. Diffraction occurs from the coherent sum of all the radiations diffused by the atoms present in the same lattice planes, and therefore placed in an orderly manner (Figure 28). Moreover, X-ray waves have to be in phase with each other to have constructive interference. From the constructive interferences a reflection pattern is obtained with typical peaks (called *Bragg peaks*), dependent on the angle of incidence and the step of the crystal lattice. From this it is possible to derive Bragg's law, which is the condition for the phenomenon to take place. It can be expressed as:

$$n \lambda = 2 d \sin\theta$$

Where:

n = integer (diffraction order)

λ = wavelength of the x-rays

d = distance between adjacent planes in the lattice

θ = incident angle of the x-ray beam

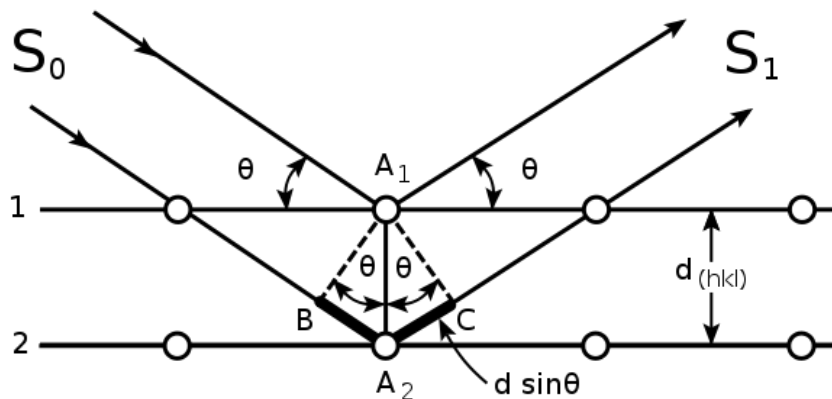


Figure 28: Bragg diffraction

It is possible to calculate the average size of gold nanoparticles applying the Scherrer Equation:

$$FWHM(2\theta) = \frac{K \lambda}{L \cos\theta}$$

FWHM = Full Width Half Maximum

λ = wavelength

L = crystallite size

K = the Scherrer constant

From this equation it can be noticed that the thickness of the peaks and the size of the crystal are inversely proportional: wider is the peak, smaller are the crystals.

The Scherrer constant k is the constant of proportionality, which depends on how the width, shape of the crystal and the size distribution are determined.

For this work, XRD analysis were performed with a Bragg-Brentano X'pertPro Panalytical diffractometer using a copper anode (K_{α} radiation at $\lambda = 1.5418 \text{ \AA}$) as source of X-radiation with $0,08^{\circ}$ step size and acquisition time of 1300 s per step in $36 - 41^{\circ} 2\theta$ range.

3.1.2.3. TEM (Transmission electron microscopy)

Transmission electron microscopy (TEM) is a high resolution technique for the characterization of nanometric materials. The instrument is composed by a source where an electron beam (generated by a tungsten filament) was created. After that, the beam passes through a section, where previously the vacuum was made, and then it crosses the sample. In this microscope there are systems capable of modifying the electromagnetic field, driving the electrons through magnetic lenses that widen the electron beam passed through the sample; in this way it is possible to obtain an enlarged image. The electron beam hits a fluorescent screen (sensitive to them) projecting on it a real and highly magnified image of the portion of the sample previously crossed. The sample must be very thin, with dimensions between 50 and 500 nm. It is placed on a copper or nickel mesh disk, generally with a diameter of 2,5 mm. The resolving power of the instrument is approximately 0,2 nm. This technique is very useful in order to calculate the average particle size, its standard deviation and particle size distribution by frequency (%). For each distribution, 300 to over 400 particles per sample are required in order to have an accurate result.

Analysis were performed using a TEM / STEM FEI TECNAI F20 microscope at 200 keV. Samples were suspended in ethanol and treated by ultrasound for 15 min. A drop of the suspension was deposited on "quantifoil-carbon film" supported by a grid of Cu. The preparation was dried at 120°.

3.1.3.Catalytic Testing-Oxidation reactions

3.1.3.1. Reactor

The oxidation reaction of glucose to glucaric acid was carried out in an autoclave batch reactor with a capacity of 50 mL. It consists of a lower part of a stainless steel container closed by a lid with a flanged joint. This part was connected to the upper one, where there was a loading and unloading line, each controlled by an interception valve, a pressure gauge and a steel cable capillary for the introduction of a thermocouple, so as not to put the thermocouple in direct contact with the solution in the reactor (Figure 29). The reactor was placed on a hot plate with magnetic stirrer in order to control temperature and stirring rate.

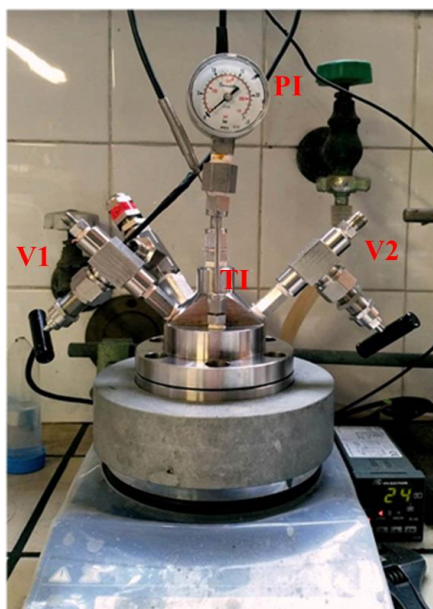


Figure 29: Photo of the batch reactor used in the oxidation of glucose

PI: Pressure gauge WIKA 315SS (0-25 bar)

V1: Valve for the load line

V2: Valve of discharge line

TI: Capillar tube for insertion of thermocouple

3.1.3.2. Preparation of the reaction solutions

Glucose oxidation

The reaction was prepared by measuring a total water volume of 15 mL. 0,7895 g of glucose and 0,0087 g of catalyst were weighed (the solution is 5% wt of glucose); a small volume of previously measured water (about 3-4 mL) was used to pour the glucose and the 1% wt gold nanoparticle catalyst into the reactor vessel (Au: glucose molar ratio of 1: 1000); the remaining water was used to dissolve the weighted NaOH (0,5259 g, molar ratio glucose: NaOH = 3:1) and to transfer this solution into the reactor vessel. A magnetic stir bar was added together with the reagents and catalyst. At this point, the reactor was carefully closed with bolts, it was then purged three times with oxygen and finally pressurized with 10 bar of O₂.

Then the reactor was placed in a heating mantle and the thermocouple was inserted in the appropriate conduit.

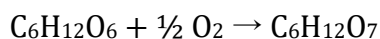
The reaction was carried out at 60 °C with a stirring of 1000 rpm for one hour (the time is measured from the moment in which the thermocouple marks the temperature of 60 °C).

At the end of the reaction the reactor was placed in an ice bath for about ten minutes to reach temperature below 10 °C, venting the unreacted oxygen and any by-products.

Oxidation using gluconic acid as reagent

To understand better the reaction pathways and reaction network and to evaluate which molecule of glucose, gluconic acid and glucaric acid adsorbs more strongly on the catalyst, leading to the blocking of the sites and therefore to a decrease in activity, it was decided to study the oxidation reaction starting from gluconic acid.

The grams of gluconic acid to be weighed were calculated considering as all the glucose had converted into gluconic acid.



Considering the weighted grams of glucose in the preparation of the previous reaction, the grams of gluconic to be measured were calculated considering a commercial solution at 50% by weight:

$$n_{\text{glucose}} = \frac{0,7895 \text{ g}}{\text{PM glucose}} = 0,00438 \text{ mol}$$

$$g_{\text{gluconic acid solution}} = 0,00438 * \text{PM gluconic acid} * 2 = 1,7193 \text{ g}$$

The reaction was prepared by measuring a total water volume of 15 mL. 1,7193 g of gluconic acid solution and 0,0087 g of catalyst were weighted; a small volume of previously measured water was used to pour the gluconic acid and the 1% wt gold nanoparticle catalyst into the reactor vessel; the remaining water was used to dissolve the NaOH and transfer this solution into the reactor vessel. The reaction was then carried out according to the same procedure at 60°C for reaction times of 15 minutes, 1 hour and two hours, to evaluate its progress as the time changed.

3.1.4. Sample treatment

The solution obtained after the reaction is collected and centrifuged at 4500 rpm for 15 minutes in order to separate the catalyst from the liquid. The solution is then poured into a cylinder, its final volume is measured, and finally it is filtered with a PTFE filter; after that, the liquid has been analysed through HPLC and the catalyst used is left to dry overnight in ambient conditions and stored.

3.1.5. Analysis of products

The quantitative analysis on the products obtained were carried out using the High-Performance Liquid Chromatography (HPLC) technique.

3.1.5.1. HPLC (High-performance liquid chromatography)

Quantitative analysis on the products obtained were carried out using the High Performance Liquid Chromatography (HPLC) technique.

HPLC is an evolution of classic normal column chromatography. The column consists of a stationary phase, placed inside it, and a mobile phase, which flows through the entire column. It is possible to separate two or more components present by exploiting the different affinities with the two phases: for example, if a substance is more similar to the stationary phase than another molecule, it will take longer to travel through the column. The time necessary to a substance to pass through the column is called retention time and it can depend on the column nature, the eluent used during the analysis, the characteristic of the molecule and the parameter (P, T) settled in the analysis.

The analysis is performed by injecting a small volume of the sample at the beginning of the column into the eluent stream; then it is carried on through the stationary phase by the mobile phase by means of pressures of the order of hundreds of atmospheres. Such a high pressure is necessary because the filling particles of the column have very small dimensions (with diameters from 3 to 10 μm) in order to have a high separation efficiency. The column packings used in liquid chromatography could be silica gel, charcoal and alumina. This kind of columns have an efficiency about 10,000 plates per column. Once the components have been separated and come out of the column, they are analysed by a detector, which can be Refractive Index detector (RI), UV-VIS, spectrofluorimetric, etc. In particular, organic compounds that possess double bonds, aromatic compounds and similar functional groups can be detected by UV radiation at different wavelengths; moreover, quantification analysis could be done correlating the amount of absorbed light with the amount of the compound. The RI detector, on the other hand, allows the detection of compounds which cause a difference in RI between the compound of interest and the mobile phase. In our case, at the end of the column, both a UV-VIS and an RI are present as detectors.

One of the advantages of this technique is that the column has small dimensions, typically 10 - 25 cm long and 4,6 mm in internal diameter. Usually the column is made of stainless steel.

The reaction mixture quantitative analyses were carried out using an Agilent 1260 Infinity Quaternary HPLC system (Figure 30). Analyses were performed using 0,0025 M sulphuric acid in ultra-pure water as eluent with a flow of 0,5 ml/min. The injection system consisted of a six-way valve with an injection volume of 20 μl . Two Rezex ROA-H+ (8%) 300x7,8 mm ion exclusion columns connected in series were used for the separation of products. A diode array detector (DAD) set to 202 nm was used to detect organic acids and a refractive index detector

(RID) was used to detect monosaccharides. The column compartment was thermostated at 80°C while the RID was kept at a constant temperature of 40°C.



Figure 30: HPLC instrument used for these analysis of the reaction mixtures

3.1.5.2. Calculation of reaction products concentration

The calibration curves were carried out by analysing with HPLC the concentrated and diluted solutions (1: 2, 1:10 and 1:20) of the glucose (reagent) and of all the main reaction products: gluconic acid, glucaric acid, glycolic acid, tartronic acid, tartaric acid, oxalic acid, lactic acid, 2-keto-D-gluconic acid, 5-keto-D-gluconic acid, fructose, mannose, arabinose, formic acid, acid glyceric and mesoxalic acid. The analysis was done keeping the same method use to analyse the reaction liquid reported in the previous part. The response factor (f_i) was achieved from the slope of the calibration curve obtained correlating the area and the concentration of the standard solution.

To calculate the moles of each component, the area of the corresponding peak of the chromatogram was divided by the response factor:

$$n_i = \frac{A_i}{f_i} * \frac{V}{1000}$$

n_i = number of moles of compound i

f_i = response factor of the compound i

A_i = area of the peak corresponding to the compound i

V = volume of the reaction mixture

In the case of gluconic acid and glucose, the situation is more complex: the peaks in the RID chromatogram are in fact overlapped. In order to quantify this two product, it has been assumed that the DAD signal of glucose was considered negligible; consequently, the quantity of glucose can be calculated by subtracting the concentration of gluconic acid (GO) obtained at the DAD from the total GO + glucose concentration obtained at the RID.

The moles of glucose are therefore obtainable from the following equation:

$$n_{glucose} = \frac{A_{RID\ GO+GLU} - \frac{A_{DAD\ GO}}{f_{DAD\ GO}} * f_{RID\ GO}}{f_{RID\ GLU}} * \frac{V}{1000}$$

$n_{glucose}$ = moles of glucose

$A_{RID\ GO+GLU}$ = Area of the peak in RID chromatogram related to gluconic acid and glucose

$A_{DAD\ GO}$ = Area of the peak in DAD chromatogram related to gluconic acid

$f_{DAD\ GO}$ = response factor of gluconic acid in DAD

$f_{RID\ GO}$ = response factor of gluconic acid in RID

$f_{RID\ GLU}$ = response factor of glucose in RID

V = volume of the reaction mixture

Similar problem of peak overlap occurs for glyceric acid and arabinose; in this case, however, we proceeded differently as there was no proportion between the theoretical sum of single areas and the area of GC peaks. Because of the two response factor compounds are similar, an average response factor was calculated:

$$C_{\text{glyceric acid+arabinose}} = \frac{A_{\text{RID glyceric acid+arabinose}}}{\frac{f_{\text{arabinose}} + f_{\text{glyceric acid}}}{2}} * \frac{V}{1000}$$

$C_{\text{glyceric acid+arabinose}}$ = Concentration of glyceric acid and arabinose in the solution

f = response factor

V = volume of the reaction mixture

$A_{\text{RID glyceric acid+arabinose}}$ = the peak's area corresponding to glyceric acid and arabinose

The glucose conversion is calculated according to the definition:

$$X = \frac{n_{\text{glucose}(t=0)} - n_{\text{glucose}(t=f)}}{n_{\text{glucose}(t=0)}} * 100$$

X = glucose conversion

$n_{\text{glucose}(t=0)}$ = initial number of moles of glucose

$n_{\text{glucose}(t=f)}$ = final number of moles of glucose

The yield of the various products was instead calculated by dividing the moles of the product generated by the initial moles of reagent; the value has been corrected with the C_f factor, which considered the ratio between carbon atoms of the product molecule to the carbons of glucose:

$$Y_i = \frac{n_i * C_f}{n_{\text{glucose}(t=0)}} * \frac{V}{1000} * 100$$

$$C_f = \frac{\text{atoms of Carbon in the molecule of the product}}{\text{atoms of Carbon in glucose}}$$

Y_i = yield of the product i

n_i = number of moles of the product i

$n_{\text{glucose}(t=0)}$ = initial number of moles of glucose

V = volume of the reaction mixture

C_f = normalization factor for carbon atoms based on the substrate

In the end, the selectivity for given compound i is calculated by dividing the yield of that compound i by the glucose conversion:

$$S_i = \frac{Y_i}{X_i} * 100$$

The sum of the selectivities of all products i represents the carbon balance.

$$C_{balance} = \sum S_i$$

3.2. Computational studies of glucose oxidation

In this work we optimized Au₅₅ clusters and Au(111) and Au(100) surfaces using the DFT theory [101]. The set of programs Gaussian16 [105] was used with the functionals B3LYP and BP86 [101,106,107], in order to compare the results obtained. Subsequently, the adsorptions of OH⁻, glucose, and gluconic acid were studied.

For the atoms of the adsorbates (H, C and O) the basis set 6-31** was used [108,109]; for gold clusters the Stuttgart effective core potential has been used to model the scalar relativistic effects [109]. In the following subsections, an overview of the methodology used is provided.

3.2.1. Fundamental of quantum mechanics

In 1900 Planck [110] proposed that the black-body radiation emitted by microscopic particles, such as electrons, was limited to discrete energies (levels). This phenomenon cannot be explained with classical mechanics, which is why there are discrepancies between classical models and experimental results. As initially proposed by de Broglie [111], microscopic particles can have properties similar to waves, which are quantized phenomena, but they also have properties of matter. This opens the concept of quantum mechanics, whose fundamental postulate is that an appropriate operator acts on the wave function, which exists for every chemical system, returning observable properties of the system. It is possible to write the fundamental equation of quantum mechanics, the *Schrödinger equation*, limiting to the non-relativistic cases and in a time-independent form as:

$$\hat{H}\psi = E\psi \quad (3.1)$$

where \hat{H} is the Hamiltonian operator describing all the interactions among the particles in the system, ψ is the system wave function and E the energy associated to the state wave function ψ . The wave function ψ is a complex-valued “probability amplitude”, with a non-trivial classical interpretation, while the product of the wave function by its complex conjugate $\psi^* \psi$ corresponds to a “probability of density”, that is the probability that a (chemical) system is found in some regions of the multi-dimensional space. The normalized integral of $|\psi|^2$ over all the space must then be one (*normalization*).

The Hamiltonian operator for a molecule (i.e. a many-body nuclei-electron problem) can be written as:

$$H = - \sum_i \frac{\hbar^2}{2m_e} \nabla_i^2 - \sum_k \frac{\hbar^2}{2m_k} \nabla_k^2 - \sum_i \sum_k \frac{e^2 Z_k}{r_{ik}} + \sum_{i<j} \frac{e^2}{r_{ij}} + \sum_{k<l} \frac{e^2 Z_k Z_l}{r_{kl}} \quad (3.2)$$

where i and j correspond to electrons, k and l to nuclei, \hbar is the Planck constant divided by 2π , ∇^2 is the Laplacian operator, m_e is the mass of the electron, m_k the mass of the nuclei k , Z the atomic number, e is the charge on the electron, r_{xy} the distance between particles x and y .

As we can see in the expression of the Hamiltonian, there is a correlation between the various particles, they do not move independently of each other. To simplify this problem, the *Born-Oppenheimer* approximation can be used: it is based on the fact that nuclei of molecular systems move much slower than electrons (neutrons and protons are about 1800 times heavier than electrons and mass is in the denominator in the kinetic energy formula), hence it is possible to consider the nuclei as fixed. It is therefore convenient to decouple the two motions and calculate the electronic energies for fixed positions of the nuclei. For fixed nuclei positions (i.e. at a given molecular geometry), obviously, the term of the kinetic energy of the nuclei is zeroed, while the term of the nucleus-nucleus repulsive potential energy becomes a constant.

The Schrödinger equation therefore becomes:

$$(H_{el} + V_N) \Psi_{el}(q_i; q_k) = E_{el} \Psi_{el}(q_i; q_k) \quad (3.3)$$

V_N is the core-core repulsive energy, constant for a set of nuclear coordinates. The electronic coordinates q_i is independent from those of the nuclei q_k . The system wave function ψ is reduced to an electronic wave function (Ψ_{el}) while the resulting energy E_{el} is the energy of a given electronic state, i.e. the "electronic energy".

3.2.2. DFT theory

The key ingredients to obtain the energy of the multi-electronic system are thus the Hamiltonian operator and the electronic wave function. In contrast with "wave function methods", where the electronic wave function is explicitly adopted to construct the Hamiltonian, the electron density ρ can be used instead within the framework of the density functional theory, namely DFT. Indeed, since the Hamiltonian only depends on the positions and atomic numbers of the nuclei

and the total number of electrons, the electron density is a good physical observable to construct it. In fact, the electron density, integrated over all space, gives the total number of electrons N :

$$N = \int \rho(\mathbf{r}) d\mathbf{r} \quad (3.4)$$

and positions of the nuclei (if approximated to point charges) obviously correspond to local maxima in the electron density.

The DFT formalism development initiated in 1927, when Thomas and Fermi [112] [113] introduced the first approximations to calculate a system energy using the electron density. They divided total energy in potential and kinetic and then derived the kinetic energy of an infinite number of electrons that move in an infinite volume of space with uniform positive charge, called uniform electronic gas. Kinetic energy, thus, is a function of the density, while the density itself is a function of the three-dimensional spatial coordinates. Kinetic energy operator, hence, is a density functional.

In 1964, Hohenberg and Kohn set the DFT formalism foundation with two fundamental theorems. In the first one, i.e. “*Hohenberg-Kohn Existence Theorem*”, they establish the dependence of the energy on the electron density. The electrons interact with one another and with an ‘external potential’, and they showed that the ground-state electron density must determine such external potential, and thus the Hamiltonian and the wave function, hence the energy of the system. With the second theorem (i.e. the ‘*Variational Theorem*’) they also found a way to predict such density of a system by invoking the variational principle. Still, the two theorems do not provide a way to compute the energy without recourse to the wave function since one has to rely on the Hamiltonian and on the wave function determined by the electron density. In 1965, Kohn and Sham solved this issue introducing the Kohn–Sham (KS) self-consistent field (SCF) methodology that simplified the main difficulties deriving from the electron–electron interaction term in the correct Hamiltonian by starting from a system of non-interacting electrons. So they used a Hamiltonian of non-interacting electrons, where the overall ground-state density is the same density as some real system where the electrons interact. Next, they divided the energy functional into specific components that facilitate further analysis while adding correction terms due to the missing contributions:

$$E[\rho(\mathbf{r})] = T_{\text{ni}}[\rho(\mathbf{r})] + V_{\text{ne}}[\rho(\mathbf{r})] + V_{\text{ee}}[\rho(\mathbf{r})] + \Delta T[\rho(\mathbf{r})] + \Delta V_{\text{ee}}[\rho(\mathbf{r})] \quad (3.5)$$

The first three terms of the right-hand side, in fact, refer to, respectively, the kinetic energy of the non-interacting electrons, the nuclear–electron interaction and the classical electron–electron repulsion, while the last two terms represent, respectively, the correction to the kinetic energy deriving from the interacting nature of the electrons and all non-classical corrections to the electron–electron repulsion energy. The ‘correction’, problematic terms $\Delta T[\rho(r)]$ and $\Delta V_{ee}[\rho(r)]$ are generally grouped together into the term E_{XC} , the *exchange-correlation energy*. This term includes not only the QM effects of exchange and correlation, but also the correction for the classic self-interaction energy and the difference in kinetic energy between the real and the fictitious (non-interacting electrons) system. This E_{XC} terms become the target of interest for developing new and more accurate density functional methods, since DFT represents an exact theory that must be resolved approximatively due to the unknown exact form of the exchange-correlation operator. In the Kohn-Sham (KS) approach, thus, the many-body problem is solved by finding the orbitals ϕ_i that minimizes the energy $E[\rho(r)]$ and thus satisfies the pseudo eigenvalue equation:

$$\left[-\frac{1}{2}\nabla_i^2 - \sum_j^{nuclei} \frac{Z_j}{|r_i-r_j|} + \int \frac{\rho(r)}{|r_i-r|} d\mathbf{r} + \frac{\delta E_{XC}}{\delta \rho} \right] \phi_i(\vec{r}) = \epsilon_i \phi_i(\vec{r}) \quad (3.6)$$

where the Hamiltonian is represented by the KS one-electron operator. The KS process, thus, must be carried out as an iterative SCF procedure quite similar to that employed in other QM methods based on the Hartree-Fock (HF) theory.

The E_{XC} dependence from electron density $\rho(r)$ can be expressed as:

$$E_{XC} = \int \rho(r) \epsilon_{XC}[\rho(r)] dr \quad (3.7)$$

where ϵ_{XC} is the energy (per particle) density and is dependent on the electron (per unit volume) density. It can also be expressed as the sum of exchange and correlation contributions:

$$\epsilon_{XC}[\rho] = \epsilon_X[\rho] + \epsilon_C[\rho] \quad (3.8)$$

Historically, the first approximation to the ϵ_{xc} is based on the ‘Local Density Approximation’ (LDA), which considers the real system as the sum of (“local”) infinitesimal space volumes with uniform electron density, such as in an uniform electron gas. LDA can be extended to the spin-polarized regime (LSDA) to include spin polarization in open-shell systems. However, since the electron density of a molecular system is not spatially uniform, it has been subsequently introduced the more accurate “Generalized Gradient Approximation” (GGA), in which the E_{xc} depends also on the gradient of the density $\nabla\rho(r)$. This contribution can be added as correction term to the LDA functional expression as

$$\epsilon_{x/c}^{GGA}[\rho(r)] = \epsilon_{x/c}^{LDA}[\rho(r)] + \Delta\epsilon_{x/c} \left[\frac{|\nabla\rho(r)|}{\rho^{3/4}(r)} \right] \quad (3.9)$$

3.2.3. The functionals

GGA functionals can be, for instance, of the ‘hybrid’ or the ‘pure’ types depending on the inclusion of HF exchanges terms or not, respectively. In this work, we adopted a pure GGA functional such as the BP86 one, composed by the Becke [114] exchange functional and the Perdew [115] correlation functional. Alternatively, we used the B3LYP functional, [101,106,107] a GGA functional defined as:

$$E_{xc}^{B3LYP} = (1 - a)E_x^{LSDA} + a E_x^{HF} + b\Delta E_x^B + (1-c) E_c^{LSDA} + c E_c^{LYP} \quad (3.10)$$

where $a = 0,218$, $b = 0,709$ and $c = 0,129$.

B3LYP is a hybrid functional, because it includes both HF and DFT exchange (E_x) terms. Indeed, experience tells us that the GGA functionals have a sort of systematic error. For instance, they tend to overestimate the barrier heights to chemical reactions; HF theory, on the other hand, tends to underestimate it. For this reason, it is common practice to add HF exchange to ‘pure’ DFT results as something of a back-titration to accuracy. In particular, for the functional B3LYP there is a 23,5% of HF exchange energy and a 76,5% of GGA.

3.2.4. Basis sets

As for other QM methods, such as HF, the orbitals needed to solve the KS process and minimize the (SCF) energy can be constructed as linear combination of atomic orbitals, where atomic orbitals are built using a basis set of mathematical functions. Slater-type orbital (STO) functions reproduce quite well the behaviour of atomic orbitals but are quite difficult to treat computationally. On the other hand, Gaussian-type orbitals (GTOs) have a good computation efficiency, but they have limitations in describing orbital functions, in particular for the radial part. For this reason, most of the basis sets use linear combination of GTOs to reproduce as much as possible STO functions:

$$\phi(x, y, z; \{\alpha\}, i, j, k) = \sum_{a=1}^M c_a \varphi(x, y, z; \alpha_a, i, j, k) \quad (3.11)$$

where M is the number of Gaussian used in the linear combination, and c is a coefficient used to optimize the shape of the basis functions and normalize them.

A basis function defined as the linear combination of Gaussians is a “contracted basis function”, where each Gaussian is called “primitive Gaussian”. The grade of contraction indicates the total number of primitives used for the contracted basis functions. In 1969 Hehre, Stewart and Pople constructed several basis sets with different M .

In this work we used the 6-31G**(d,p) [107] for carbon, hydrogen and oxygen. 6-31G is a split-valence basis set [108] of Pople and al. This means that the core orbitals are represented with a single base function contracted, while the valence orbitals are split into several arbitral functions. The nomenclature is a guide of the contraction scheme. The first number (in this case ‘6’) represents the number of primitives used in the contracted functions of core. The number after the hyphen indicates the number of primitives used for the valence functions. In this case there are two numbers, ‘31’. It means that it is a valence-double- ζ basis.

Split-valence sets use basis functions sp-type, with common exponents. Pople and his co-workers chose the exponents and coefficients of the contracted functions based on variational principle. Coefficients and exponents are optimized to find the minimal energy. The “**” indicate that these are “polarization functions”, which include angular momenta higher than those in the valence orbitals of each atom. They "embrace" the flexibility of atoms to form bonds in any direction.

3.2.5. Effective Core Potentials

Using all-electron basis sets, i.e. treating all electrons of each atom by a given basis set, might be computationally unaffordable for heavy atoms. Effective Core Potentials (ECP) [109] are a linear combination of specially designed Gaussian functions that can model the core electrons. They have been introduced to replace core electrons with an effective potential which is added to a Hamiltonian and can be used in combination with standard basis set for the (non-core) remaining electrons of a given atom. They have been employed in our study to describe the gold atoms. Their main functions are two: one is to decrease the computational cost of our calculation: the ECPs, in fact, allow us to describe with an effective potential the electrons closest to the nucleus and therefore less reactive from a chemical point of view, while the outermost (and therefore most interesting) electrons are explicitly described. The second is to best describe the relativistic effects, strongly present for heavy and transition metals. Figure 31 [108] describes the ECPs: core electrons are modeled with an effective potential while valence electrons are described by basis set functions.

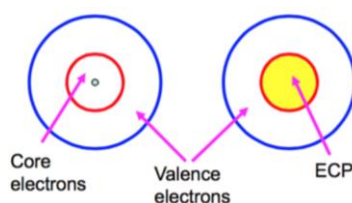


Figure 31: Scheme to describe the ECP idea [109]

Possible disadvantages should be considered: if the core considered is too large, the system will be poorly described by the ECPs, since they do not consider polarization and core relaxation; so, a reasoned choice of the core size must be made. Furthermore, errors due to the core-valence overlap must be considered. In this work, we use Stuttgart ECP to model the scalar relativistic effect and to allow reproducing experimental observables of a single atom, such as ionization potentials and excitation energies.

4. Results and discussion

4.1. Experimental results

4.1.1. Synthesis and characterization of materials



Figure 32: On the left: solution of the gold precursor; on the right: solution of gold nanoparticles

The catalysts were prepared with the sol-immobilization method described in Chapter 3. Figure 32 shows the gold precursor solution and the solution with the colloidal system. The solution of the precursor, extremely diluted, appears with a pale yellow colour; following the addition of the reductant (NaBH_4), the solution immediately changes to a bright "wine red" colour, indicating the successful formation of small gold nanoparticles, which typically have this shade. Subsequently, the addition of support (Active Carbon) during the immobilization phase do not permit to observe any shade changing because of the black colour of the solid.

4.1.1.1. *Uv-Vis analysis*

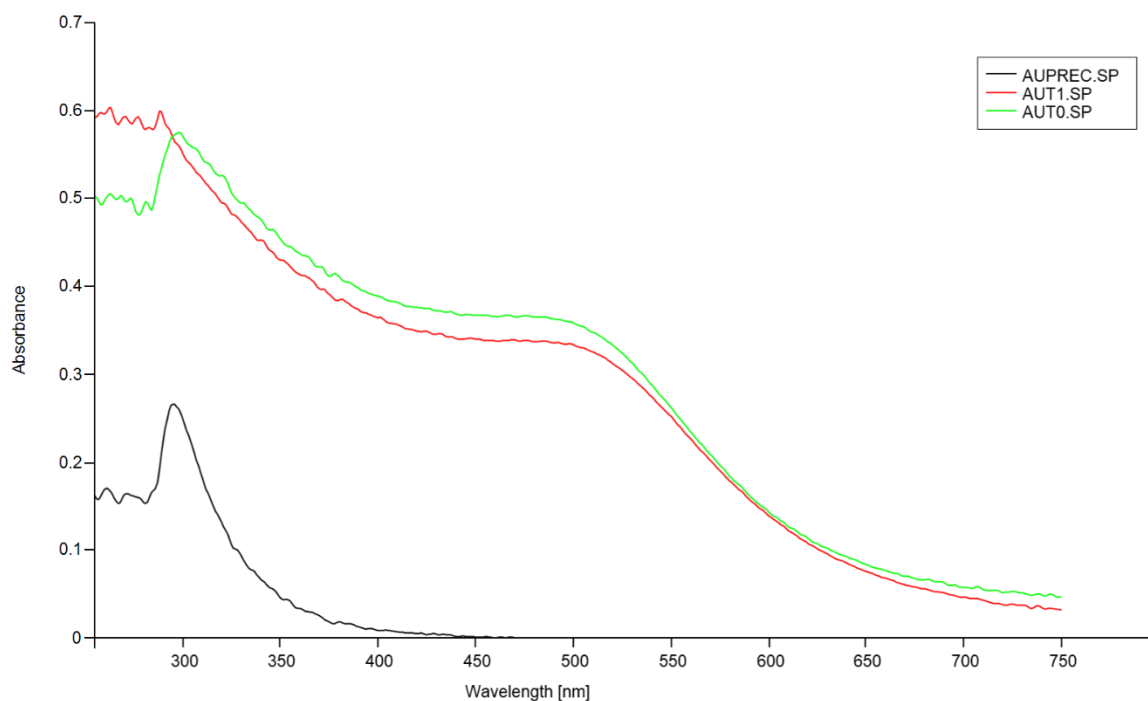


Figure 33: UV-VIS spectra of gold precursor and gold nanoparticles after 3 and 25 minutes from the addition of NaBH₄

In the Figure 33, it was reported the UV-Vis spectra related all the catalyst synthesis steps: the gold precursor solution, the solutions after 3 and 25 minutes from the addition of the reducing agent NaBH₄.

Regarding the spectrum of the gold precursor there is a peak at 300 nm due to the hydrolysed complexes of gold. Instead the two spectra at $t = 0$ (after 3 minutes from the addition of NaBH₄) and at $t = 1$ (after 25 minutes after the addition of NaBH₄) show a peak at 502 nm, due to the surface plasmon resonance of the nanoparticles of gold. Since the spectra are very similar, it is not possible to estimate properly a dimension enlargement, but it can be deduced that the size of the nanoparticles does not vary significantly from $t = 0$ to $t = 1$.

4.1.1.2. XRD analysis

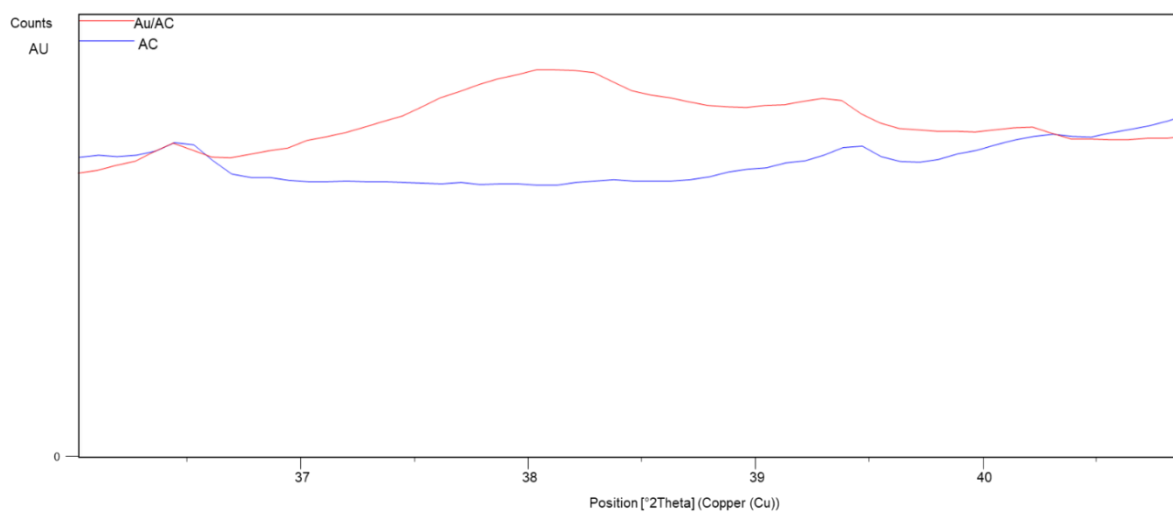


Figure 34: XRD pattern of Au/AC catalyst prepared and of the support (AC)

As it was showed in the previous session, the UV analysis could give information about the nanoparticles dimension in the colloidal solution, and the spectra analysed confirm the presence of small nanoparticles. However, the immobilization step and the interaction with the support could affect the final diameter of Au NPs and this is why XRD analysis was performed on the final catalyst. Figure 34 shows the XRD patterns of the support (AC) and of the catalyst after the immobilization and post-treatment phase. For the XRD pattern of the catalyst, the peak at 38.2 must be highlighted, which is the one with the greatest intensity. Through the Scherrer equation, considering the crystallites as spherical, their size was estimated using the Au(111) plane at 38.2 ° 2θ (Table 2).

Catalyst	Average crystallite size (nm)
Au/AC PVA0,6	3,1

Table 2: Average crystallite size calculated with Scherrer equation

4.1.1.3. TEM analysis

TEM analysis were performed to establish the nanoparticle size of the synthesized catalysts.

Over 400 nanoparticles were considered in order to obtain a representative model for the analysis. From Figure 35, it can be seen that the nanoparticles synthesized possess small diameter, excepted for some larger nanoparticles, obtained by agglomeration of some of them: the average size of the nanoparticles is 2,43 nm (Figure 36).

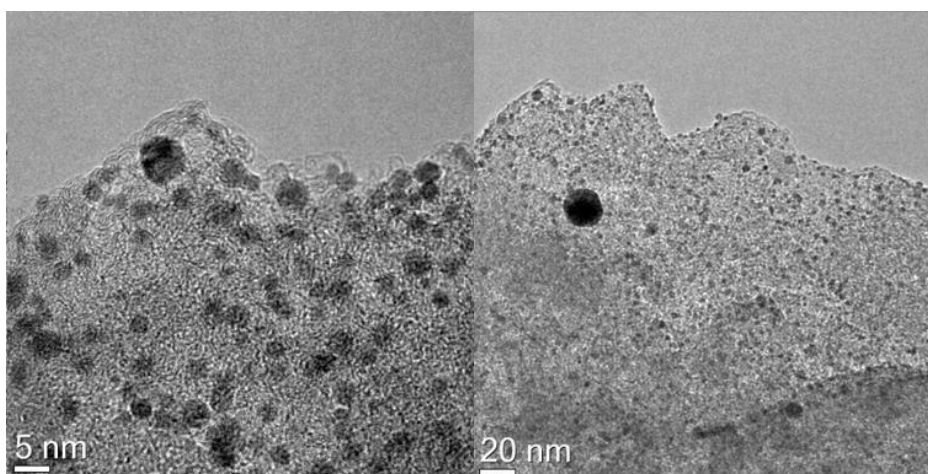


Figure 35: TEM images of Au/AC catalyst prepared

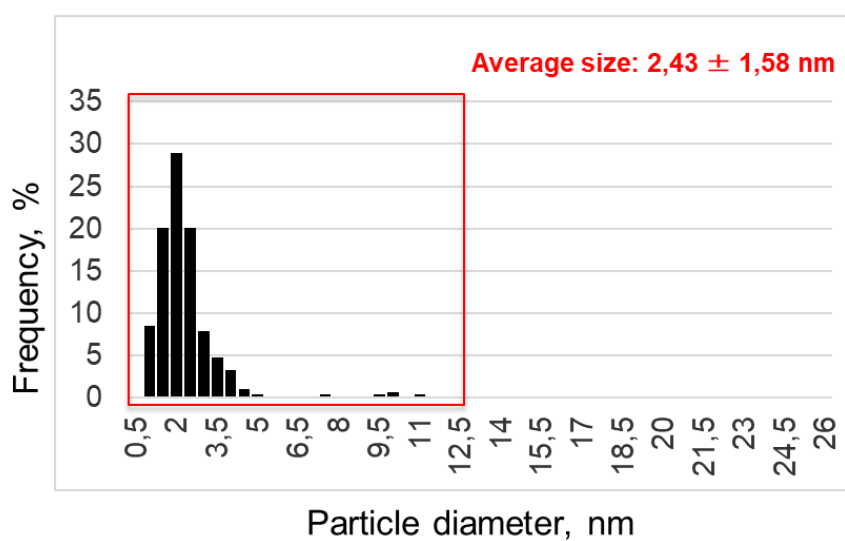


Figure 36: Particle size distribution of the Au/AC catalyst prepared

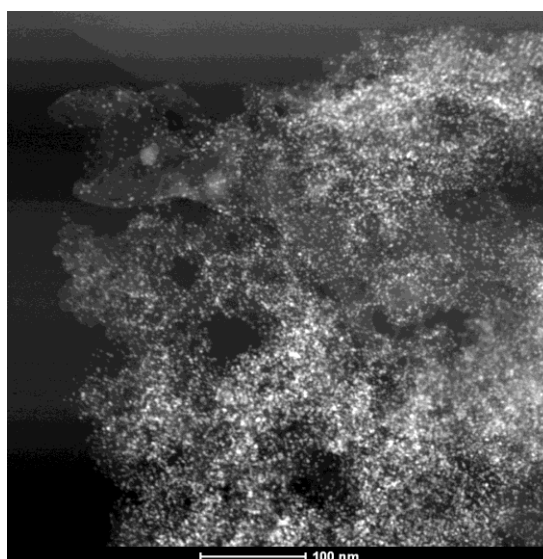
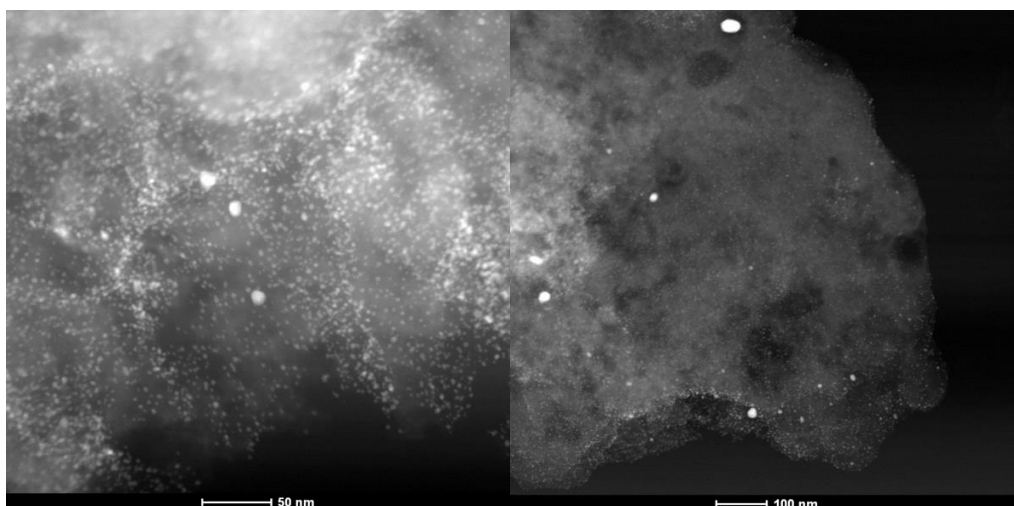


Figure 37: STEM-HAADF images of Au/AC catalyst prepared

In Figure 37 the images obtained from the scanning transmission electron microscopy analysis (STEM) are reported. This technique has the advantage of allowing to obtain sharp images that allow to clearly distinguish the nanoparticles from the support with a strong colour contrast. STEM, in fact, focuses an electron beam on a point and scans it on the sample to be analysed; the scattered electrons are then collected by the HAADF detector: this is very sensitive to the differences in the atomic number (Z) of the irradiated elements, where heavier atoms look

brighter than lighter ones. From the STEM-HAADF image at 100 nm it is possible to see that the nanoparticles are well dispersed, thanks to the presence of the stabilizer agent, except in areas where agglomerations can be found; however, STEM confirms the presence of agglomeration zones leading to larger particles (up to 38 nm).

4.1.2. Glucose oxidation

Reproducibility

To evaluate the reproducibility dealing with the catalyst preparation step and the catalytic reactions, and therefore the reproducibility of the operator, it is necessary to perform the same procedure at least three times. Thereby, it was synthesized three batch of catalysts using the sol immobilization technique (as reported above in Section 3), keeping all the parameter constant. These three batch of catalysts was tested on the glucose oxidation in the presence of base under standard conditions as reported in Section 3 ($T = 60\text{ }^{\circ}\text{C}$; $t = 1\text{ h}$; $\text{rpm} = 1000$; $\text{PO}_2 = 10\text{ bar}$; Glu: Au: NaOH molar ratio of 1000:1:3000).

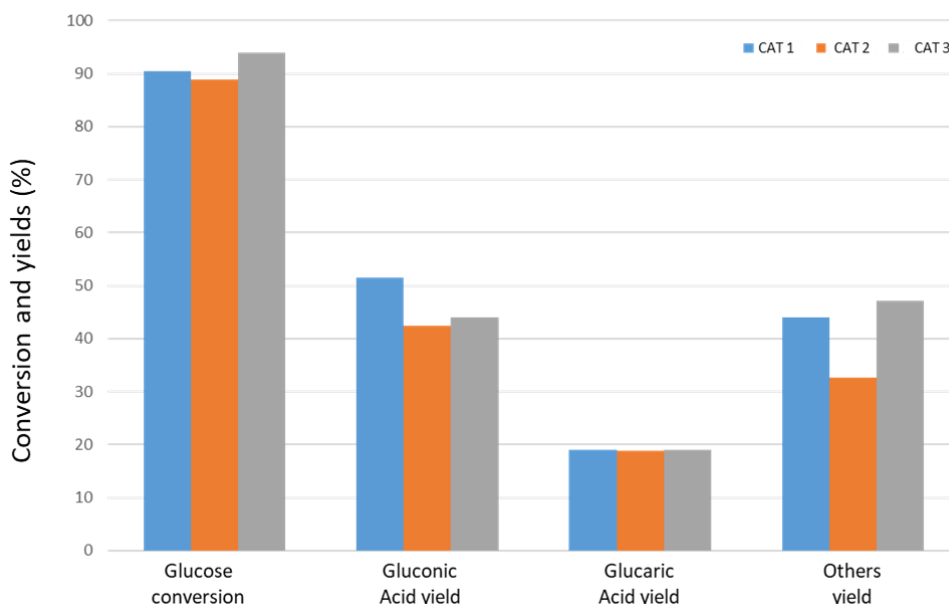


Figure 38: Reproducibility test on catalyst Au/AC-PVA 0,65 in standard conditions ($\text{PO}_2 = 10\text{ bar}$; $t = 1\text{ hour}$; $T = 60\text{ }^{\circ}\text{C}$; $\text{rpm} = 1000$; Glu: Au: NaOH molar ratio of 1000:1:3000). Three repetitions were carried out with three catalysts prepared with the same method.

Figure 38 shows the results obtained: in details, the three catalysts prepared similar value for glucose conversion (around 90%), gluconic and glucaric acid yield and other byproduct. All the catalytic data obtained was summarized in Table 3, where it has been reported also the average and the deviation standard for each species.

	Glucose conversion %	Gluconic Acid yield %	Glucaric Acid yield %	Others yield %
CAT 1	90	51	19	44
CAT2	89	42	19	33
CAT3	94	44	19	47
Average	91 ± 2	$46 \pm 3,7$	19 ± 1	$41 \pm 4,7$

Table 3: Glucose conversion and yield products for the three catalysts in order to test reproducibility

Gluconic acid oxidation with different time of reaction

In effort to study the mechanism of the reaction and some possible poisoning and deactivation effect, it was performed tests using Gluconic acid as starting material. In particular, it was tested in different reaction time (15 minutes, 1 hour and 2 hours) in standard conditions (reported in Section 3), with the aim of evaluating the effects on conversion and yields.

In Table 4 it was reported the results obtained:

	Gluconic Acid conversion %	Glucaric Acid yield %	Others yield %
t=15 min	16	7	7
t=1 h	35	21	21
t=2h	46	21	19

Table 4: Glucose conversion and yield products for reactions at different times ($PO_2=10$ bar; $t=15$ min/1 hour/ 2 hours; $T=60^\circ C$; rpm=1000; GO: Au:NaOH molar ratio of 1000:1:3000)

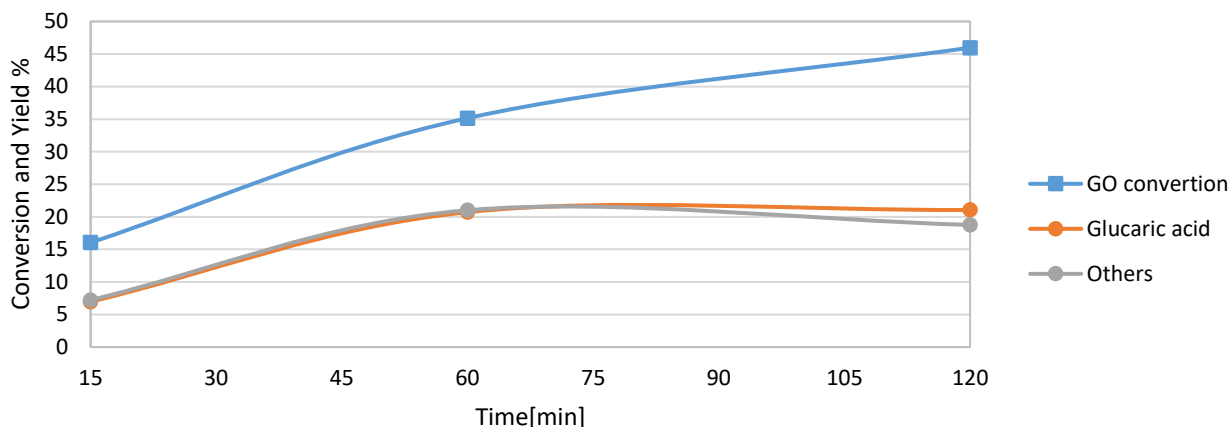


Figure 39: Conversion of gluconic acid and yields as a function of reaction time ($PO_2=10$ bar; $t=15$ min/ 1 hour/ 2 hour; $T=60^\circ C$; $rpm=1000$; Glu: Au: NaOH molar ratio of 1000:1:3000)

As shown in Figure 39, the conversion of gluconic acid increases as the reaction time increases. The yield of glucaric acid increases with increasing reaction time up to one hour; after one hour of reaction the glucaric acid yield (21%) does not increase but remains constant.

The yield of others, however, increases as the reaction time increases up to one hour; after one hour, for longer times (2 h), it decreases slightly. Since, for a reaction time of two hours, the conversion of glucose, is higher than the sum of the product yields, this could indicate that it decomposes leading to the formation of light products or that some products or reagents remains adsorbed on the surface of the catalyst, in both cases not identifiable by analytical methods.

The absence of an GA yield increases after 1 hour of reaction is in agreement with the data obtained with glucose (Figure 40); this phenomenon could be ascribe to the effect of Gluconic acid or some other by-product from it that could decrease the catalyst activity, blocking the active sites of supported gold nanoparticles.

From these results we understand that increasing the reaction time beyond an hour is useless in not useful to obtain the product of interest.

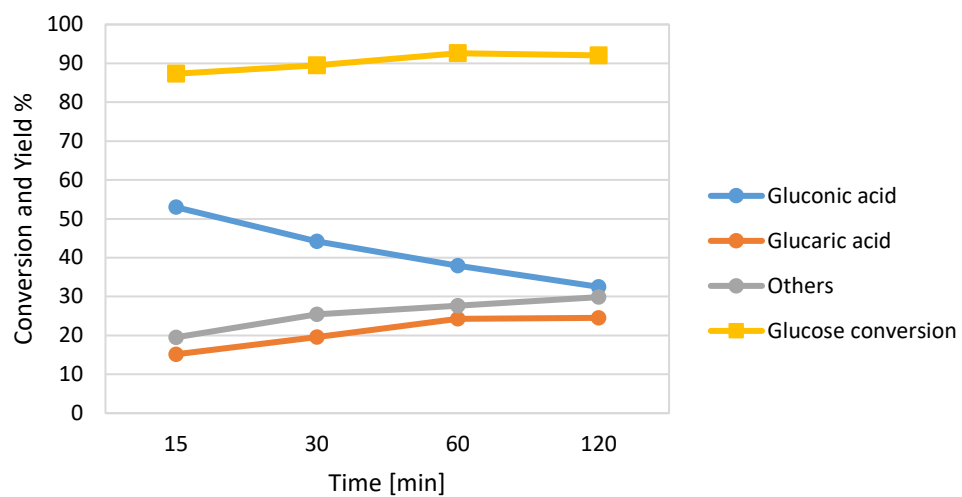


Figure 40: Conversion of glucose and yields as a function of reaction time ($PO_2=10$ bar; $t=15$ min/ 1 hour/ 2 hour; $T=60^\circ C$; rpm=1000; Glu: Au: NaOH molar ratio of 1000:1:3000)

4.2. Computational results

4.2.1 Modeling Gold Nanoparticles: structures and reactivity

To study the catalysts used in the laboratory we decided to simulate the gold nanoparticles using a so-called “cluster” approach. A cluster is a set of finite number of atoms that can assume different structures and can be treated as any molecular systems, thus allowing the use of standard computational tools generally employed in quantum molecular chemistry. Still, these computational tools allow QM treatment of limited size, which depends on the atomic number of the atoms involved. In the case of gold, we are limited to gold cluster with less than 70 atoms if one wants to obtain the desired results in a reasonable computational time. This implies that our clusters represent realistic models of small nanoparticles (ca. 1 nm) and just simplified models of the 4-5 nm nanoparticles obtained in the laboratory. Anyway, we considered different type of (ca. 1 nm) gold clusters in order to model various possible exposed surfaces that could be present in experimental nanoparticles larger than 1 nm. In particular, we considered 4 types of structures, as described below, according to the state-of-the-art knowledge of metal nanoparticle structures. Studies using photoelectronic spectroscopy combined with computational calculations [116,117] have allowed us to understand that gold clusters of 55 atoms and more have a distorted, irregular structure, as a result of relativistic effects that induce strong surface contractions analogous to bulk surface reconstructions. The fact that the gold clusters have a low symmetry structure can be a cause of the high reactivity of the gold in the nanoparticle form (which instead in bulk form, as we recall, is inactive) [117]. Indeed, the key for the reactivity of the catalytic systems is the low surface coordination, which leads to the formation of interactions with the reactants, to the breaking and formation of new bonds and therefore of the products of interest. These distorted gold structures are strongly under-coordinated and with surface defects, leading to an increase in catalytic reactivity. For nanoparticles larger than 5 nm the surface area (and therefore the sub-coordinated sites) tends to decrease, also corresponding to a decrease in the catalytic activity. Similar effect occurs with the metals Pt and Pd, while for other metals, such as copper and silver, the Mackay icosahedron (ICO) is the lowest-energy configuration [118,119], so the most stable. Still, for experimental nanoparticles of 4-5 nm, we could expect that clean Au(100) and Au(111) surfaces are (at least partially) exposed. Thus, we have modelled these types of gold clusters, as reported in Figure 41. We also decided to optimize a cubo-octahedral (CUBO) Au₅₅ structure, in order to compare

the results obtained with those of Ishimoto and co-workers, who studied the glucose oxidation reaction in presence of base on such cluster model [102].

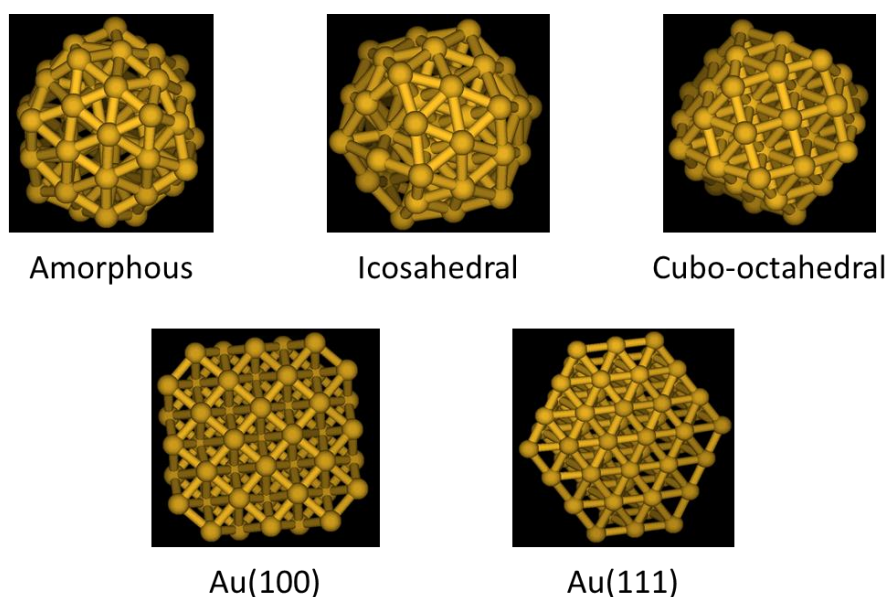


Figure 41: Modelled gold clusters

4.2.2. Bare gold Nanoparticles

We optimized the Au_{55} clusters and Au(111) and Au(100) surfaces using DFT approaches [101] as implemented in the Gaussian16 QM code. [105] Along with the commonly used B3LYP hybrid functional, we employed the pure BP86 functional [101,106,107] previously employed for the study of PdAu bimetallic clusters. The Stuttgart effective core potential have been used to model the scalar relativistic effects [109].

Amorphous structures

We considered the five lowest energy distorted structures obtained with density functional tight-binding theory (DFT-B) in the work of Van den Bossche [118], re-optimizing them at DFT level in order to obtain more accurate results. We also decided to optimize a positively charged structure Au_{55}^+ and a negatively charged one Au_{55}^- : during the glucose oxidation reaction, indeed, the nanoparticle is reduced, becoming negatively charged.

Ideal structure: icosahedral symmetry (ICO)

As previously mentioned, the other noble metals (Ag and Cu) have the icosahedral structure as stable structure. For this reason, it was decided to optimize an icosahedral Au_{55} cluster at DFT

level, in order to compare the results obtained with those in the literature and to have a comparison with other (amorphous or surface) structures considered in this work. The starting structure was obtained with the MATLAB software "Cluster generator" [120].

Ideal structure: cubo-octahedral symmetry (CUBO)

It was also decided to optimize the cubo-octahedral Au₅₅ structure, in order to compare our study with that of Ishimoto and co-workers, which studied the glucose oxidation mechanism for the first step of the reaction, up to gluconic acid [102]. The starting structure was obtained with the same MATLAB software used for the icosahedral structure [120].

4.2.3. Bare gold Nanoparticles: Au₅₅ models

In figure 42 are reported the figures of the five DFT-B Au₅₅ amorphous/distorted structures after the DFT optimization: they are called "S_n", with n=1-5.

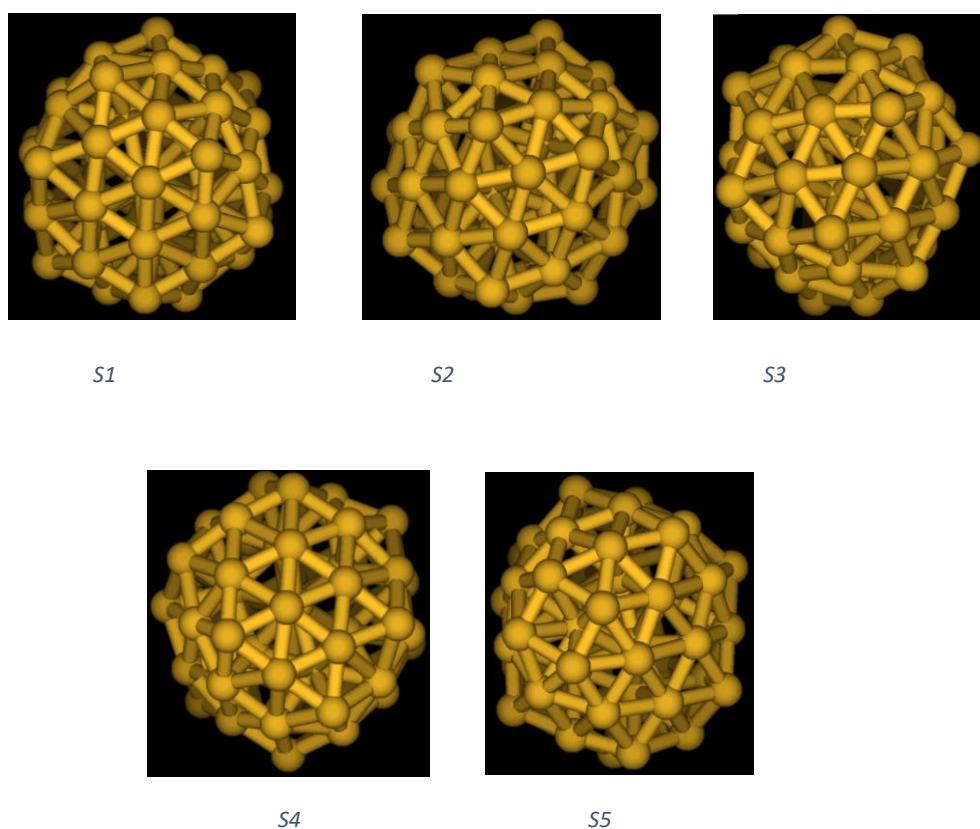


Figure 42: Au₅₅ distorted structures optimized

In Table 5 we summarized the results relative to the total energy of all the Au₅₅ structures, optimized with the functional BP86: we reported the five distorted clusters and ICO and CUBO clusters. In Table 6 we reported the same results but using the B3LYP functional.

	Deviation from the lowest energy structure
S1	0,0
S2	0,8
S3	0,9
S4	0,6
S5	0,4
ICO	30,2
CUBO	57,7

Table 5: Energies (in kcal/mol) for Au₅₅ structures using the functional BP86

	Deviation from the lowest energy structure
S1	0,6
S2	0,6
S3	0,0
S4	0,6
S5	0,8
ICO	33,9
CUBO	59,5

Table 6: Energies (in kcal/mol) for Au₅₅ structures using the functional B3LYP

As we can see, the most stable structure calculated with the functional BP86 is the distorted structure S1. With the functional B3LYP, on the other hand, the most stable structure is the distorted S3. In both cases the distorted structures are much more stable than the icosahedral and cubo-octahedral ones: both with the functional BP86 and with the B3LYP, ICO is higher

in energy by over 30 kcal/mol compared to the distorted structure more stable; CUBO structure is even higher in energy by over 50 kcal/mol. Although with the two functionals two different structures are highlighted as more stable, among all the distorted clusters the difference in energy is really negligible (< 1 kcal/mol).

These optimizations have allowed us to confirm that, as seen in the literature, gold nanoparticles prefer a disordered geometry unlike other transition metals.

To compare the electronic structures of various models, it was decided to calculate the Density of State (DOS) using the program *Multifwn* [121]. Below we report the DOS of the five distorted structures optimized with the functional BP86 and the plot with their overlay (Figure 43). The vertical dashed line represents the HOMO energy reference, set to zero.

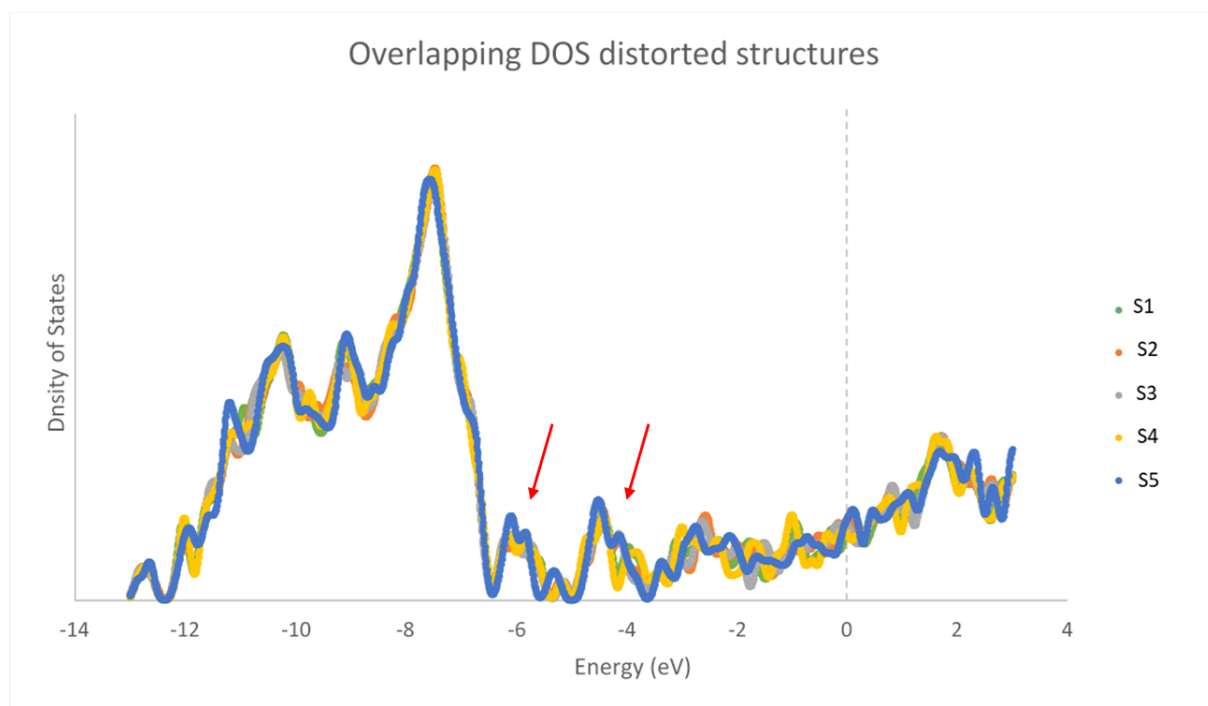


Figure 43: overlapping DOS distorted structures

The graphs are very similar, indicating a similar electronic structures in the various models. It is possible to compare the DOS with experimental data from Photoelectron spectra (PES)[117]. Both, in fact, show peaks (indicated in the figure by the arrows) towards 4.5 and 6 eV.

Au₅₅: positive, negative and neutral distorted structures

It was decided to optimize, using the functional BP86, the first distorted structure both positively and negatively charged. We then compared the DOS of the Au₅₅, Au₅₅⁺ and Au₅₅⁻ optimized geometries, as depicted in Figure 44.

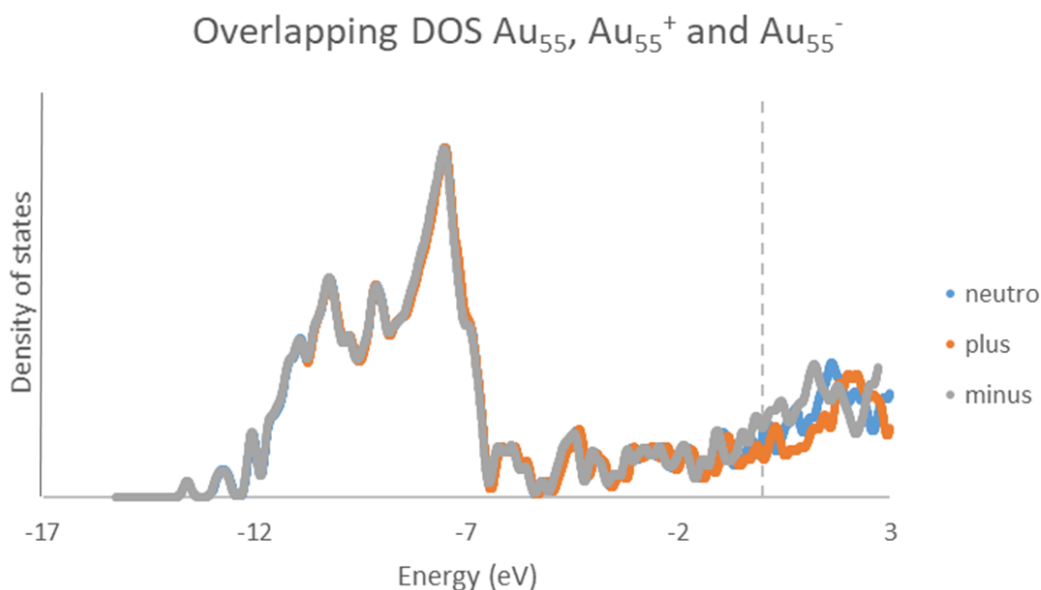


Figure 44: Overlapping DOS positive, negative and neutral S1 structures

The charged gold clusters feature DOS very similar to the neutral one, except in the area of frontier orbitals/bands (i.e. near 0 eV) where the extra charge has a sizeable effect.

4.2.4. Bare gold Nanoparticles: Au(100) and Au(111)

The model clusters for the Au(100) and Au(111) surfaces, featuring 57 atoms and 64 atoms, respectively, have been optimized with the same DFT methodology used for the Au₅₅ clusters amorphous and symmetric clusters. The starting structures were adapted from the work of I. Rivalta and co-workers [122], where PdAu bimetallic cluster (with Pd dimeric ensembles) were successfully used to study absorption and reactivity of organic molecules, but replacing two Pd atoms (present in the surface core of the bimetallic cluster) with two gold atoms. The Au clean surfaces clusters were thus constructed in the following way: the clusters were initially formed by 4 (core) gold atoms linked together (see Figure 45); the first neighbor atoms were added to

these Au atoms in the first and second layers, so that the active sites of Au(100) and Au(111) surfaces are represented by the Au₂₁ and Au₂₂ clusters, respectively. These atoms are generally considered mobile during any geometry optimization. The clusters were completed by adding the set of the first neighbor atoms for all the peripheral atoms of the active site atoms, obtaining three layer clusters: an Au₅₇ cluster for the Au(100) surface and an Au₆₄ cluster for the Au(111) surface (see Figure 45). The position of all these additional atoms (beyond the fully optimized Au₂₁ and Au₂₂ clusters) are generally kept frozen during geometry optimizations. In our work we reoptimized the initially constructed Au₅₇ and Au₆₄ clusters using both the BP86 and B3LYP functionals.

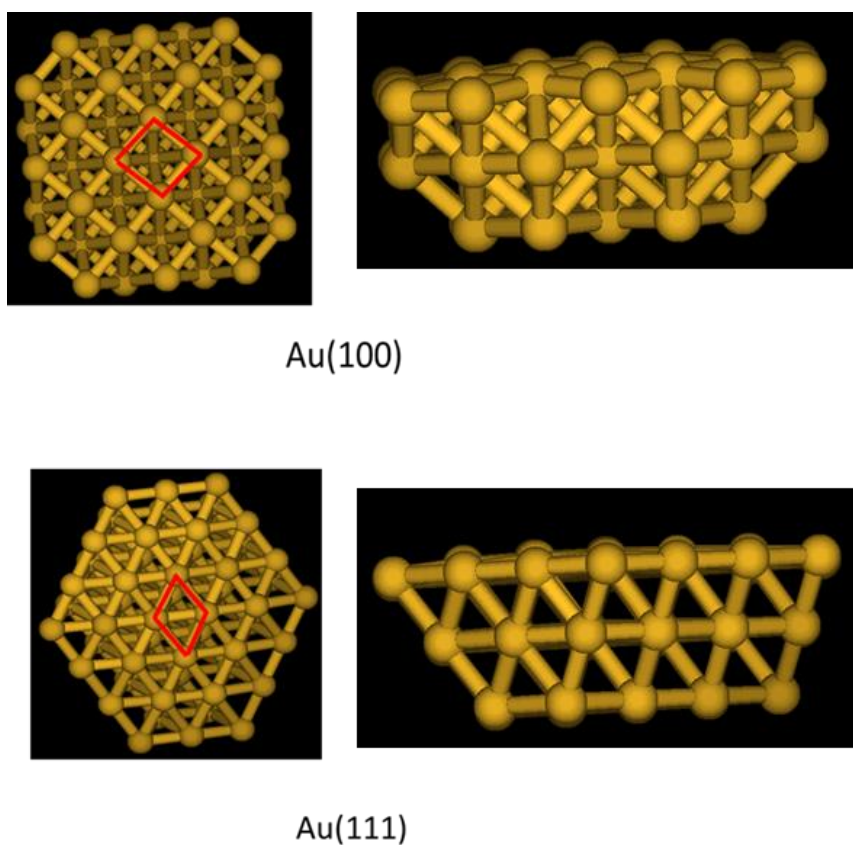


Figure 45: optimized surfaces Au(100) and Au(111) from a side and a top view

4.2.5. Study of the reaction mechanism: Preliminary considerations

It was decided to study the glucose oxidation reaction by taking into consideration the conditions of the reactions carried out in the laboratory and the Ishimoto's theoretical work on a symmetric model. As seen above, the reaction was treated, for the experimental part, with a heterogeneous catalyst of gold nanoparticles in presence of a base (NaOH). Therefore, the OH⁻ adsorption on the various optimized clusters was studied first. Subsequently, the study of the adsorption of glucose and gluconic acid, the reaction intermediate, was performed.

4.2.6. OH⁻ adsorption on Au₅₅ clusters

For the atoms of the adsorbates (H, C and O) the basis set 6-31** was used [108,109]. It was chosen to use only the BP86 as functional: this because we observed that it gave good results and in shorter times than the B3LYP.

First, we decided to investigate OH⁻ adsorption on Au₅₅ clusters. For the distorted structures we focused on the first (S1) and third (S3) structures, which appear to be the lowest energy ones with the B3LYP and BP86 calculations, respectively. We studied the OH⁻ adsorption also on the ICO and CUBO structures for comparison. In the work of Ishimoto and co-workers [102], where the adsorption of OH⁻ and ·OH radical on Au(100) and Au(111) extended surfaces and on CUBO Au₅₅ is studied, it is seen that the OH⁻ for the cube-octahedral nanoparticle structure is more stable on the vertex (top) position. For this reason, we have decided to focus the OH⁻ adsorption on the vertex position as regards the symmetrical structures (ICO and CUBO).

As regards the distorted structures, however, we have studied two different cases: one with the OH⁻ adsorbed in the position at the vertex and another with a less "protruding" position: to distinguish them, the rows (or chain) of atoms starting from the vertex (gold) atom considered were analyzed (see Figure 46): in particular, we considered as vertex either the gold atom connected to 3 rows featuring 3 atoms each and to 2 rows with 2 atoms or, for the less protruding position, the gold atom connected to 2 rows featuring 3 atoms each and to 3 rows with 2 atoms each.

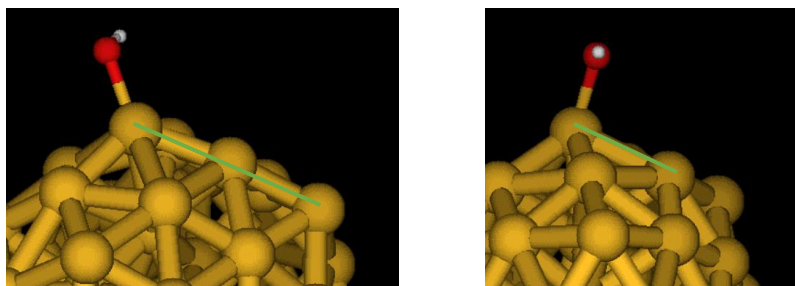


Figure 46: Example of (from left to right) a rows of 3 atoms and a rows of 2 atoms

For the distorted structures we observed that (see Figure 47) when the OH⁻ is initially positioned on a vertex with 3 rows of 3 atoms and 2 rows of 2 atoms it tends to remain in the same position; when instead (as for S3) it is initially bound to the alternative less "protruding" vertex it tends to move to a Au-Au bridge position.

	INITIAL STRUCTURE	FINAL STRUCTURE
S1(I)		
S1(II)		
S3		

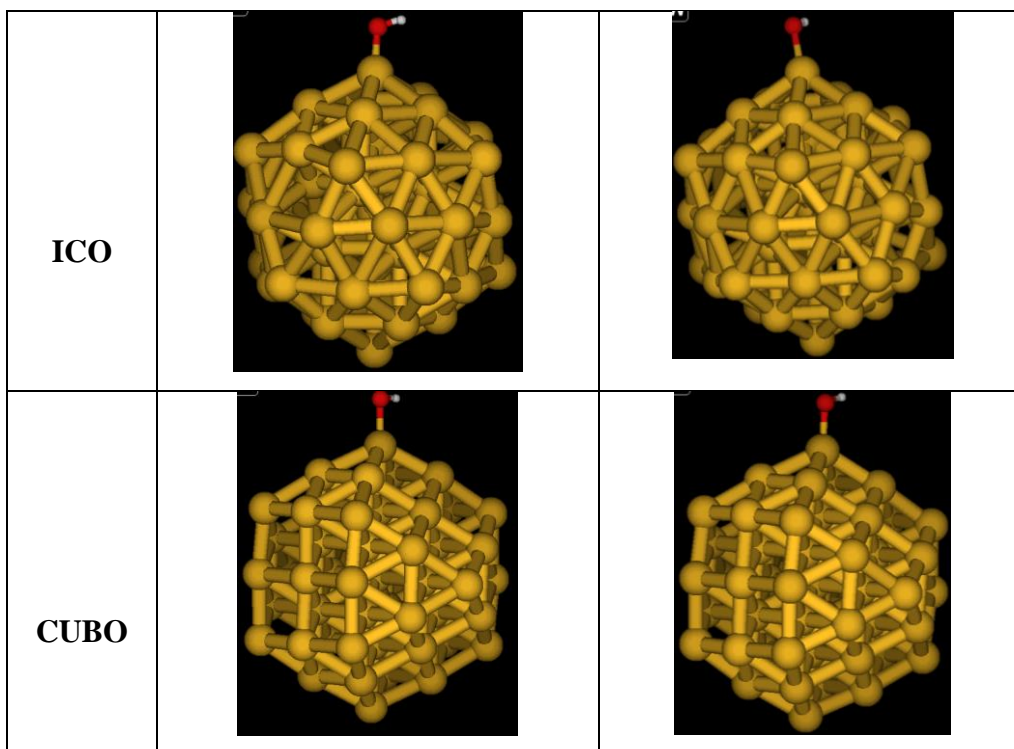


Figure 47: Structures of OH minus adsorbed on Au₅₅ clusters before and after optimization

In table 7, the relative energies associated with these different adsorptions are reported, showing that the OH⁻ is adsorbed more stably on distorted structures than symmetrical ones. Furthermore, the most stable structure is the S3, for which the OH⁻ move to a bridge position.

	Deviation from the lowest energy structure	Change position of OH ⁻
ICO	34,1	/
CUBO	62,6	/
S1 (I)	2,6	/
S1 (II)	3,6	/
S3	0,0	top→bridge

Table 7: Energies (in kcal/mol) for Au₅₅ structures with OH⁻ adsorbed

In table 8 we report the bond lengths and the angles of the OH⁻ adsorbed on the clusters. For the structures with OH⁻ in vertex position and that with OH⁻ in bridge we measured the AuAuO angles, as reported in Figure 48.



Figure 48: Example of angles measured for OH⁻ in vertex position (left) and in bridge position (right)

	Au _m -O(1) (Å)	Au _n -O(2) (Å)	O-H (Å)	Au _m Au _n O (°)	Au _m OH (°)
S1 (I)	2,063	/	0,980	126;149;122;102;99	105
S1 (II)	2,065	/	0,980	131;162;114;96;99	106
S3	2,281	2,255	0,981	48;48	84
ICO	2,069	/	0,980	99;115;138;135;105	105
CUBO	2,140	/	0,976	115;115;118;118	118

Table 8: bond lengths and angles for OH⁻ on Au₅₅

It can be seen that the O-Au bond length is more or less the same for S1(I), S1(II) and ICO structures. For the CUBO structure, the O-Au bond is a little bit longer. For the S3 structure, the only one where the OH⁻ is in bridge on two gold atoms, the two O-Au bonds lengthen with respect to the previous cases; the AuAuO angles instead are equal (48°), forming an isosceles triangle.

4.2.7. OH⁻ adsorption on Au(100) and Au(111) surface models

For the surfaces Au(100) and Au(111) surfaces we decided to study the adsorption of OH⁻ both when it is found on a top and on a bridge adsorption site (see Figure 49).

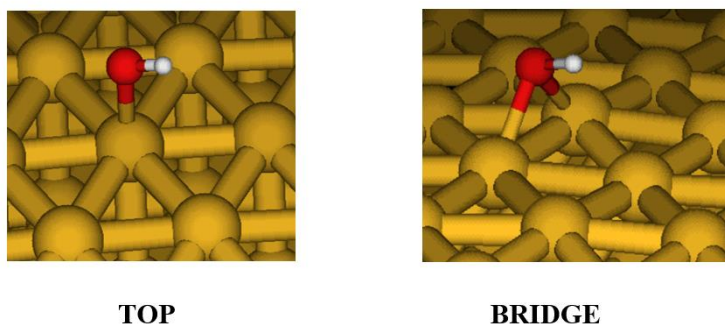
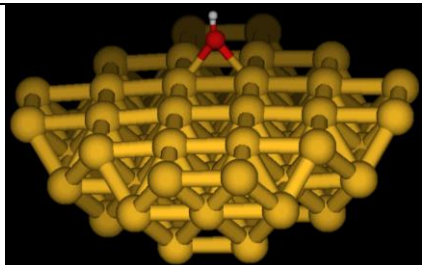
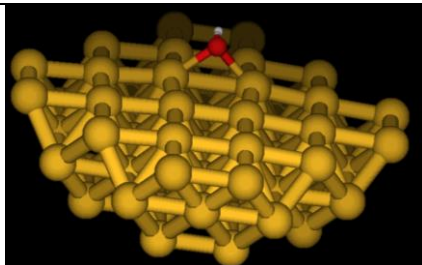
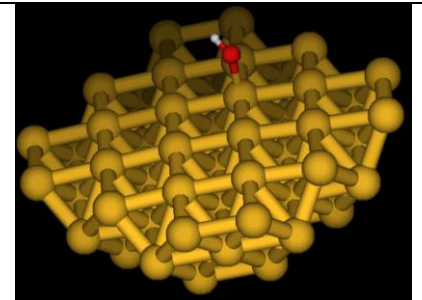
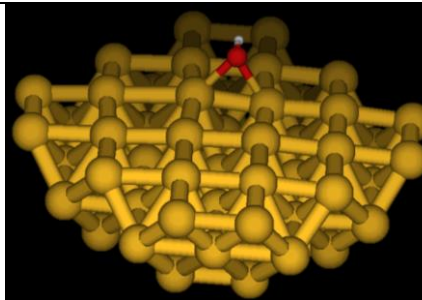


Figure 49: Example of the top and bridge structures of the OH on Au(100) and Au(111) surfaces

We report the initial and final structures of optimizations on various geometries (see Figure 50), named as “Sx”, with x=a-d.

	INIZIAL STRUCTURE	FINAL STRUCTURE
Sa: Au (100) Starting from bridge		
Sb: Au (100) Starting from top		

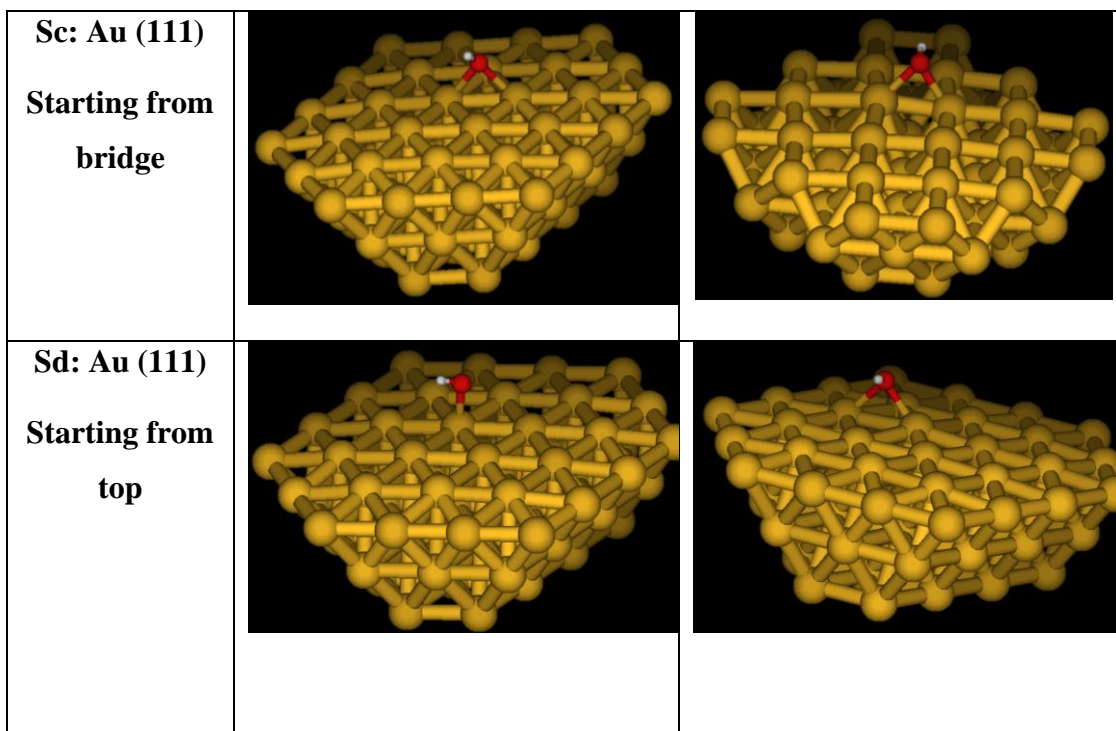


Figure 50: OH minus adsorption on gold surfaces before and after optimization

We see that for all structures, starting either from top or bridge sites, the final optimized one is the structure on the bridge sites, for both the negative and the radical OH group.

It is worth noting that for some models, (in particular Sb and Sc) the OH⁻ group tends to pull a gold atom to which it is bonded out of the surface. This phenomenon resembles that of gold surface reconstructions induced by charged adsorbate.

Computations have also been carried out considering the ·OH on the same gold surfaces. Also in this case, there was a tendency of the ·OH to prefer a bridge position over the top one.

Tables 10 and 11 show the relative energies obtained for the Au(100) and Au(111) surface models, respectively, while Table 12 shows some corresponding geometrical parameters (i.e. bond lengths and angles).

	Deviation from the lowest energy structure	Change position of OH⁻ / ·OH
Au(100) OH⁻ : Sa	0,0	/
Au(100) OH⁻: Sb	2,5	top→bridge

Table 10: energy of optimized Au(100) surface with OH⁻

	Deviation from the lowest energy structure	Change position of OH⁻ / ·OH
Au(111) OH⁻ : Sc	2,8	/
Au(111) OH⁻ : Sd	0,0	top→bridge

Table 11: Energies (in kcal/mol) for Au(111) surfaces with OH⁻

	O-Au(1)(Å)	O-Au(2) (Å)	O-H (Å)	AuOAu (°)	AuAuO(1) (°)	AuAuO(2) (°)
Au(100) OH⁻ bridge: Sa	2,238	2,239	0,983	88	43	43
Au(100) OH⁻ top: Sb	2,265	2,331	0,983	74	54	52
Au(111) OH⁻ bridge: Sc	2,914	2,214	0,982	90	44	46
Au(111) OH⁻ top: Sd	2,324	2,304	0,983	80	50	50

Table 12: bond lengths and angles for OH⁻ on Au(100) and Au(111) surfaces

For the Sa structure, we observed that the OH⁻ binds to the two gold atoms with bonds of the same length, forming an isosceles triangle. For the other structures we observed that one O-Au bond is longer than the other; in particular, for the structure Sc the difference is high, of 0,7 Å. This happens when the OH pulls one atom of gold out of the surface plane, thus making one bond shorter than the other. Consequently, the two angles AuAuO are also different.

For the Sd structure the difference between the two bonds is small, about 0.2 Å, and the two AuAu angles are identical: the OH⁻ therefore forms an isosceles triangle with the gold surface.

4.2.8. Glucose and OH⁻ adsorption on Au₅₅ clusters

We analyzed the oxidation reaction of glucose. First, we studied the adsorption of glucose on Au₅₅-OH⁻ clusters previously optimized. To decide where to place the glucose approaching the nanoparticle, we considered the outcome of the computations of Ishimoto and co-workers [102]: in particular, the adsorption of glucose on Au surface was assumed on the atom of gold near to the one on which the OH⁻ is bound and with carbon chain axe perpendicular to the surface plane, as reported in Figure 51.

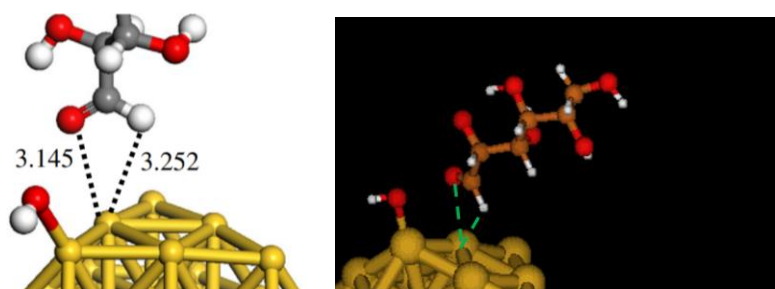


Figure 51: Example of initial position for OH + glucose in Ishimoto article [102] (left) and in our work (right)

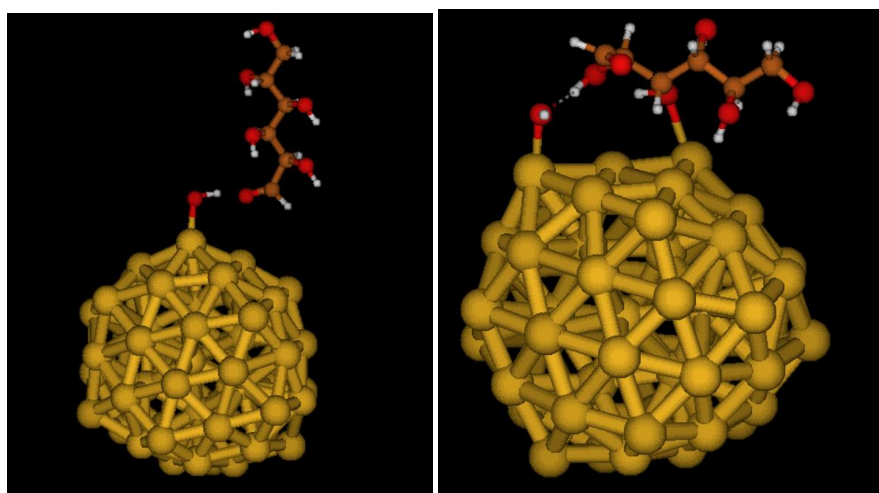


Figure 52: Glucose and OH⁻ adsorption on S1 structure: initial (left) and final (right) position

As depicted in Figure 52, upon geometry optimization of the initial structure showed in Figure 51, we observed that the glucose carbon chain moves horizontally with respect to the Au(111) surface plane of the nanoparticle S1. Moreover, there is a hydrogen bond (1,58 Å) between the (acceptor) oxygen of the adsorbed OH⁻ and the hydrogen of one of the glucose hydroxyl group

(working as H-bond donor). This H-bond stabilizes the structure along with an interaction between one surface gold atom (at a vertex) and the oxygen of the hydroxyl group at the third atom of the glucose carbon chain (with Au-O distance of 2,52 Å).

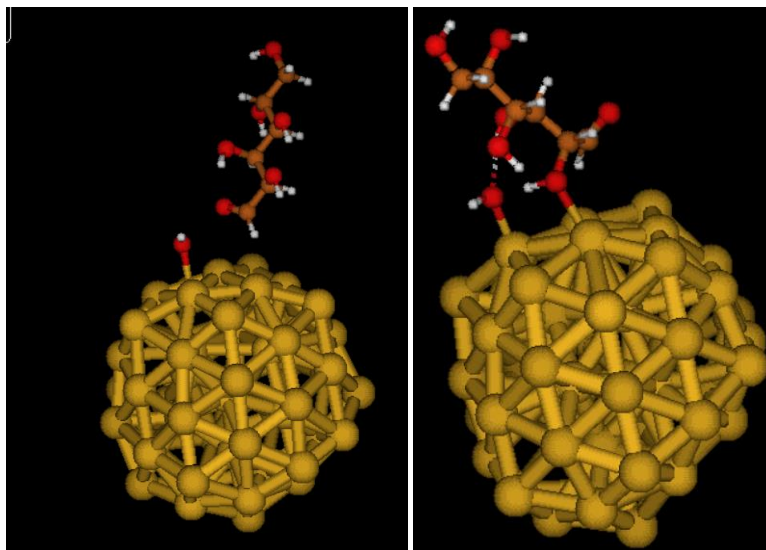


Figure 53: Glucose and OH⁻ adsorption on S3 structure: initial (left) and final (right) position

In Figure 53 the adsorption of Glucose and OH⁻ on S3 is reported. In this case, we obtained a glucose adsorbed vertically to the Au surface by the hydroxyl oxygen of the second carbon of the chain, with Au-O(H) distance of 2,45 Å. There is an hydrogen bond (1,76 Å) between the oxygen of the surface OH⁻ and the hydrogen of the OH group of the third carbon of glucose. It is important to note that, with the presence of the glucose on the S3 structure (stabilized by the H-bond between the surface OH⁻ and the glucose), the OH⁻ prefers a top position, while on the clean S3 nanostructure it prefers a bridge position.

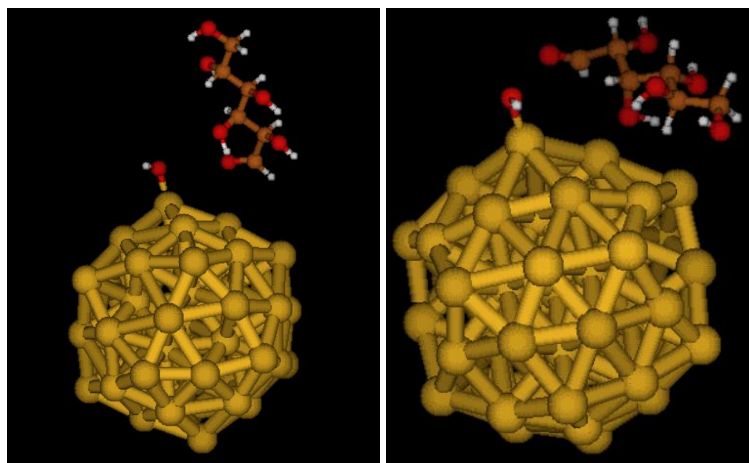


Figure 54: Glucose and OH⁻ adsorption on ICO structure: initial (left) and final (right) position

On the ICO structure we observed (see Figure 54) that glucose adsorbs horizontally to the Au(111) surface of the nanoparticle. In this case there are no interactions between glucose and OH⁻, which remains in the position at the top as in the initial structure.

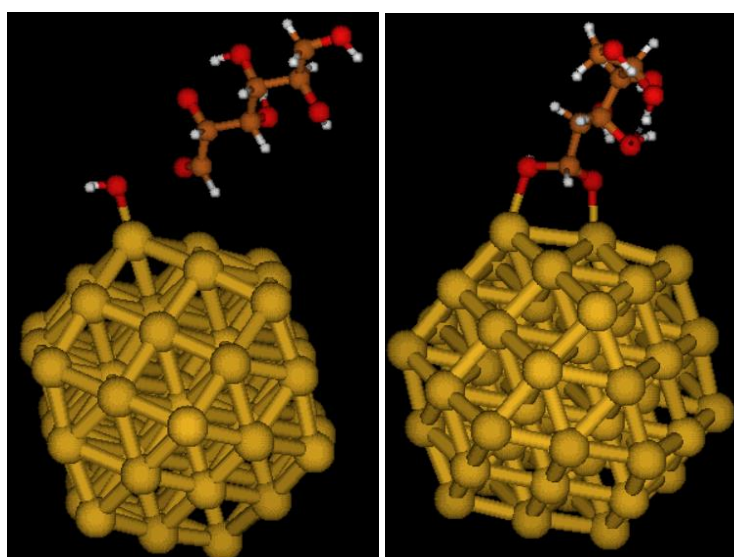


Figure 55: Glucose and OH⁻ adsorption on CUBO structure: initial (left) and final (right) position

In Figure 55 we report the adsorption of glucose and OH⁻ on the CUBO structure: while the initial structure was prepared with separated OH⁻ and glucose (distance 3,07 Å), as in the remaining cluster models, during the geometry optimization the OH⁻ spontaneously attacks the carbon of the aldehyde group, forming a bidentate tetrahedral intermediate (the OH⁻ and aldehyde carbon are now linked by a bond of 1.5 Å): this is in accordance with the reaction intermediate reported in the article of Ishimoto and co-workers [102].

	Deviation from the lowest energy structure
S1	0,0
S3	5,5
ICO	41,8
CUBO	*

Table 13. Energies (in kcal/mol) for Au₅₅ structures with glucose + OH⁻

*For the CUBO structure, during the optimization, the formation of a tetrahedral intermediate happens.

As reported in Table 13, the lowest energy is that found for the structure S1: also in this case, indeed, the amorphous structures are the most stable.

4.2.9. Gluconic acid adsorption on Au₅₅ clusters

We also carried out a first study regarding gluconic acid, linking back to Ishimoto's article. In particular, we initially focused on amorphous (distorted) nanoparticles that more realistic models of the experimental nanoparticles. In figure 56 we report the starting structure for the S3 cluster and the one at the end of the optimization.

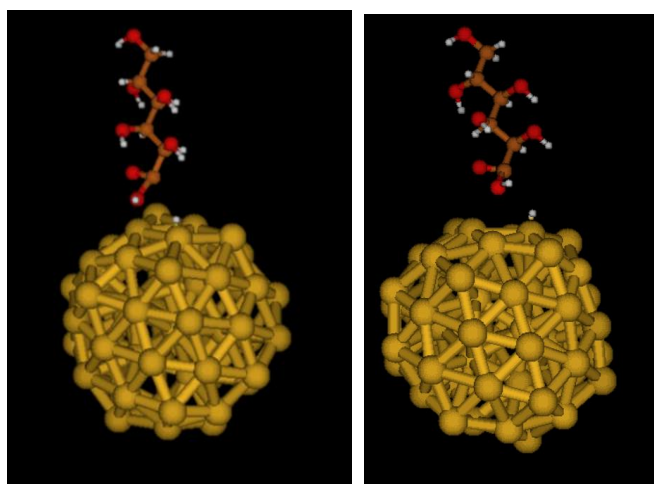


Figure 56: Gluconic Acid and H⁻ on S3 structure: initial (left) and final (right) position

As depicted in Figure 56, the gluconic acid adsorbs perpendicularly to the gold surface, as was previously also seen for glucose on the same S3 structure. The distance between the oxygen of the carboxylic OH⁻ and the nearest gold is 2.99 Å. The hydride ion, obtained from the aldehyde group of glucose following the attack of the OH group, is positioned at the top of a gold atom, with a distance of 1.08 Å. Starting from this important structure, future computational work can establish for the first time the thermodynamics and kinetics of the glucose oxidation on amorphous gold nanoparticles.

5. Conclusions

Nanoparticle gold-based catalysts were synthesized by the sol-immobilization method and characterized by the UV-Vis, XRD and TEM techniques, from which it was possible to confirm that nanoparticles of small size (approximately 2-3 nm) and well dispersed, thanks to the use of stabilized PVA, have been obtained. Subsequently, the catalysts were tested for the oxidation reaction of glucose to glucaric acid: to evaluate the reproducibility of the synthetic process, three different batches of catalyst were tested for the glucose oxidation reaction under standard conditions ($t = 1$ hour, $T = 60^\circ\text{C}$, $P = 10$ bar O_2 , Glu: Au: NaOH molar ratio of 1000:1:3000). From the data obtained it has been seen that the synthesis is reproducible, as well as the reaction, with an average conversion of gluconic of 91%, a yield of gluconic acid of 46%, of glucaric acid of 19% and of others 41%. Subsequently, the effect of the reaction time on the oxidation reaction from gluconic acid to glucaric acid was then tested (time of reaction: 15 minutes, 1 hour and 2 hours): the results show that the conversion of gluconic acid increases as the reaction time increases up to one hour; after one hour of reaction the conversion continues to increase till 40%; instead, the yield of glucaric acid and other by product follow a different trend: both the yields increase with increasing reaction time up to one hour, but after one hour of reaction the glucaric acid yield (21%) does not increase but remains constant and the yield of others decreases slightly. The data obtained are in agreement with the trend of the oxidation reaction of glucose to glucaric acid at the same reaction times (15 minutes, 1 hour and two hours) and suggest a possible catalyst deactivation due to gluconic acid or other byproduct.

For the computational part of the work, both symmetrical (icosahedron and cubo-octahedron) and distorted gold clusters of 55 atoms (approximately 1 nm) have been optimized by means of DFT methods. The results obtained show that distorted structures are the preferred ones due to relativistic effects, in agreement with previous studies. The surfaces Au(111) and Au(100), which are the main surfaces of large gold nanoparticles, were also optimized at the DFT levels using tailored cluster models. On these clusters, the adsorption of OH^- , glucose and gluconic acid has been studied. It has been observed that, on both exposed gold surfaces, the OH^- prefers a bridge position than a top one. On the other hand, for amorphous structures the OH^- adsorbed at the vertices are the most stable. In order to start investigations on the glucose oxidation reaction, the adsorption of glucose and gluconic acid on the Au_{55} clusters was studied. The study carried out aims to provide a method for approaching the study of gold-based nanosized

catalytic systems. The outcome provides important information that will be extremely useful to carry out more studies that are necessary to determine the full reaction mechanism and the corresponding energetics.

6. Future work

The results of this work serve as a starting point for understanding the activity of the gold-based catalysts prepared according to the procedure reported for the oxidation reaction of glucose to glucaric acid. To better evaluate the structure of the synthesized catalysts, TEM and XRD analysis should be carried out on each of them, in order to understand the size of the nanoparticles, the shape, the crystalline phase and the distribution.

In order to understand better the possible poisoning effect of gluconic acid on the catalyst, the idea to add different amount of GO at the beginning of the reaction could give us some clue on the interaction between GO and Au. Furthermore, the reaction could be carried out by adding also glucaric acid at the beginning, in order to evaluate if this adsorbs on the catalyst, modifying its activity. At the end, to better understand the effect of the reaction parameters on the catalytic activity, tests could be carried out at different oxygen pressures and at different temperatures (over and below 60 ° C).

For the computational the analysis of the second step of the reaction, and therefore the adsorption of glucaric acid on the surface of the catalyst should be performed. Furthermore, all the possible positions of adsorption of glucose and products could be analysed in more detail. Moreover, the study of the reactive mechanism could be carried out, in particular for the step from gluconic acid to glucaric acid, as there are no relevant data in the literature, in order to better understand the catalytic activity.

7. References

- [1] (a) G. B. Kauffman, *Chem. Educator* 4, 186 (1999); (b) J. J. Berzelius, Årsberättelsen om framsteg i fysik och kemi, Royal Swedish Academy of Sciences (1835); (c) J. J. Berzelius, Edinburgh, *New Philosophical Journal* XXI, 223 (1836); (d) J. J. Berzelius, Jahres-Bericht, 14, 237 (1836); (e) J. J. Berzelius, *Ann. Chim.*, 61, 146 (1836)
- [2] (a) W. Ostwald, *Z. Phys. Chem.*, 15, 705 (1984); (b) R. Zott, *Angew. Chem. Int. Ed. Engl.* 34, 3990 (2003)
- [3] Sebastian Kozuch and Jan M. L. Martin, Turning Over” Definitions in Catalytic Cycles, *ACS catal.* 2787-2794 (2012)
- [4] J Hagen, *Industrial Catalysis, a practical approach*, second edition (2006)
- [5] C. Tolman, The 16 and 18 electron rule in organometallic chemistry and homogeneous catalysis, *Chem. Soc. Rev.* 1 (3), 337–353 (1972)
- [6] M. Faraday, *Philosophical Transactions of the Royal Society* (1834)
- [7] a) I. Langmuir, *J. Am. Chem. Soc.* 37, 1139 (1915); (b) I. Langmuir, *J. Am. Chem. Soc.* 38, 2221, (1916); (c) I. Langmuir, *Phys. Rev.* 8, 149, (1916)
- [8] K. Vasanth Kumar, K. Porkodi, F. Rocha, Langmuir–Hinshelwood kinetics – A theoretical study
- [9] Frieder W. Lichtenthaler, Carbohydrates as Organic Raw Materials, *Ullmann’s Encyclopedia of Industrial Chemistry* vol.6 – pag. 584
- [10] Solomon S, Qin D, Manning M, Chen Z, Marquis M, Averyt KB, et al., editors, IPCC. Climate change 2007: the physical science basis. Contribution of working group 1 to the fourth assessment report of the intergovernmental panel on climate change. Cambridge, United Kingdom and New York, NY, USA: Cambridge University Press (2007)
- [11] IPCC. Climate change 2007: mitigation. In: Metz B, Davidson OR, Bosch PR, Dave R, Meyer LA, editors. Contribution of working group 3 to the fourth assessment report of the intergovernmental panel on climate change. Cambridge, United Kingdom and New York, USA: Cambridge University Press (2007)
- [12] Nossin PMM, White biotechnology: replacing black gold? In: Fifth international conference on renewable resources and biorefineries. Ghent, Belgium; (10–12 June 2009)
- [13] TRS – The Royal Society Sustainable biofuels: prospects and challenges. Policy document 01/08, ISBN 978 0 85403 662 2 (2008)
- [14] EC. Towards, a European knowledge-based bioeconomy – workshop conclusions on the use of plant biotechnology for the production of industrial biobased products. EUR 21459. European Commission, Directorate-General for Research. Brussels, Belgium (2004)
- [15] Kenneth J. Moore Hans-Joachim G. Jung: Lignin and Fiber Digestion, *Journal of Range Management*, 420-430, (July 2001)
- [16] Werpy, T., and G. Petersen., Top. value added chemicals from biomass, volume 1—results of screening for potential candidates from sugars and synthesis gas. U.S. Department of Energy, Washington, DC (2004)
- [17] Thomas Becker, Dietmar Breithaupt, Horst Werner Doelle, Armin Fiechter, Günther Schlegel, Sakayu Shimizu, Hideaki Yamada: Biotechnology, *Ullmann’s Encyclopedia of Industrial Chemistry*, 7th Edition, Wiley-VCH ISBN 978-3-527-32943-4. Volume 6, p. 48 (2011)
- [18] Robert Żółtaszek, Margaret Hanausek, Zofi M. Kiliańska, Zbigniew Walaszek: The biological role of D-glucaric acid and its derivatives; *Postepy Hig Med Dosw* (online), issue 62, 451-462 (2008)

- [19] Z. Walaszek: Potential use of D-glucaric acid derivatives in cancer prevention; *Cancer Lett.* 54, 1–8 (1990)
- [20] Narula, J.; Petrov, A.; Pak, K.-Y.; Lister, B.C.; Khaw, B.-A: Very early non-invasive detection of acute non perfused myocardial infarction with ^{99m}Tc glucarate; *Circulation* 95 (6), 1577–1584 (1997)
- [21] Walaszek, Z., Szemraj, J., Hanausek, M., Adams, A. K., Sherman: D-Glucaric acid content of various fruits and vegetables and cholesterol-lowering effects of dietary Dglucarate in the rat; *U. Nutr. Res.*, 16, 673–681 (1996)
- [22] Korzh, E. N.; Sukhotin, A. M: Zh. Prikl. Khim. 54, 2404–2407 (1981)
- [23] Abbadi, A.; Gotlieb, K. F.; Meiberg, J. B. M.; Peters, J. A.; van Bekkum, H: New sequestering materials based on the oxidation of the hydrolysis products of lactose; *Green Chem.*, 1, 231–235(1999)
- [24] Devin G. Barrett and Muhammad N. Yousaf: Poly(triol α -ketoglutarate) as Biodegradable, Chemoselective, and Mechanically Tunable Elastomers; *Macromolecules*, 41 (17), pp 6347–6352 (2008)
- [25] Jang, Y. S., Kim, B., Shin, J. H., Choi, Y. J., Choi, S., Song, C. W., ... & Lee, S. Y., Bio-based production of C2–C6 platform chemicals. *Biotechnology and bioengineering*, 109(10), 2437-2459 (2012)
- [26] Beerthuis, R., Rothenberg, G., & Shiju, N. R, Catalytic routes towards acrylic acid, adipic acid and ϵ -caprolactam starting from biorenewables. *Green Chemistry*, 17(3), 1341-1361 (2015)
- [27] National Pollutant inventory, Department of Agriculture, water, and the Environment, Australian Government
- [28] H. Roper: Selective Oxidation of Glucose; *Starch/Starke*, 42, p. 346 (1990)
- [29] O. Sohst, B. Tollens: Über krystallisirte Zuckersäure (Zuckerlactonsäure); *Liebigs Ann. Chem.* 245, 1–27 (1888)
- [30] Tae Seok Moon, Sang-Hwal Yoon, Amanda M. Lanza, Joseph D. Roy-Mayhew, Kristala L. Jones Prather: Production of Glucaric Acid from a Synthetic Pathway in Recombinant Escherichia coli; *Appl. Environ. Microbiol.* 75, 589–595 (2009)
- [31] V. Pamuk, M. Yılmaz, A. Alicilar: The preparation of D-glucaric acid by oxidation of molasses in packed beds; *J. Chem. Technol. Biotechnol.* 76, 186-190 (2001)
- [32] N. Merbouh, Jean Francois Thaburet, Mathias Ibert, Francis Marsais, James M. Bobbitt: Facile nitroxide-mediated oxidations of D-glucose to D-glucaric acid; *Carbohydrate Research* 336 75–78 (2001)
- [33] National Institute for Occupational Safety and Health (NIOSH): Approaches to Safe Nanotechnology: Managing the Health and Safety Concerns Associated with Engineered Nanomaterials (March 2009)
- [34] D. Bin, H. Wang, J. Li, Z. Yin, J. Kang, B. He, Z. Li: Controllable oxidation of glucose to gluconic acid and glucaric acid using an electrocatalytic reactor; *Electrochimica Acta* 130, 170–178 (2014)
- [35] Zhang, Z. & Huber, G. W. Catalytic oxidation of carbohydrates into organic acids and furan chemicals. *Chem. Soc. Rev.* 47, 1351–1390 (2018)
- [36] C. Tiloke, A.A. Chuturgoon, in *Nanoarchitectonics for Smart Delivery and Drug Targeting* (2016)
- [37] Karmani L, Labar D, Valembois V, Bouchat V, Nagaswaran PG: Antibodyfunctionalized nanoparticles for imaging cancer: influence of conjugation to gold nanoparticles on the biodistribution of Zr-labeled cetuximab in mice; *Contrast Media Mol Imaging.* 8, 402-408 (2013)
- [38] (EN) The Textiles Nanotechnology Laboratory, su nanotextiles.human.cornell.edu
- [39] Kawazome, M., Kim K., Hatamura, M., Suganuma, K.: *Funsai* 50, 27 – 31 (2007)

- [40] Haruta, M., Kobayashi, T., Sano, H. & Yamada, N. Novel Gold Catalysts for the Oxidation of Carbon Monoxide at a Temperature far Below 0 °C. *Chem. Lett.* 16, 405–408 (1987)
- [41] Hutchings, G. J. Vapor phase hydrochlorination of acetylene: correlation of catalytic activity of supported metal chloride catalysts. *J. Catal.* 96, 292–295 (1985)
- [42] Kim, K. J., & Ahn, H. G. Complete oxidation of toluene over bimetallic Pt–Au catalysts supported on ZnO/Al₂O₃. *Applied Catalysis B: Environmental*, 91(1-2), 308-318 (2009)
- [43] Ivanova, S., Petit, C., & Pitchon, V. A new preparation method for the formation of gold nanoparticles on an oxide support. *Applied Catalysis A: General*, 267(1-2), 191-201 (2004)
- [44] Ivanova, S., Pitchon, V., & Petit, C., Application of the direct exchange method in the preparation of gold catalysts supported on different oxide materials, *Journal of Molecular Catalysis A: Chemical*, 256(1-2), 278-283 (2006)
- [45] Haruta, M. Size- and support-dependency in the catalysis of gold. *Catal. Today* 36, 153–166 (1997)
- [46] Qian, Z., & Park, S. J., Silver seeds and aromatic surfactants facilitate the growth of anisotropic metal nanoparticles: gold triangular nanoprisms and ultrathin nanowires. *Chemistry of Materials*, 26(21), 6172-6177 (2014)
- [47] Prati, L. & Martra, G., New gold catalysts for liquid phase oxidation. *Gold Bull.* 32, 96–101 (1999)
- [48] Ramo'n Pamies, Jose' Gine's Herna'ndez Cifre, Vanesa Ferna'ndez Espi'n ,Mar Collado-Gonzalez, Francisco Guillermo Di'az Ban'os, Jose' Garcí'a de la Torre, Aggregation behaviour of gold nanoparticles in saline aqueous media
- [49] C.E. Hoppe, M. Lazzari, I. Blanco, M.A. Lopez-Quintela, *Langmuir* 22, 7027-7034 (2006)
- [50] Dimitratos, N. et al. Effect of the preparation method of supported Au nanoparticles in the liquid phase oxidation of glycerol. *Appl. Catal. Gen.* 514, 267–275 (2016)
- [51] Jia, C.-J. & Schüth, F. Colloidal metal nanoparticles as a component of designed catalyst. *Phys. Chem.* 13, 2457–2487 (2011)
- [52] Megías-Sayago, C., Santos, J. L., Ammari, F., Chenouf, M., Ivanova, S., Centeno, M. A., & Odriozola, J. A., Influence of gold particle size in Au/C catalysts for base-free oxidation of glucose. *Catalysis Today*, 306, 183-190 (2018)
- [53] Rodolfo Zanella, Laurent Delannoy, Catherine Louis, Mechanism of deposition of gold precursors onto TiO₂ during the preparation by cation adsorption and deposition–precipitation with NaOH. *Sciencedirect* 291, 62–72 (2005)
- [54] P.L. Murphy, G. Stevens, M.S. LaGrange, *Geochim. Cosmochim. Acta* 64, 479(2000)
- [55] M. Manfait, A.J.P. Alix, C. Kappenstein, *Inorg. Chem. Acta* 50, 147 (1981); L.H. Skibsted, *Acta Chem. Sand. Ser. A*33, 113 (1979); L.H. Skibsted, J. Bjerrum, *Acta Chem. Sand. Ser. A*28 (1974) 740
- [56] W.R. Mason, H.B. Gray, *J. Am. Chem. Soc.* 90, 5721 (1968)
- [57] Carolina Alejandra Garcia Soto Thesis, Investigation of gold-based catalysts for liquid phase oxidation of glucose to glucaric acid (2018-2019)
- [58] Delannoy, L., El Hassan, N., Musi, A., Le To, N. N., Krafft, J. M., & Louis, C., Preparation of supported gold nanoparticles by a modified incipient wetness impregnation method. *The Journal of Physical Chemistry B*, 110(45), 22471-22478 (2006)

- [59] Nasrabadi, Hamid; Abasi, Elham; Davaran, Soodabeh; Kouhi, Mohammad; Akbarzadeh, Abolfazl. "Bimetallic nanoparticles: Preparation, properties, and biomedical applications". *Artificial Cells, Nanomedicine, and Biotechnology*. Researchgate. 44 (2014-09-09)
- [60] Sharma, Gaurav; Kumar, Amit; Sharma, Shweta; Naushad, Mu.; Prakash Dwivedi, Ram; ALOthman, Zeid A.; Mola, Geneve Tessema, Novel development of nanoparticles to bimetallic nanoparticles and their composites: A review, *Journal of King Saud University - Science*. *ScienceDirect*. 31 (2): 257–269 (2019-04-01)
- [61] Blosi, Magda; Orтели, Simona; Costa, Anna Luisa; Dondi, Michele; Lolli, Alice; Andreoli, Sara; Benito, Patricia; Albonetti, Stefania, Bimetallic Nanoparticles as Efficient Catalysts: Facile and Green Microwave Synthesis, *Materials*. 9 (7): 550. doi:10.3390/ma9070550. PMC 5456855. PMID 28773672, (2016-07-08)
- [62] S. Zhou, M. Zhao, T. H. Yang, Y. N. Xia, *Mater. Today*, 22, 108 (2019)
- [63] D. Zhang, B. Gökce, S. Barcikowski, *Chem. Rev.*, 117, 3990(2017)
- [64] L. Zhang, Z. Xie, J. Gong, *Chem. Soc. Rev.*, 45, 3916 (2016)
- [65] Y. Xu, L. Chen, X. Wang, W. Yao, Q. Zhang, *Nanoscale*, 7, 10559 (2015)
- [66] H. L. Liu, F. Nosheen, X. Wang, *Chem. Soc. Rev.*, 44, 3056 (2015)
- [67] M. B. Cortie, A. M. McDonagh, *Chem. Rev.*, 111, 3713 (2011)
- [68] R. Ferrando, J. Jellinek, R. L. Johnston, *Chem. Rev.*, 108, 845 (2008)
- [69] H. Mistry, A. S. Varela, S. Kuhl, P. Strasser, B. R. Cuenya, *Nat. Rev. Mater.*, 1, 16009(2016)
- [70] C. Z. Zhu, D. Du, A. Eychmuller, Y. H. Lin, *Chem. Rev.*, 115, 8896 (2015)
- [71] J. B. Zhao, R. C. Jin, *Nano Today*, 18, 86 (2018)
- [72] G. F. Liao, J. S. Fang, Q. Li, S. H. Li, Z. S. Xu, B. Z. Fang, *Nanoscale*, 11, 7062 (2019); J. Gu, Y. W. Zhang, F. Tao, *Chem. Soc. Rev.*, 41, 8050 (2012)
- [73] G. Guisbiers, R. Mendoza-Cruz, L. Bazan-Diaz, J. J. Velazquez-Salazar, R. Mendoza-Perez, J. A. Robledo-Torres, J. L. Rodriguez-Lopez, J. M. Montejano-Carrizales, R. L. Whetten, M. Jose-Yacamán, *ACS Nano*, 10, 188 (2016)
- [74] K. McNamara, S. A. Tofail, *Chem. Phys.*, 17, 27981(2015)
- [75] F. Calvo, *Phys. Chem. Chem. Phys.* 17, 27922 (2015)
- [76] M. Sankar, N. Dimitratos, P. J. Miedziak, P. P. Wells, C. J. Kiely, G. J. Hutchings, *Chem. Soc. Rev.*, 41, 8099 (2012)
- [77] C. M. Copley, J. Y. Chen, E. C. Cho, L. V. Wang, Y. N. Xia, *Chem. Soc. Rev.* 40, 44 (2011)
- [78] S. Krishnan, M. Estevez-González, R. Perez, R. Esparza, M. Meyyappan, *RSC Adv.*, 7, 27170 (2017)
- [79] Y. G. Sun, Y. N. Xia, *Science*, 298, 2176 (2002)
- [80] C. M. Copley, M. Rycenga, F. Zhou, Z. Y. Li, Y. N. Xia, *Angew. Chem., Int. Ed.*, 48, 4824 (2009)
- [81] S. Krishnan, M. Estevez-González, R. Perez, R. Esparza, M. Meyyappan, *RSC Adv.*, 7, (2017)
- [82] T. Fu, J. Fang, C. Wang, J. Zhao, *J. Mater. Chem.* 4, 8803 (2016)
- [83] C. Bock, C. Paquet, M. Couillard, G. A. Botton, B. R. MacDougall, *J. Am. Chem. Soc.*, 126, 8028 (2004)
- [84] F. Papa, C. Negrila, A. Miyazaki, I. Balint, *J. Nanopart. Res.* 13, 5057 (2011)

- [85] D. Zhang, B. Gökce, S. Barcikowski, *Chem. Rev.*, 117, 3990 (2017)
- [86] I. Lee, S. W. Han, K. Kim, *Chem. Commun.*, 1782 (2001)
- [87] D. Tiedemann, U. Taylor, C. Rehbock, J. Jakobi, S. Klein, W. A. Kues, S. Barcikowski, D. Rath, *Analyst*, 139, 931 (2014)
- [88] A. Neumeister, J. Jakobi, C. Rehbock, J. Moysig, S. Barcikowski, *Phys. Chem. Chem. Phys.*, 16, 23671 (2014)
- [89] C. Rehbock, J. Jakobi, L. Gamrad, S. van der Meer, D. Tiedemann, U. Taylor, W. Kues, D. Rath, S. Barcikowski, *Beilstein J. Nanotechnol.*, 5, 1523 (2014)
- [90] D. Thompson: *Gold Bulletin*, vol 31, 111-118 (1998)
- [91] B. Grigorova, J. Mellor, A. Palazov, F. Greyling, Selective catalytic oxidation of CO in presence of hydrogen, Patent PCT/IB00/00390 (2000)
- [92] N. Lopez, T.V.W. Janssens, B.S. Clausen, Y. Xu, M. Mavrikakis, T. Bligaard and J.K. Nørskov, On the origin of the catalytic activity of gold nanoparticles for low-temperature CO oxidation, *J. Catal.* 223, 232 (2004)
- [93] S. Carrettin, P. McMorn, P. Johnston, K. Griffin, G.J. Hutchings; Selective oxidation of glycerol to glyceric acid using a gold catalyst in aqueous sodium hydroxide; *Chem. Commun.*, 696–69(2002)
- [94] A. Villa, D. Wang, D. Sheng Su, L. Prati: Gold Sols as Catalysts for Glycerol Oxidation: The Role of Stabilizer; *ChemCatChem*, 1, 510 – 514 (2009)
- [95] Biella, S., Prati, L. & Rossi, M. Selective Oxidation of D-Glucose on Gold Catalyst. *J. Catal.*, 206, 242–247 (2002)
- [96] Comotti, M., Della Pina, C., Falletta, E., & Rossi, M., Aerobic oxidation of glucose with gold catalyst: hydrogen peroxide as intermediate and reagent, *Advanced Synthesis & Catalysis*, 348(3), 313-316 (2006)
- [97] Saliger, R., Decker, N., & Prüße, U., D-Glucose oxidation with H₂O₂ on an Au/Al₂O₃ catalyst, *Applied Catalysis B: Environmental*, 102(3-4), 584-589 (2011)
- [98] F. Besenbacher, I. Chorkendorff, B.S. Clausen, B. Hammer, A.M. Molenbroek, J.K. Nørskov, I. Stensgaard, *Science*, 279, 1913(1998)
- [99] K. Honkala, A. Hellman, I.N. Remediakis, A. Logadottir, A. Carlsson, S. Dahl, C.H. Christensen, J.K. Nørskov, *Science* 307, 555 (2005)
- [100] E. Schrödinger, Nobel Lecture (1933)
- [101] Christopher J. Cramer, *Essentials of Computational Chemistry*, 165-179, 249-268, 393- 394 (2004)
- [102] Takayoshi Ishimoto, Hiroki Kazuno, Takayuki Kishida, Michihisa Koyama: Theoretical study on oxidation reaction mechanism on Au catalyst in direct alkaline fuel cell, *Solid State Ionics*, Volume 262, Pages 328-331(2014)
- [103] Takayoshi Ishimoto, Yumi Hamatake, Hiroki Kazuno, Takayuki Kishida, Michihisa Koyama: Theoretical study of support effect of Au catalyst for glucose oxidation of alkaline fuel cell anode, *Applied Surface Science*, Volume 324, 76-81(1 January 2015)
- [104] Weidong Gong, Matthew C Mowlem, Michael Kraft, Hywel Morgan, A Simple, Low-Cost Double Beam Spectrophotometer for Colorimetric Detection of Nitrite in Seawater, (2009)
- [105] Gaussian 16, Revision C.01, M. J. Frisch, G. W. Trucks, H. B. Schlegel, G. E. Scuseria, M. A. Robb, J. R. Cheeseman, G. Scalmani, V. Barone, G. A. Petersson, H. Nakatsuji, X. Li, M. Caricato, A. V. Marenich, J. Bloino, B. G. Janesko, R. Gomperts, B. Mennucci, H. P. Hratchian, J. V. Ortiz, A. F. Izmaylov, J. L.

- Sonnenberg, D. Williams-Young, F. Ding, F. Lipparini, F. Egidi, J. Goings, B. Peng, A. Petrone, T. Henderson, D. Ranasinghe, V. G. Zakrzewski, J. Gao, N. Rega, G. Zheng, W. Liang, M. Hada, M. Ehara, K. Toyota, R. Fukuda, J. Hasegawa, M. Ishida, T. Nakajima, Y. Honda, O. Kitao, H. Nakai, T. Vreven, K. Throssell, J. A. Montgomery, Jr., J. E. Peralta, F. Ogliaro, M. J. Bearpark, J. J. Heyd, E. N. Brothers, K. N. Kudin, V. N. Staroverov, T. A. Keith, R. Kobayashi, J. Normand, K. Raghavachari, A. P. Rendell, J. C. Burant, S. S. Iyengar, J. Tomasi, M. Cossi, J. M. Millam, M. Klene, C. Adamo, R. Cammi, J. W. Ochterski, R. L. Martin, K. Morokuma, O. Farkas, J. B. Foresman, and D. J. Fox, Gaussian, Inc., Wallingford CT (2016)
- [106] P.J. Stephens, F.J. Devlin, C.F. Chabalowski, M.J. Frisch, *J. Phys. Chem.*, 98, 11623- 11627 (1994)
- [107] A. D. McLean and G. S. Chandler, *J. Chem. Phys.*, 72, 5639-5948 (1980)
- [108] A. Schäfer, H. Horn, R. Ahlrichs, *J. Chem. Phys.*, 97, 2571-2577 (1992)
- [109] Dmytro Ivashchenko, A step towards artificial photosynthesis: theoretical study of photoelectrocatalytic CO₂ conversion to fuel, *Research Project*, 9-16(2015)
- [110] Boyer T H 2018 Blackbody radiation in classical physics: A historical perspective, *Am J phys* 86 (7) July (2018)
- [111] Louis De Broglie, Recherches sur la théorie des Quanta, *Ann. Phys.*, vol. 10, n. 3, 22 - 128(1925)
- [112] L.H. Thomas, Proc. Cambridge Phil. Soc., 23, 542 (1927)
- [113] E. Fermi, Rend. Accad. Naz. Lincei, 6, 602(1927)
- [114] Becke, A. D., *J. Chem. Phys.*, 84, 4524 (1986)
- [115] Perdew, J.P., *Phys. Rev. B*, 33, 8822 (1986)
- [116] Hannu Haikkinen, Michael Moseler, Symmetry and Electronic Structure of Noble-Metal Nanoparticles and the Role of Relativity, *physical review letters*, volume 93, number 9(2004)
- [117] Wei Huang, Min Ji, Chuan-Ding Dong, Xiao Gu, Lei-Ming Wang, Xin Gao Gong, and Lai-Sheng Wang, Relativistic Effects and the Unique Low Symmetry Structures of Gold Nanoclusters, *acs nano*, vol.2, no. 5, 897–904 (2008)
- [118] Maxime Van den Bossche, DFTB-Assisted Global Structure Optimization of 13- and 55-Atom Late Transition Metal Clusters, *J. Phys. Chem. A*, 123, 3038–3045 (2019)
- [119] Nathalie Tarrat, Mathias Rapacioli, Jérôme Cuny, Joseph Morillo, Jean-Louis Heully, et al., Global optimization of neutral and charged 20- and 55-atom silver and gold clusters at the DFTB level. Computational and Theoretical Chemistry, *Elsevier*, 1107, pp.102-114 (2017)
- [120] Dmitry (2020). Cluster generator (<https://www.mathworks.com/matlabcentral/fileexchange/33449-cluster-generator>), MATLAB Central File Exchange, August 7, (2020)
- [121] Tian Lu, Feiwu Chen, Multiwfn: A Multifunctional Wavefunction Analyzer, *J. Comput. Chem.* 33, 580-592 (2012)
- [122] Gloria Mazzone, Ivan Rivalta, Nino Russo, and Emilia Sicilia, Interaction of CO with PdAu(111) and PdAu(100) Bimetallic Surfaces: A Theoretical Cluster Model Study, *J. Phys. Chem. C*, 112, 6073-6081 (2008)